

1-1-1991

# Hindered diffusion of polymers in porous materials/

Yihong, Guo

*University of Massachusetts Amherst*

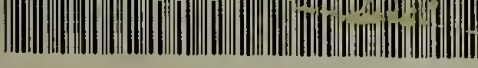
Follow this and additional works at: [https://scholarworks.umass.edu/dissertations\\_1](https://scholarworks.umass.edu/dissertations_1)

---

## Recommended Citation

Guo, Yihong, "Hindered diffusion of polymers in porous materials/" (1991). *Doctoral Dissertations 1896 - February 2014*. 777.  
[https://scholarworks.umass.edu/dissertations\\_1/777](https://scholarworks.umass.edu/dissertations_1/777)

This Open Access Dissertation is brought to you for free and open access by ScholarWorks@UMass Amherst. It has been accepted for inclusion in Doctoral Dissertations 1896 - February 2014 by an authorized administrator of ScholarWorks@UMass Amherst. For more information, please contact [scholarworks@library.umass.edu](mailto:scholarworks@library.umass.edu).



312066007768784

**HINDERED DIFFUSION OF POLYMERS  
IN POROUS MATERIALS**

A Dissertation Presented

by

**YIHONG GUO**

Submitted to the Graduate School of the  
University of Massachusetts in partial fulfillment  
of the requirements for the degree of

**DOCTOR OF PHILOSOPHY**

February 1991

Department of Polymer Science and Engineering

© Copyright by Yihong Guo 1991

All Rights Reserved

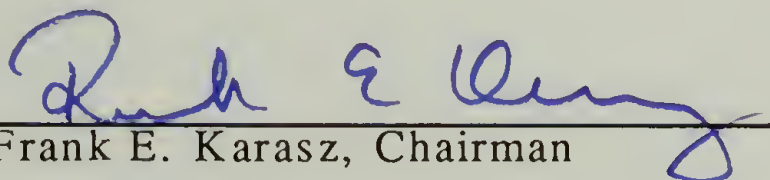
# HINDERED DIFFUSION OF POLYMERS IN POROUS MATERIALS


A Dissertation Presented

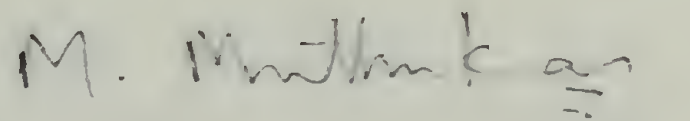
by

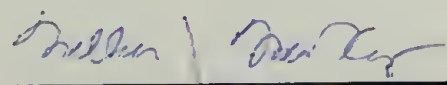
YIHONG GUO

Approved as to style and content by:

  
Frank E. Karasz, Chairman

  
Kenneth H. Langley, Member

  
Murugappan Muthukumar, Member

  
William J. MacKnight, Head  
Department of Polymer Science and  
Engineering

Dedicated to my wife, Hongyi

## ACKNOWLEDGEMENTS

I am truly grateful to my advisors: Professor Frank E. Karasz for his inspiration, guidance and making everything possible for me; Professor Kenneth H. Langley for his continuous support, instruction, and training me to be a better scientist.

I acknowledge my gratitude to Professors Murugappan Muthukumar and Robert A. Guyer for their valuable insights in the problems in my project. It was a great pleasure to have worked with Dr. Stephen J. O'Donohue, who helped me in numerous ways on my experiments, and who also started setting up the forced Rayleigh scattering spectrometer. I sincerely thank Dr. Kimin Eum for his generous help when I started working in the light scattering laboratory. I thank Dr. Nalini Easwar and Richard Bonanno for their contributions to this study. I also feel obliged to Dr. Matthew T. Bishop, who initialized, in our laboratory, the study of polymer diffusion in a porous medium. I benefited from the dynamic light scattering apparatus he set up and his inclusive Ph.D. thesis. Machinist A. B. Webb is thanked; many important parts in the forced Rayleigh scattering apparatus were custom made by him.

The Polymer Science and Engineering Department has provided me an excellent opportunity of learning much about the fascinating polymers.

This work has been supported by the Air Force Office of Scientific Research.

I am most deeply indebted to my wife, Hongyi, for her love, encouragement and companionship over the years in the “dark tunnel”. A debt of gratitude is owed to my parents for all they have given me in my life.



# ABSTRACT

HINDERED DIFFUSION OF POLYMERS IN POROUS MATERIALS

FEBRUARY 1991

YIHONG GUO, B.S., JIAO TONG UNIVERSITY, SHANGHAI, CHINA

Ph.D., UNIVERSITY OF MASSACHUSETTS

Directed by: Professor Frank E. Karasz

Professor Kenneth H. Langley

Dynamic light scattering (DLS) and forced Rayleigh scattering (FRS) were used to study polymer diffusion in solution in two kinds of porous materials: porous glasses and suspensions and gels formed from fumed silica particles. The diffusants were: dendritic polyamidoamines, linear polystyrenes, and dye-labeled polystyrenes.

Polymer diffusion in porous glasses was investigated, by using DLS, as a function of time scale ( $t$ ), polymer hydrodynamic radius ( $R_H$ ), and pore radius ( $R_P$ ). As  $t$  increases, the apparent diffusion crosses over from single pore diffusion (in which steric obstruction is weak) to macroscopic diffusion (in which the tortuosity of the pore networks is fully effective). Computer simulated diffusion agreed qualitatively with the crossover observed by DLS.

The dependence of hindered diffusion on the size ratio  $\lambda_H=R_H/R_P$  was studied for dendritic polyamidoamines and linear polystyrenes in porous glasses. For  $\lambda_H \ll 1$ , when hydrodynamic interactions dominate, dendritic polymers diffuse more slowly than linear polymers of comparable  $\lambda_H$ . The diffusion results of the dendritic polymer and of the linear flexible polymer agreed quantitatively with the hydrodynamic theories for a hard sphere in a cylindrical pore, and for a random-coil macromolecule in a cylindrical pore, respectively. At large  $\lambda_H$ , irregularities in local pore size lead to conformational entropy changes as the macromolecule moves. The experimental data agree qualitatively with the entropy barrier theory.

Diffusion of dye-labeled polystyrenes within gels and suspensions formed from fumed silica was studied using FRS. Untreated silica was found to adsorb the labeled polymer, leading to strong hindrance even at very low silica concentration. Thorough quenching of the silica surface by silanization prevented polymer adsorption. The dependence on silica volume fraction of the resulting weakly hindered diffusion in treated silica was found to be consistent with simple theories of steric obstruction.

# TABLE OF CONTENTS

	<u>Page</u>
ACKNOWLEDGEMENT .....	v
ABSTRACT.....	vii
LIST OF TABLES .....	xi
LIST OF FIGURES .....	xii
Chapter	
I INTRODUCTION.....	1
II LIGHT SCATTERING THEORIES AND EXPERIMENTS .....	14
A. Dynamic Light Scattering Theories.....	14
B. Forced Rayleigh Scattering Theory .....	20
C. Polymer Samples .....	26
D. Porous Materials and Surface Treatment .....	35
E. Apparatus and Experimental Procedures.....	41
III TIME SCALE DEPENDENCE OF DIFFUSION IN POROUS MATERIALS .....	55
A. Background.....	55
B. Computer Simulation.....	57
C. Results and Discussion.....	60
D. Conclusions .....	68
IV MACROSCOPIC DIFFUSION OF POLYMERS IN POROUS GLASSES .....	79
A. Background.....	79
B. Effect of Hydrodynamic Drag.....	85

	C. Diffusion of Polymer Chains under Strong Confinement .....	92
	D. Diffusion of Polystyrenes in Vycor Glass with Very Small Pores .....	97
	E. Conclusions.....	100
V	DIFFUSION IN POROUS MEDIA FORMED FROM FUMED SILICA .....	115
	A. Background.....	115
	B. Results and Discussions .....	117
	C. Conclusions .....	126
VI	CONCLUSIONS .....	137
	A. Summary.....	137
	B. Suggestions for Future Work .....	142
APPENDICES		
	A. SOME PROPERTIES OF THE SOLVENTS.....	149
	B. TECHNICAL DETAILS OF FORCED RAYLEIGH SCATTERING ....	152
	REFERENCES.....	160

# LIST OF TABLES

Table	Page
2.1 Characteristics of polystyrene samples .....	49
2.2 Characteristics of the porous glass samples .....	50
4.1 Hydrodynamic radius( $R_H$ ), size ratio( $\lambda_H$ ), diffusivity in unbounded solution( $D_0$ ), macroscopic diffusion coefficient( $D$ ), and diffusivity ratio( $D/(D_0X)$ ) for starburst-dendritic s polyamidoamine in porous glasses .....	103
6.1 Systems studied in this dissertation .....	147

# LIST OF FIGURES

Figure	Page
2.1	Dynamic light scattering spectrometer.....51
2.2	Forced Rayleigh scattering spectrometer .....52
2.3	The spatially periodic interference pattern in the sample created by the two writing beams crossing at an angle $\theta$ .....53
2.4	Timing diagram of the forced Rayleigh scattering measurements .....54
3.1	Model pore structure used in the computer simulation.....69
3.2	The inverse friction ratio $K^{-1}(\beta)$ used in the computer simulation.....70
3.3	Field autocorrelation function $g(t)$ (normalized after baseline subtraction) measured by dynamic light scattering from a solution of polystyrene ( $M=50,000$ , $R_H=52 \text{ \AA}$ ) in the controlled pore silica glass R893 ( $R_P=893 \text{ \AA}$ ).....71
3.4	The apparent diffusion coefficient as a function of time, proportional to the slope of the ACF in Figure 3.3(b) and (c).....74
3.5	Mean square displacement $\langle R^2(t) \rangle$ versus random walk step number (equivalent to time), obtained from computer simulation.....75
3.6	Computer simulation calculation of the apparent diffusion coefficient obtained from the slope of the curve in Figure 3.5.....76

3.7	Dependence of the crossover time on polymer radius $R_H$ and pore radius $R_P$ , from computer simulation.....	77
3.8	Dependence of the crossover time $t_1$ on polymer radius $R_H$ , measured using DLS .....	78
4.1	The ratio of the diffusivity, $D/(XD_0)$ , for dendritic polyamidoamines in porous glasses R893 ( $R_P=893\text{\AA}$ ) and G275 ( $R_P=275\text{\AA}$ ) versus the size ratio $\lambda_H$ (filled squares) .....	104
4.2	Semilogarithmic plot of the intensity autocorrelation function for polystyrene P100 in glass G75 ( $\lambda_H = 1.01$ ) measured at a scattering angle of $35^\circ$ .....	105
4.3	Autocorrelation decay rate spectrum based on scattered intensity, calculated from the ACF shown in Figure 4.2 using CONTIN program.....	106
4.4	Hindrance factor for macroscopic diffusion ( $D/D_0$ ) versus polymer to pore size ratio ( $\lambda_H$ ) .....	107
4.5	Molecular weight dependence of the macroscopic diffusion coefficients of polystyrene fractions ( $7 \times 10^3 < MW < 2.05 \times 10^6$ ) inside the porous glasses G75 and G275 .....	108
4.6	Logarithmic plot of the hindrance factor ( $D/D_0$ ) versus size ratio ( $\lambda_H$ ).....	109
4.7	A schematic representation of the pore structure .....	110
4.8	A comparison of the experimental data to the predictions of the entropy barrier theory .....	111
4.9	Decay rate of DLS autocorrelation function ( $1/\tau$ ) versus squared wavevector $q^2$ , for polystyrene ( $MW=7,000$ ) in Vycor glass .....	113
4.10	Hindrance factor $D/D_0$ as a function of size ratio $\lambda_H$ for polystyrenes ( $MW=2,500$ to $13,000$ ) in Vycor ( $R_P=20\text{\AA}$ ) ..	114

5.1	Transient diffraction intensity $V(t)$ for a dye-labeled polystyrene ( $MW=1.13\times 10^6$ ) in a silica gel composed of R972-M which has negligible adsorption of the polymer .....	127
5.2	A plot of the residuals of a non-linear least square fit of the data points in Figure 5.1 to equation (2.27).....	128
5.3	Transient diffraction intensity $V(t)$ for a dye-labeled polystyrene ( $MW = 1.13\times 10^6$ ) in a silica gel of R972 which has a finite surface silanol density resulting in surface adsorption .....	129
5.4	A plot of the residuals of a non-linear least square fit of the data points in Figure 5.4 to equation (2.27) .....	130
5.5	The decay rate $1/\tau$ of the intensity diffracted from the transient grating of photo-excited dye attached to polystyrene ( $MW=1.13\times 10^6$ ) as a function of the squared wavevector $q^2$ in three different systems .....	132
5.6	Hindrance factor $D/D_0$ versus silica volume fraction $\Phi$ for two polystyrene samples ( $MW = 4.8\times 10^4$ and $1.13\times 10^6$ ) in R972-M gels .....	133
5.7	Hindrance factor $D/D_0$ versus silica volume fraction $\Phi$ for polystyrene ( $MW = 1.13\times 10^6$ ) in R972 gels .....	134
5.8	Diffusion coefficient $D$ versus time during the gelation process for a R972-M gel ( $\Phi = 7.1\%$ ) .....	135
5.9	Diffusion coefficient $D$ versus time during the gelation process for a R972 gel ( $\Phi = 2.6\%$ ) .....	136
6.1	Systematic scheme of diffusion behavior in different regimes..	148
B.1	Connections among different units of the forced Rayleigh scattering apparatus.....	158
B.2	Optical layout of the for forced Rayleigh scattering spectroweter.....	159



# CHAPTER I

## INTRODUCTION

Reported in this dissertation is the study of diffusion of macromolecules in porous materials using light scattering spectroscopies. This "Introduction" places the current work in the context of general studies of transport in porous materials, illustrates the motivation of this study, describes briefly the experimental systems and techniques, and outlines the contents of the dissertation.

Generally speaking, the transport processes within porous media can be classified as diffusion, convection, electric conduction, thermal conduction, and hydrodynamic flow[1-7]. These processes are governed by interactions between the fluid continuum and the confining solid-fluid interfaces. In absence of any chemical reactions such as adsorption, the geometries of these interfaces establish the fields with which the fluid interacts in many ways.

Practically, many of these elementary processes occur simultaneously. However, a fuller understanding must first be developed for the elementary processes in order to make meaningful predictions concerning such complex phenomena within a porous medium. This dissertation is devoted to the study of diffusion of polymers in porous

materials; the restricted diffusion process is intimately related to the other transport processes, and to many aspects of the pore structure such as tortuosity, porosity and pore dimensions. This work is part of the general pursuit of understanding molecular dynamics in confining spaces.

The diffusion of polymer solutes and other species in liquid-filled pores has attracted great interest from different disciplines because it is central to many important processes such as chromatographic separation of macromolecules, enhanced oil recovery, membrane separation, polymerization using heterogeneous catalysts, and biological transport processes. Theoretically, the study of hindered polymer diffusion furnishes much insight into topics such as transport in porous media and dynamics of confined polymer chains in gels, pores and melts.

A macromolecule diffuses more slowly in a porous medium than in a free solution ultimately due to the presence of an obstructing solid phase. A polymer diffusant experiences size dependent hydrodynamic interactions with the pore walls while it translates inside the tortuous pores. Relative to the overall scheme of transport in porous media, our system of polymer diffusion in pores bears certain features that give rise to a higher degree of complexity. This is mostly due to two inherent attributes of polymer: a larger polymer size often comparable to the pore sizes, and a complex polymer conformation. As opposed to small diffusants or simple fluids, a polymer molecule experiences hydrodynamic drag from the pore walls. This drag is increasingly stronger when the polymer molecule is closer to the walls. The prediction of the effect of hydrodynamic interactions is complicated by the difference in polymer conformation between confined

polymer and unbounded polymer (in free solution), or by the difficulty of finding a characteristic polymer dimension which is most directly related to the hydrodynamic interactions. Also, the hindrance to diffusion is partly dependent on the chemical and architectural structure of the polymer. More complication arises when the size of the macromolecule is similar to or larger than that of the pores. At that time, the polymer conformation is perturbed to suit the local pore structure, thus is different at different positions within the porous medium. The conformational change during the polymer movement greatly affects the diffusion behavior.

Previous studies of diffusion of polymers in porous materials may be divided into two categories: those using systems with well defined pore geometry such as track-etched membranes[8-15], and those using systems with relatively random pore structures exemplified by porous glasses[16-22]. The objective of these studies has been to relate the experimentally obtained results to the microscopic parameters characterizing the polymer and the porous material. For the diffusion of a flexible polymer across a membrane, which can be modeled by a diffusion process in cylindrical pores, the experimental results have been generally consistent with theories of hard sphere diffusion[23-26] and with scaling theories[27-30].

However, a good understanding of polymer diffusion in pores of non-ideal geometry has not been attained for several reasons: 1) the pore structure has not been unambiguously characterized; 2) the statics and dynamics of polymers in random pores have not been studied as completely as in pores of idealized geometry; 3) there are discrepancies among the experimental results. Systematic measurements of diffusion in porous media are

therefore desirable to test further the current models and to stimulate additional theoretical developments, and thereby to acquire more knowledge in this area.

The objective of this dissertation is to achieve a better understanding of the transport of polymers in porous materials. Specifically, our study is aimed at revealing mechanisms of diffusion hindrance in porous materials with pore geometries more complicated than ideal geometries (e.g. cylindrical pores). The systems that have been studied in this dissertation project are described here. Two kinds of porous materials were investigated: (1) silica glasses with controlled pore size; and (2) porous media (suspensions and gels) composed of fumed silica with random pore structures. The polymer diffusants used in this work were: linear polystyrene, starburst-dendritic polyamidoamine diffusing in porous glasses studied by dynamic light scattering (DLS); and dye-labeled polystyrene in gels and suspensions of fumed silica studied by forced Rayleigh scattering (FRS). Details about the polymer samples and porous materials can be found in Chapter II. Three solvents, which are 2-fluorotoluene, transdecahydronaphthalene, and fluorobenzene, have been used. These solvents have indices of refraction very similar to that of the porous materials (silica in this work) thus allowing direct measurement of polymer diffusion within the porous sample by light scattering. Some relevant properties of these solvents are listed in Appendix A. The working temperatures were selected such that the indices of refraction of the silica and of the solution are optimally matched for the light scattering experiments.

Pragmatically, the reduced diffusion rate of various polymers within several porous materials were measured by light scattering techniques (DLS and FRS), and were correlated to the characteristic parameters including polymer molecular weight, hydrodynamic radius of polymer, nominal pore radius, and porosity of the porous material, which are all independently measurable.

In this laboratory, my predecessor Dr. Matthew T. Bishop employed dynamic light scattering to measure directly the mutual diffusion coefficient of linear polystyrene in porous glasses under macroscopic equilibrium [19,20]. DLS has significant advantages compared to other techniques as it is insensitive to boundary layer resistance and partition coefficient effects. The results of Bishop's work were highlighted in the following.

The diffusion at different length scales, or exactly at different values of  $qR_p$  were studied, where  $q$  is the amplitude of the scattering wavevector, and  $R_p$  is the pore radius. At large  $qR_p$  ( $>1$ ), the phenomenological diffusion coefficient is larger than that at small  $qR_p$  corresponding to diffusion within a single pore segment. At small  $qR_p$  ( $<1$ ), the macroscopic diffusion coefficient  $D$  ( $D_\infty$  in Bishop's notation) was obtained, which is the phenomenological coefficient for diffusion over large distances in porous glass. The reduction in macroscopic diffusion coefficient ( $D$ ) relative to the diffusivity in free solution ( $D_0$ ) was investigated as a function of the size ratio  $\lambda_H = R_H/R_p$ , where  $R_H$  is the hydrodynamic radius of the polymer diffusant. The diffusion behavior was interpreted in terms of two separable factors: (1) the tortuosity[6] of the pore spaces; and (2) the hydrodynamic interactions with the pore walls in cylindrical pores[24-

30]. For the three glasses being studied, the tortuosities (obtained as the inverse of  $D/D_0$  in the limit  $\lambda_H=0$ ) were independent of  $\lambda_H$  and were related to the pore space geometries. The prediction of the hindrance due to hydrodynamic interactions was based on theories[24-26] for hard sphere diffusion at small  $\lambda_H$  values and scaling theories[27-30] at higher  $\lambda_H$  values. It was found that the dimension ratio  $\lambda_S=R_S/R_P$  obtained from fitting the experimental data to the hydrodynamic predictions, where  $R_S$  is the effective hard-sphere radius for the polymer, is different from the size ratio  $\lambda_H$ . The causes of this difference were left to be uncovered.

Dr. M. T. Bishop's work was followed by Dr. N. Easwar, who extended in two directions the study of polystyrene diffusion in porous glasses. First, The diffusion measurements were extended from linear polystyrene to 4-arm and 8-arm star-branched polyisoprenes which have higher architectural compactness. It was found that for a given  $\lambda_H$ , the branched polymers diffuse more slowly than the linear polymers; it was also found that 8-arm stars diffuse more slowly than 4-arm stars of the same hydrodynamic radius[21]. The results indicated that the effective hard-sphere radius ( $R_S$ ) is often different from the free solution hydrodynamic radius ( $R_H$ ), and is generally different for different polymers with different architectures. The difference between  $R_H$  and  $R_S$  is smaller for macromolecules with higher structural compactness. Second, the diffusion measurements were also extended from a lower  $\lambda_H$  regime ( $\lambda_H \leq 0.47$  in Bishop's work) to a higher  $\lambda_H$  regime ( $\lambda_H \leq 0.74$ ). The results suggested that the diffusion of strongly confined polymer chains is in qualitative agreement with the theoretical prediction based on the

conformational entropy changes[31] accompanying the diffusive motion of polymer chains within the porous glass.

This dissertation work can be viewed, in some sense, as extension and expansion of the previous works of Bishop et al.[19,20] and Easwar et al.[21] The connections between this work and the previous works done in this laboratory are in several respects. First, the transition region ( $1/q \approx R_p$ ) is studied in which the dynamic light scattering autocorrelation function was dominated by single pore diffusion at early times, and crossed over to a relaxation characteristic of macroscopic diffusion at later times. Second, the study on the effect of molecular architecture was extended from linear and star-branched polymers to a starburst-dendritic polymer that has a much higher structural compactness. Third, the measurements of the diffusion of linear polystyrene in porous glasses were extended to new regimes of much higher confinement; measurements at size ratios up to  $\lambda_H = 1.4$  (compared to  $\lambda_H = 0.74$  in Easwar's work) was achieved. Fourth, a new technique, forced Rayleigh scattering, was established in this laboratory and was employed, in addition to the dynamic light scattering, for measuring diffusion rate in porous materials. Fifth, new porous materials — gels and suspensions of fumed silica, were used for the study of diffusion in random porous materials.

The principles of the analytical techniques employed in this work are briefly described here. Dynamic light scattering measures the intensity autocorrelation function (ACF) which is a measure of the correlation between the molecular configuration at a given time and that at some later time, as such, this correlation function is related to the dynamic processes

in the scattering medium. The decay rate of this ACF is determined by the diffusion rate, provided that this decay of correlation is only due to the diffusive motion of the molecules. Forced Rayleigh scattering is fundamentally similar to dynamic light scattering. It monitors the decay of an externally modulated concentration grating, instead of the decay of spontaneous thermal fluctuations of polymer concentration in DLS. In our experiments, FRS follows the transient diffraction intensity from a grating of photochemically excited probes which is created by a laser pulse. The decay of the diffraction intensity in FRS is also related to the diffusive motion of the probes which erases the gradient of the index of refraction in the sample.

There are other dynamic methods available for the study of transport in porous materials. Among those often used are pulsed field gradient NMR (PFGNMR)[32-34], fluorescence recovery after photobleaching (FRAP)[35], ionic conductivity measurement[36-39], size exclusion chromatography (SEC) peak broadening[40], trace exchange[41,42], and membrane transport measurement[8-15]. DLS, FRS, PFGNMR, FRAP directly monitor dynamics in porous materials, as opposed to other methods (mentioned here) which are generally complicated by partitioning and boundary resistance effects.

The remainder of this chapter describes the contents of this dissertation.

Chapter II presents the relevant theories of dynamic light scattering[43-45] and forced Rayleigh scattering[46-84] which were employed in this work, describes the polymer samples and porous materials



studied, and outlines the experimental procedures and data analysis methods for all experiments. The results from these experiments are presented in chapters III, IV and V.

Chapter III reports the work on the study of time scale dependence of diffusion in porous materials. In this part, diffusion of polystyrene molecules in controlled-pore glasses was studied experimentally using DLS, and by computer simulation based on a hydrodynamic theory of a hard sphere in a cylindrical pore[24]. Dynamic light scattering at fixed scattering wavevector revealed faster apparent diffusion at short times (corresponding to diffusion within a single pore) followed by a slower relaxation which we attribute to macroscopic diffusion over distances large enough to average out the microscopic nonuniformities of the glass-pore matrix. The measured time at which the behavior crosses over from faster to slower diffusion was found to be independent of the light scattering wavevector, and is roughly equal to the time required for a polymer molecule to diffuse a distance comparable to the pore dimension. At small ratio of polymer to pore radius, the crossover time was found to increase linearly with the polymer radius, both in DLS measurements and in the computer simulation.

Chapter IV is a systematic study of the diffusion of different polymers in porous glasses with different pore sizes, using the technique of dynamic light scattering. Polymer diffusants with drastically different architectures have been studied, as part of the effort of understanding the effect of molecular architecture on the hindered diffusion in porous materials. The diffusion of a relatively compact polymer molecule –

starburst dendritic polyamidoamine (PAMAM) was measured, and the results were compared to the diffusion of linear polystyrenes[19,20] and star-branched polyisoprenes(PI)[21], and to the Brenner-Gaydos(BG)[25] theory which is a hydrodynamic theory based on a model of hard sphere in cylindrical pores. For the same  $\lambda_H$  and same  $D_0$ , it was found that,

$$D(\text{dendritic PAMAM}) < D(\text{star-branched PI}) < D(\text{linear PS})$$

because the PAMAM molecules are least compressed when they diffuse inside the confining pores. Quantitative agreement exists between our experimental results on the diffusion of PAMAM and the BG theory, with the assumed relation  $R_S = R_H$ . This supports the direct applicability of the BG theory to controlled-pore glasses.

Another part of Chapter IV is on diffusion of linear polystyrenes in controlled pore glasses. It was studied in a very large range of polymer-to-pore size ratio  $\lambda_H = R_H/R_P$ , where  $R_H$  and  $R_P$  are the hydrodynamic radius of polymer and the nominal pore radius, respectively. Fickian diffusion was observed up to confinements as high as  $\lambda_H = 1.4$ . The macroscopic diffusion coefficient  $D$  in the porous medium (measured on length scales large compared to  $R_P$ ) was found to decrease monotonically with increasing molecular weight and  $\lambda_H$ . At  $\lambda_H < 0.3$ , the diffusion coefficients were in good agreement with those predicted by the hydrodynamic theory for the diffusion of a flexible macromolecule in cylindrical pores[9,15]. At  $\lambda_H > 0.6$ , a stronger molecular weight dependence emerges, inconsistent with the "elongated cigar" model[27-30] which successfully explained the diffusion behavior of macromolecules in cylindrical pores of porous membrane. At

large values of  $\lambda_H$ , irregularities in local pore size lead to alterations in polymer conformation and hence changes in entropy as the chain moves. The experimental data agree qualitatively with the prediction of the recently developed entropy barrier theory[31] which is a scaling analysis of the diffusion hindrance based on entropy changes.

Chapter V presents the diffusion study of a dye-labeled polystyrene chain inside a random porous medium composed of fumed silica particles, studied by forced Rayleigh scattering. Two forms of silica porous media were involved: silica suspension and silica gel; the former can transform into the latter if the silica concentration is high enough. The surfaces of a fumed silica, R972 (Degussa), were chemically treated to replace hydroxyl groups by alkyl groups thus minimizing surface adsorption; the treated silica was referred as R972-M. Significant difference was observed between silica R972 which adsorbs labeled polystyrene and the silica R972-M which does not adsorb. In a porous medium of R972-M, the FRS signal was normal, and the proportionality of  $1/\tau \propto q^2$  was found indicating Fickian diffusion at macroscopic scales, where  $\tau$  is the characteristic decay time and  $q$  is the scattering wavevector. On the contrary in a porous medium of R972, the FRS signal was abnormal and there was an obvious curvature in the plot of  $1/\tau$  versus  $q^2$ . We studied the effect of porosity on the hindrance to diffusion in the porous media of both types of fumed silica. For polymer diffusion inside a R972-M porous medium, the hindrance is weak owing to the large pores and the high porosity and is attributed to geometric obstruction and hydrodynamic interactions with the silica surfaces. The experimental results for R972-M were compared to

some theories, which were based on simpler models than the actual pore structure; the models are: (1) a homogeneous swarm of spheres of arbitrary size distribution[36]; and (2) minimum entropy production model[85]. Since these models are not truly parallel to our experimental system, the comparisons were only intended to put our work in the context of transport in a random medium. In a porous medium of R972, adsorption dominated the polymer diffusion behavior, and the diffusion was drastically hindered even at very low silica concentration. The changing diffusion rate during gelation was also monitored. A difference in the time preceding the stabilization of the diffusion coefficient was found between two different systems, relating to the different mechanisms that govern the diffusion behavior.

Chapter VI starts by summarizing the works done in this dissertation project. I used dynamic light scattering to study diffusion of a dendritic polymer and a linear polymer in porous glasses. The time scale dependence of diffusion was studied using both DLS and computer simulation. Diffusion of dye-labeled polymer in a random porous medium of fumed silica was studied using forced Rayleigh scattering, which was set up by Dr. S. J. O'Donohue and myself under the direction of Professor. K. H. Langley and Professor F. E. Karasz.

Later in Chapter VI the mechanisms of diffusion hindrance were summarized in a schematic plot that systematically depicts different regimes of diffusion behavior. These regimes are defined by three most important parameters: time scale of observation ( $t$ ), hydrodynamic radius of polymer diffusant ( $R_H$ ), and pore radius ( $R_P$ ). At small time scales, the measured

apparent diffusion is single pore diffusion without fully experiencing the steric obstruction. At large  $t$ , macroscopic diffusion was measured, which was found to be slower than single pore diffusion. The region of macroscopic diffusion is influenced by different factors that manifest their effects differently in different regimes characterized by the size ratio  $\lambda_H$ . At  $\lambda_H \ll 1$ , the diffusion is hindered, for the most part, by the steric obstruction, and the diffusion is determined by the characteristics of the porous material, independent of the polymer structure. At  $\lambda_H < 1$ , the diffusion hindrance is due to both the hydrodynamic effect and the geometric effect. In this regime, it was found that the dendritic polymer diffuses more slowly than the linear polymer, which is attributed to the architectural effects. Quantitative agreement was found between the diffusion of the dendritic polymer and a hard sphere diffusion model, and between diffusion of the linear polystyrene chain and a model of random coil macromolecule. At  $\lambda_H \approx 1$ , the diffusion of highly confined polymer chains is largely determined by conformational changes. We found qualitative agreement between our measured diffusion and the entropy barrier model.

# CHAPTER II

## LIGHT SCATTERING THEORIES AND EXPERIMENTS

### A. Dynamic Light Scattering Theories

Dynamic light scattering offers one of the most precise methods of measuring polymer diffusion coefficients. Basic light scattering theories and applications have been elaborately reviewed in several books[43-45]. This section briefly summarizes those aspects of dynamic light scattering theory relevant to the work of this dissertation. The practical measurements and data analysis are described in the "Experimental Procedures" section.

The basic DLS experiment is shown schematically in Figure 2.1. Incident light with propagating wavevector  $q_0$  impinges on a sample, and induces re-radiation from oscillating dipoles, thereby giving rise to a pattern of scattered light. The photomultiplier tube at a scattering angle  $\theta$  measures the intensity (photon count rate) of the scattered light with propagating wavevector  $q_s$ . This optical setup determines the most important parameter, the light scattering wavevector  $q$ ,

$$q = q_s - q_0. \quad (2.1)$$

Since the scattering is nearly elastic (this gives DLS another name of quasielastic light scattering), i.e.  $|\mathbf{q}_0| \approx |\mathbf{q}_s|$ , the magnitude of  $\mathbf{q}$  is

$$q = \frac{4\pi n}{\lambda_0} \sin \frac{\theta}{2} \quad (2.2)$$

where  $\lambda_0$  is the vacuum wavelength of the incident light, and  $n$  is the index of refraction of the scattering medium.

The scattered light intensity  $I$  is determined by the amplitudes and phase relationships of the components of the scattered electric field, in turn determined by the configuration of the molecules in the sample. In the polymer solution, that configuration changes with time due to molecular motion, giving rise to fluctuations in the intensity of the scattered light.

Experimentally, at a certain scattering angle, the dynamic light scattering spectrometer measures the intensity autocorrelation function (ACF) of the fluctuating intensity; this ACF is defined as:

$$G^{(2)}(t) = \langle I(\tau)I(\tau+t) \rangle = \lim_{T \rightarrow \infty} \frac{1}{2T} \int_{-T}^T I(\tau)I(\tau+t)d\tau \quad (2.3)$$

where  $t$  is the delay time, and  $\tau$  is the real time over which the average is taken. The intensity ACF is a measure of the correlation between the molecular configuration at a given time, to the configuration at some later time  $t$ ; as such the intensity ACF is related to dynamic processes in the scattering medium.

Though intensity ACF is measured in DLS experiments, it is the scattered electric field autocorrelation function that is fundamentally related to the dynamics of the scattering medium. We denote the scattered electric field ACF by  $G^{(1)}(t)$ , which is defined as:

$$\begin{aligned} G^{(1)}(t) &= \langle E_s^*(\tau)E_s(\tau+t) \rangle \\ &= \lim_{T \rightarrow \infty} \frac{1}{2T} \int_{-T}^T E_s^*(\tau)E_s(\tau+t)d\tau \end{aligned} \quad (2.4)$$

The more convenient, normalized intensity and electric field ACFs are introduced as:

$$g^{(2)}(t) = \frac{\langle I(0)I(t) \rangle}{\langle I(t) \rangle^2} \quad (2.5)$$

and

$$g^{(1)}(t) = \frac{\langle E_s^*(0)E_s(t) \rangle}{\langle E_s^*(0)E_s(0) \rangle} = \frac{\langle E_s^*(0)E_s(t) \rangle}{\langle I \rangle} \quad (2.6)$$

We use  $\langle I(t) \rangle$  or  $\langle I \rangle$  to denote the average scattering intensity. Caution must be taken in using the normalized intensity ACF (equation 2.5) as there exist different ways of normalization; instead of normalization to  $\langle I(t) \rangle^2$  in equation (2.5),  $g^{(2)}(t)$  may be normalized to  $\langle [I(t)]^2 \rangle$ .

In the ensuing paragraphs, we first relate the intensity ACF (measured experimentally) to the field ACF (related to molecular



dynamics), and then demonstrate the extraction of information on polymer diffusion from the field ACF.

Two optical arrangements have been used in this work to measure diffusion coefficients: homodyne method for diffusion in free solution, and heterodyne method for diffusion in porous materials. In the homodyne (self-beating) arrangement, only light scattered from the polymer molecules hits the detector. If the scattered field  $E_S$  obeys Gaussian distribution, then the relation between  $g^{(1)}(t)$  and  $g^{(2)}(t)$  is given by the Siegert relation[45]:

$$g^{(2)}(t) = 1 + |g^{(1)}(t)|^2 \quad (2.7)$$

Experimentally, due to the finite size of the scattering volume and the finite area of the detecting photocathode surface, spatial coherence must be considered. The intensity ACF in homodyne method can then be written as

$$G^{(2)}(t) = B(1 + f_c |g^{(1)}(t)|^2) \quad (2.8)$$

where  $f_c$  is the coherence factor that depends mainly on the optical arrangement, and  $B$  is the ACF baseline value which is theoretically equal to  $\langle I \rangle^2$ . The calculation of  $B$  from other experimentally measured quantities is shown in the "Experimental Procedures" section of this chapter.

In the heterodyne arrangement, a coherent local field  $E_{LO}$  (which is the scattered light from the glass matrix in our work) is mixed with the scattered field  $E_S$  on the photocathode, and the intensity ACF is,

$$G^{(2)}(t) = \langle I(0)I(t) \rangle = \langle |E_S(0) + E_{LO}(0)|^2 |E_S(t) + E_{LO}(t)|^2 \rangle \quad (2.9)$$

The expansion of this equation results in a expression with sixteen terms. This expression can be significantly simplified for the “strong heterodyne” limit ( $E_{LO} \gg E_S$ ), assuming two conditions: (a) fluctuations of the local oscillator field are negligible; and (b) the local oscillator field and the scattered field are statistically independent. With these assumptions, equation (2.9) reduces to,

$$G^{(2)}(t) = \langle I \rangle^2 + 2\langle I_S \rangle \langle I_{LO} \rangle g^{(1)}(t) \quad (2.10)$$

With the spatial coherence taken into account, we have,

$$G^{(2)}(t) = B(1 + f_c |g^{(1)}(t)|) \quad (2.11)$$

for our practical data analysis.

Discussed next are some existing theories on the relation between the electric field ACF  $g^{(1)}(t)$  and the underlying molecular dynamics, which in our case is the microscopic Brownian motion of polymer solutes. For a dilute solution of monodisperse isotropic scatterers, small compared to the wavelength of light, the scattered field is

$$E_S(\mathbf{q}, t) = \sum_i \alpha \exp i\mathbf{q} \cdot \mathbf{r}_i(t) \quad (2.12)$$

where  $\mathbf{r}_i(t)$  is the position of the  $i^{\text{th}}$  particle at time  $t$ , and  $\alpha$  is the polarizability. Using this result with equation (2.6), the normalized scattered field ACF can be written as

$$g^{(1)}(t) = \frac{\left\langle \sum_i \sum_j \exp \{ i \mathbf{q} \cdot [\mathbf{r}_j(t) - \mathbf{r}_i(0)] \} \right\rangle}{\left\langle \sum_i \sum_j \exp \{ i \mathbf{q} \cdot [\mathbf{r}_j(0) - \mathbf{r}_i(0)] \} \right\rangle} \quad (2.13)$$

Under the assumption of statistically independent particles[44], equation (2.13) can be simplified as

$$g^{(1)}(t) = \left\langle \exp i \mathbf{q} \cdot \Delta \mathbf{R}_i(t) \right\rangle \quad (2.14)$$

where  $\Delta \mathbf{R}_i(t) = \mathbf{r}_i(t) - \mathbf{r}_i(0)$  is the displacement of the  $i^{\text{th}}$  particle in time  $t$ , and the average is over all particles in the scattering volume. The right hand side of equation (2.14) is often referred to as the intermediate scattering function. For Brownian motion, equation (2.14) reduces to

$$g^{(1)}(t) = \exp \left( - \frac{q^2 \langle R^2(t) \rangle}{6} \right) \quad (2.15)$$

with  $\langle R^2(t) \rangle$  being the mean square displacement in time period  $t$ . Equations (2.14) and (2.15) are obtained under the assumption of statistical independence of particles, which is strictly true only in infinitely dilute solutions. Without this rigorous assumption, the more general equation (2.13) can be expressed in terms of concentration fluctuations as

$$g^{(1)}(t) = \frac{\langle \delta c^*(\mathbf{q}, 0) \delta c(\mathbf{q}, t) \rangle}{\langle |\delta c(\mathbf{q}, 0)|^2 \rangle} \quad (2.16)$$

Where  $\delta c(\mathbf{q}, t)$  is the  $\mathbf{q}^{\text{th}}$  Fourier component of the concentration fluctuation. From the first and second Fickian laws, equation (2.16) leads to

$$g^{(1)}(t) = \exp(-q^2 D_c t) \quad (2.17)$$

where  $D_c$  is the collective or mutual diffusion coefficient.

### B. Forced Rayleigh Scattering Theory

Dynamic light scattering has revolutionized dynamical studies in fluids. In spite of its many successes, DLS has several drawbacks. First, the amplitude of the spontaneous, statistical fluctuations is small and this severely limits the sensitivity. Second, all the motions that contribute to intensity fluctuations can not be distinguished from one another. For example, in our system of polymer in silica gels, the oscillating silica particles give a contribution to the ACF, which can not be separated from the contribution of polymer movements. Third, DLS does not have sufficient frequency resolution to study slow relaxation processes with decay times much over one second.

Some of the difficulties of DLS can be overcome by forced Rayleigh scattering spectroscopy which was developed in the early 1970s by several groups working independently [46-48]. The essence of FRS is to replace the weak statistical thermal fluctuations of DLS by strong, coherent fluctuations induced externally. The thermodynamic properties of interest such as temperature, concentration, or molecular orientation, can be spatially modulated with a modulation depth large compared to the spontaneous thermal fluctuations but weak enough to stay close to equilibrium. Since this perturbation is spatially modulated, it can be easily

observed through the concomitant refractive index changes as an optical grating with well defined diffraction properties. The light of an incident reading laser will be diffracted into angles directly related to the wavevector  $q$  of the spatial modulation. In most FRS experiments, the external modulating source is turned off after a grating has been induced in the sample. Diffusive motions and relaxational processes gradually smear or erase the induced grating. In this eventuality, the diffracted intensity decays towards its initial value. The decay of this diffraction, which proves to be exponential for diffusive motion and relaxational processes, contains the useful information about the molecular dynamics. From the spatial dependence of the characteristic decay time, it is possible to differentiate between a purely intramolecular relaxation and a transport process.

FRS is also complementary to DLS. It can be used to study diffusion at much larger length scales, equivalent to much smaller scattering wavevector. Most DLS instruments are not suitable scattering angles smaller than 10 degrees. For FRS, it is possible to study polymer dynamics at crossing angles (between the two crossing beams) below 1 degree. This is mainly due to the much larger coherence factor in FRS, because the diffraction intensity does not contribute to the baseline, in contrary to the situation in DLS.

The principles, techniques, and applications of forced Rayleigh scattering were reviewed to limited extents by Pohl[49], and Rondelez[50] with emphasis on thermal transport processes, and by Urbach et al.[51] on the topic of mass diffusion measurements. Several groups have contributed to the theoretical understanding[52-56] and instrumentation[57-59] of the

forced Rayleigh scattering technique. As an excellent method for investigating polymer dynamics, FRS has been widely employed to study the diffusion behavior of liquid crystalline polymers[60-63], diffusion of small (dye) molecules in polymer matrices such as solids[64,65], gels[66], concentrated solution and melts[67,68], and diffusion of polymers in solutions[69-74], polymer networks[75,76], and solid-state polymers[77,78]. FRS combined with electrophoresis can measure mobilities and diffusivities at the same time[79,80]. Diffusion of proteins was also studied using FRS[81]. The results obtained from FRS experiments have been compared with other dynamic techniques that directly measure the diffusion coefficients. Comparisons were made against DLS[82], PFGNMR[83], and FRAP[84].

The remainder of this section discusses those aspects of forced Rayleigh scattering that are relevant to this dissertation.

The spatially-varying, amplitude controlled, external modulation can be achieved by various methods. We used a sinusoidal interference pattern generated by crossing two coherent laser beams at an angle  $\theta$ . The experimental setup is shown in Figure 2.2. The writing light beam is split into two beams of equal intensity, which are later converged onto the sample after traveling the same optical path length. A linear interference pattern is thus created which has the intensity profile

$$I(x,t) = I_0 + \delta I(t) \sin(qx) \quad (2.18)$$

where  $x$  is the coordinate on the axis perpendicular to the bisector of angle  $\theta$ ,  $I_0$  is the average intensity,  $\delta I(t)$  is the amplitude of the fluctuation in writing light intensity, and the scattering wavevector  $q$  is defined as,

$$q = \frac{4\pi}{\lambda_0} \sin \frac{\theta}{2} \quad (2.19)$$

where  $\lambda_0$  is the wavelength of the writing laser. Equation (2.19) is different from equation (2.2) in that  $q$ , or the fringe pattern is not affected by the index of refraction of the scattering medium. Figure 2.3 schematically shows an expanded view of the area where the two writing beams cross. The interference pattern is contained within the intersection of the beams, thus having finite extent. The optical grating pattern is an array of successive bright and dark fringes. A real image of this interference pattern can be projected to a distant screen using a telescope to measure the fringe spacing which is

$$d = \frac{2\pi}{q} = \frac{\lambda_0}{2 \sin \frac{\theta}{2}} \quad (2.20)$$

The external modulation interacts with the sample through various means. In our work, the polymer sample is photochromic, and thus a fringe pattern of photoexcited states is induced by the optical grating. The concentration of the excited species is

$$C(x, t) = C_0 + \delta C(t) \sin(qx) \quad (2.21)$$

where  $C_0$  is the average concentration,  $\delta C(t)$  is the amplitude of the concentration fluctuation at time  $t$ . The concentration change of the excited species in the sample due to diffusion can be described by Fick's law:

$$\frac{\partial C}{\partial t} = -D \nabla^2 C \quad (2.22)$$

The solution of equations (2.21) and (2.22) gives

$$\delta C(t) = \delta C(0) \exp(-Dq^2 t) \quad (2.23)$$

If the excited states have a finite half life time  $\tau_{\text{life}}$ , as opposed to permanent excitation, equation (2.23) is modified as

$$\delta C(t) = \delta C(0) \exp(-t/\tau_{\text{life}}) \exp(-Dq^2 t) \quad (2.24)$$

The change in the spatially periodic concentration grating results in a same change in the grating of refractive index. The decay of this grating is detected by a reading laser beam which is diffracted by the grating. The intensity of this reading beam has to be weak not to perturb the sample under examination, and the incidence of this beam satisfies the Bragg's condition, which in our experiments requires the angle  $\theta_R$  between the reading beam and the fringe axis to satisfy

$$\frac{\lambda_R}{\sin \theta_R} = \frac{\lambda_0}{2 \sin \frac{\theta}{2}} \quad (2.25)$$

where  $\lambda_R$  is the wave length of the reading beam. The diffraction field ( $E_{\text{diff}}(t)$ ) follows the decay of the concentration grating, such that



$$E_{\text{diff}}(t) \propto \exp\left(-\frac{t}{\tau_{\text{life}}}\right) \exp(-Dq^2t) \quad (2.26)$$

Finally, the transient intensity of the diffracted light is a sum of the coherent scattering intensity and the incoherent scattering intensity, which can be expressed in the following formula

$$I(t) = [A \exp(-t/\tau) + B]^2 + C \quad (2.27)$$

where the decay rate is

$$\frac{1}{\tau} = Dq^2 + \frac{1}{\tau_{\text{life}}} \quad (2.28)$$

and A is the preexponential amplitude of the diffracted optical field, B is the coherent scattering background optical field, and C is the background intensity due to incoherent scattering and stray light. In our experiments, the measured transient intensity of diffraction  $I(t)$  is fitted to equation (2.27) and the decay rate is thus extracted. Through the spatial dependence of decay rate  $\tau$ , the diffusion coefficient is obtained from the slope of  $1/\tau$  versus  $q^2$  (equation 2.28).

The diffusion coefficients measured by FRS were compared with those measured by DLS for the same polymers. It was found that the difference between the data from these techniques is within 5% for polymers with  $MW > 20,000$ . It is noted that for labeling ratio of about 1:1000 the diffusion coefficients of polystyrene and that of dye-labeled polystyrene both measured by DLS are almost the same with difference less than 3%.

## C. Polymer Samples

### 1. Polystyrene

Many polystyrene fractions have been used in this study, spanning almost three decades of molecular weights ( $2.5 \times 10^3$  to  $2.05 \times 10^6$ ). Linear anionic polystyrenes, each with narrow molecular weight distribution ( $M_w/M_n < 1.06$ ), were used as received, without fractionation. Table 2.1 lists the characteristics and sources of the polystyrene samples used in this dissertation project. The peak molecular weight,  $M_p$ , obtained from size exclusion chromatography (by the suppliers), is used to describe the polystyrene molecular weight noted herein as  $M$ . The mutual diffusion coefficient,  $D_0$ , in unbounded 2-fluorotoluene solution is measured by DLS at concentrations  $C \approx C^*/8$  where  $C^*$  is the overlap concentration[29]. At  $C^*/8$ ,  $D_0$  is greater than that at the limit  $C = 0$  by about 5%. In this dissertation  $D_0$  is referred to as the free solution diffusivity. For polystyrene with  $M > 3 \times 10^4$  a power law was obtained:

$$D_0(37.8^\circ\text{C}, 0.55 \text{ cp}) = 4.63 \times 10^{-4} \times M^{-0.587} \text{ (cm}^2/\text{s)} \quad (2.29)$$

The value of the scaling exponent ( $0.587 \pm 0.005$ ) indicates that 2-fluorotoluene is a thermodynamically good solvent, chosen to minimize interchain entanglement and to enable comparison of our results with most existing theories. The hydrodynamic radius was calculated from the Stokes-Einstein equation:

$$R_H = k_B T / 6\pi\eta D_0 \quad (2.30)$$

where  $k_B$  is the Boltzmann constant,  $\eta$  is the the solvent viscosity used here instead of the dilute solution viscosity. Polystyrene was dissolved in 2-fluorotoluene (Aldrich, 99+% pure). The solvent was filtered through a 0.2  $\mu\text{m}$  pore diameter teflon membrane (Millipore) before use. The concentration of each solution was normalized to  $C^*/8$ , where  $C^*$  was estimated from  $M_p$  as

$$C^* = [\eta]^{-1}. \quad (2.31)$$

where the intrinsic viscosity  $[\eta]$  of the polymer can be calculated from

$$[\eta] = 1.35 \times 10^{-4} M^{0.716} \quad (2.32)$$

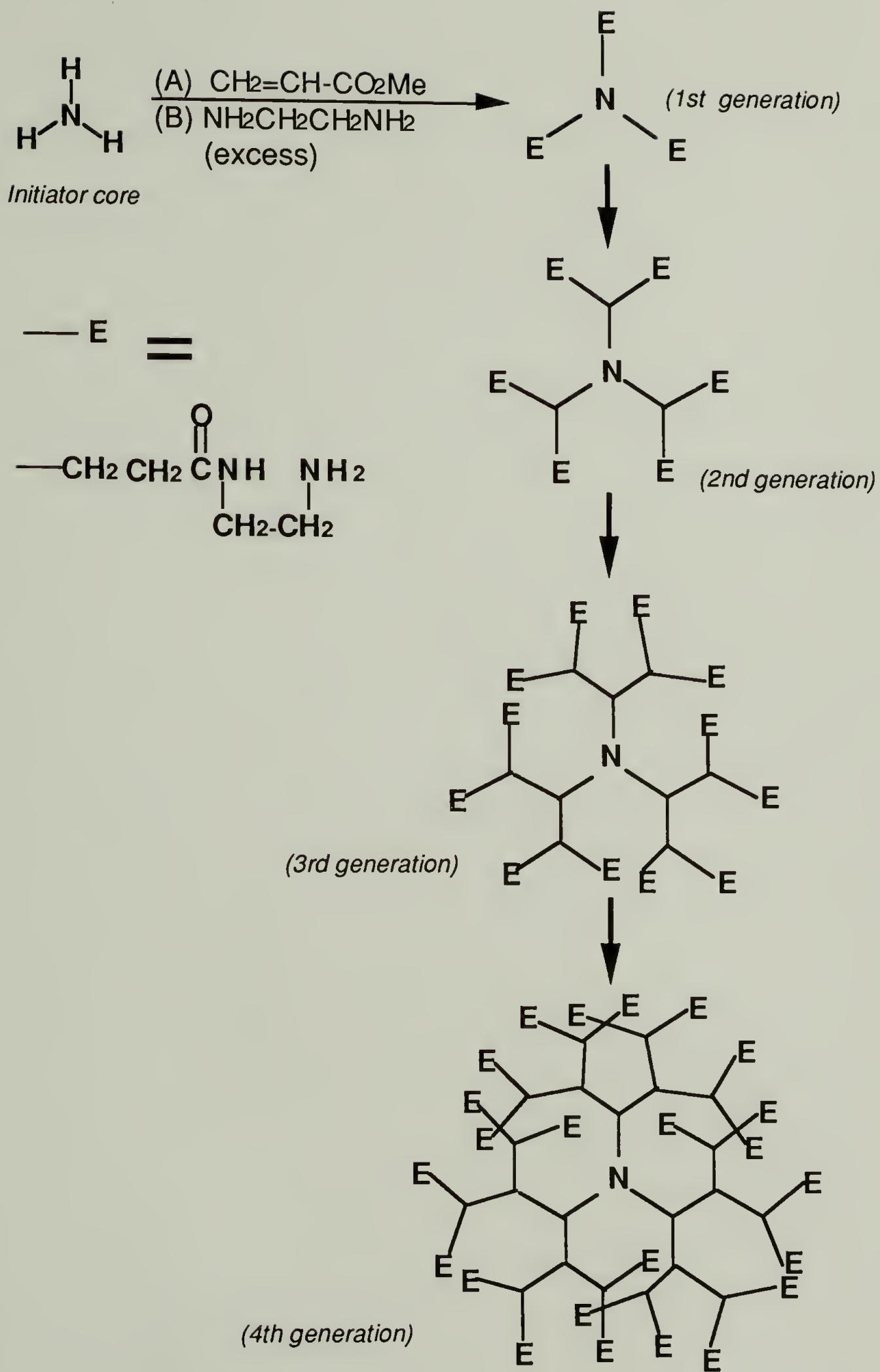
Equation (2.32) was obtained by Bishop[20] from the characterization results (supplied by the manufacturers) for polystyrene chains in toluene.

The results and discussions of the diffusion measurements of polystyrene chains in porous glasses are presented in Chapter III and IV.

## 2. Starburst-Dendritic Polyamidoamines

The dendritic polyamidoamines were a precious gift from Dr. David M. Hestrand at DOW Chemical Co. The fundamental building blocks for this class of polymer are referred to as dendrimers[86] which have extraordinary symmetry, high branching and maximized (telechelic) terminal functionality density. Scheme I shows the diagram of making

**Scheme I** Diagram of synthesizing starburst-dendritic polyamidoamine.  
“--E” stands for the terminal group, which is formally derived from N-(2-aminoethyl) acrylamide.



starburst polymers. The initiator core is ammonia. The repeating unit is formally derived from N-(2-aminoethyl) acrylamide. The dendritic polymers were formed by chemically bridging the repeating units in a starburst topology[86]. The chemical reactions involved in the polymerization are (A) Michael reaction and (B) Amidation. Due to the high functionality of the dendrimers, the number of terminal groups increases very rapidly with generation number. Therefore, several layers of repeating units will result in a molecule of high structural compactness.

The dendritic polyamidoamine samples received from DOW Chemical Co. were the 5<sup>th</sup>, 7<sup>th</sup>, and 10<sup>th</sup> generations. The generation number here means the number of layers of repeating units outside the initiator core. These samples had the surface amines modified by reaction with epoxyoctane, so that they are soluble in organic solvents. The hydrophobic surface (after modification) outside the hydrophilic inner body has an effect of reducing permeation of organic solvent molecules.

The molecular weight of the ideal starburst-dendritic polymers can be calculated for each generation[86]. The relation between molecular weight and size is always of great interest because it gives information about the shape and compactness of the polymers. In our study, the exact molecular weights were unknown, and could not be calculated since the number of the attached epoxyoctane groups is unknown as there were a number of terminal amines ending inside the "ball" instead of being at the surface. To have a rough sense of the relation of molecular weight to overall size, the theoretical molecular weights for the unmodified starburst polyamidoamines were used, which are 10619, 43415, and 349883 for the 5<sup>th</sup>, 7<sup>th</sup>, and 10<sup>th</sup>

generation polymers. The values were plotted versus the hydrodynamic radii measured in free solution by DLS using equation (2.30). It was found that

$$M \propto R_H^{4.1 \pm 0.4} \quad (2.33)$$

The exponent ( $4.1 \pm 0.4$ ) is somewhat surprising in a sense that it is even higher than that of a rigid body ( $M \propto R^3$ ). This can be explained in that a low generation starburst polymer has some empty inner spaces, and as the polymer grows, the terminal units can fold back and fill the initially available spaces, resulting in an exponent (in equation 2.33) even higher than 3.

In our experiments, all the starburst polyamidoamines were dissolved in transdecahydronaphthalene (Aldrich). Some properties of this solvent were listed in Appendix A. The results and discussion of the diffusion behavior of polyamidoamines are presented in Chapter IV.

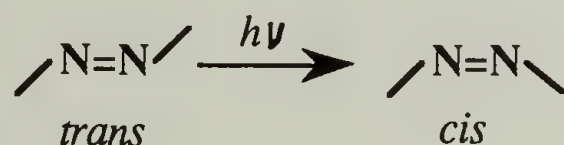
### **3. Dye-Labeled Polystyrene**

In the forced Rayleigh scattering experiments, the polymer chains are “tagged” with chromophores that can be excited by the writing impulse. The grating of the concentration of excited species effects a grating of refractive index which is probed by the reading beam in a diffusion measurement.

Dye-labeled polystyrene chain was used in our study, because of the commercial availability, monodispersity and popularity of polystyrene. Roughly speaking, there are three approaches to make labeled polystyrenes: (1) randomly label previously synthesized polystyrene; (2) stop the

propagating chain with a functional group in the living anionic polymerization, and later react the terminal function with dye molecules to produce end-labeled (either single end or double end) polystyrenes; and (3) copolymerize styrene and derivatized styrene monomers, and later substitute the incorporated functional groups in the derivatized styrene monomers by dye molecules. The first approach was chosen in our study, because it does not involve the difficult polymerization procedures and because most of the characterization data of unlabeled polystyrene can still be used since the labeling ratio is very low, typically 1 dye per about 1000 monomers.

4-Dimethylaminoazobenzene-4'-isothiocyanate (DABITC, from Pierce) was attached to polystyrene chains to obtain photochromically active polymers. The use of this dye was proved successful by Yu et al. [73] in that it gives a long life time and a good contrast in refractive index between excited and ground states. The double bond of the azo function is responsible for the photoisomerization. When irradiated in solution, azobenzene which is in *trans* conformation at ground state, is excited to form *cis* isomer:[87]



The principal absorption band ( $\pi-\pi^*$ ) for azobenzene is in the ultraviolet region. Substitutions of positions *ortho* or *para* to the azo function with strongly electron-donating groups such as amino or dimethylamino shifts the main absorption band into the visible spectrum. The 4-Dimethylamino-

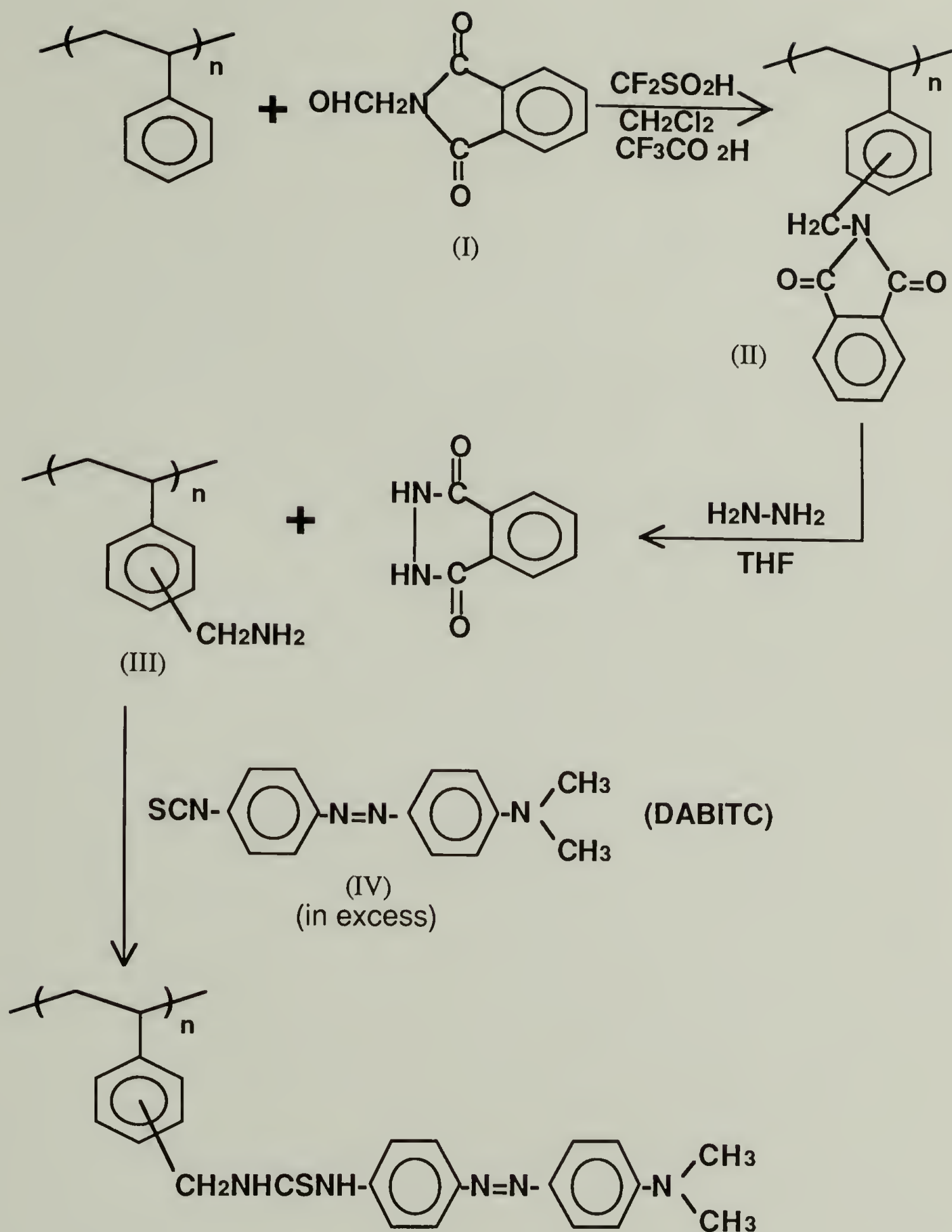


azobenzene-4'-isothiocyanate molecule absorbs at around 420 to 430 nm. The substitution of the isothiocyanate group by phenol groups in the labeling process further shifts the absorption band toward the longer wavelength by 10 to 20 nm.

The thermal *cis*  $\rightarrow$  *trans* reaction determines the lifetime of the excited states. This decay process is much faster for substituted azobenzenes than for simpler azobenzenes[88]. The reported half-life time for 4-Dimethylaminoazobenzene is about 220 min at 25°C in toluene[89] which is a factor of 25 times as fast as azobenzene. The energy of activation is 21kcal/mol. This half-life time, though not long enough for the diffusion measurements in solid state polymers, is long compared to the diffusion process of interest to this study.

The labeling procedure involves two steps: (1) random aminomethylation of phenyl rings in polystyrene; and (2) the subsequent reaction of aminomethyl groups with an azobenzene dye. Detailed procedures are shown in Scheme II, and discussed as follows.

Linear polystyrene with narrow molecular weight distribution was dissolved in CH<sub>2</sub>Cl<sub>2</sub>. Trifluoroacetic acid as a catalyst was dissolved in the polymer solution. Hydroxymethylphthalimide (I) and trifluoromethanesulfonic acid were then added to the solution, and the solution was stirred for 8 hours at room temperature. At the end of the reaction, the intermediate polymer (II) is precipitated in methanol and washed by dissolving in tetrahydrofuran (THF) and reprecipitating in methanol. The polymer was converted to the amine form by refluxing with



Scheme II Synthesis of dye-labeled polystyrene.

hydrazine in THF overnight. After the reflux, the aminomethylated polystyrene (III) was purified by precipitating it into methanol.

The aminomethylated polystyrene (III) was dissolved in THF containing an excess of 4-Dimethylaminoazobenzene-4'-isothiocyanate (IV). The solution was stirred at room temperature for 2 days. The resultant polymer was precipitated into methanol, and was then extracted in a soxhlet extractor. The final DABITC-labeled polystyrene had one attached dye per approximately one thousand monomer units. It was dissolved in fluorobenzene (Aldrich) which is a good solvent for polystyrene and which has a index of refraction closely matching that of the fumed silica thus allowing direct measurement of polymer diffusion inside a porous medium by FRS. Chapter V presents the results of diffusion of dye-labeled polystyrene chains in the porous media of fumed silica.

#### D. Porous Materials and Surface Treatment

##### **1. Porous Glasses**

Porous silica glasses are widely used as model restricted geometries to study the dynamic and thermodynamic properties of confined molecular systems. These glasses are highly pure, optically transparent, mechanically stable and chemically inert (after surface treatment), and therefore they are ideally suited for probe measurements using light scattering.

All the porous glasses used in this dissertation were made by a phase separation and leaching process[90-92]. There are three controlled-pore glass (CPG) samples and a Vycor porous glass sample; the three CPGs

were named G75, G275 and R893. Glass R893 has also been used by Bishop. In manufacturing these porous glasses, sodium borosilicate ( $\text{Na}_2\text{O}-\text{B}_2\text{O}_3-\text{SiO}_2$ ) glass was heated to above the melting point, at which temperature all three components are miscible. The mixture is then heat treated below the liquidus temperature to induce separation into two bicontinuous phases. The nascent structure produced upon phase separation of these ternary glasses depends on both thermodynamic (e.g., temperature, composition) and kinetic (e.g., time, temperature) factors. It is by varying these factors that glasses with different properties, for example, pore size and porosity, can be made. The  $\text{Na}_2\text{O}-\text{B}_2\text{O}_3$  rich phase is etched out by hydrochloric acid (HCl). Colloidal silica, which comes from  $\text{SiO}_2$  initially present in the  $\text{Na}_2\text{O}-\text{B}_2\text{O}_3$  rich phase and which is deposited in the pores during the acid leaching treatment, can be removed by controlled etching with NaOH. The microstructure of the pore space that is ultimately produced depends not only on the phase separation process but also on the etching processes. All CPGs undergo a second etching process to remove the silica deposits, whereas Vycor does not.

Relevant data from the suppliers are shown in Table 2.2. The nominal pore radius was measured by mercury porosimetry,[93] and the surface area by BET nitrogen absorption[94]. The porous glasses were amorphous. The local pore structure over small dimensions was believed to be approximately cylindrical in shape, branched and highly connected. This view is supported by the electron micrographs in the Ph.D. thesis of Matthew T. Bishop[20].

## 2. Fumed Silica

Fumed silica, also called pyrogenic silica, is produced from hydrolysis of silicon chloride ( $\text{SiCl}_4$ ) in presence of a hydrogen-oxygen flame[95]. These silica powders have extremely high surface areas, and are used as binders, thixotropic agents, thickeners, anticaking agents, etc. The growth and structure of fumed silica was studied by Schaefer et al.[96] using small-angle X-ray scattering (SAXS) and neutron scattering (SANS) techniques. These authors found the fumed silica powders to be fractal and proposed a model based on ballistic polymerization, sintering, and diffusion-limited aggregation to explain the observation.

The fumed silica used in this study was Aerosil R972 (Degussa). It has basic units of 10 to 20 nm in diameter and a surface silanol group density of 0.25 to 0.33  $\text{nm}^2/\text{SiOH}$ [95]. The precursor silica (the product of the hydrolysis) had been treated (by the manufacturer) with  $(\text{CH}_3)_2\text{SiCl}_2$  to yield the hydrophobic product R972, which has about 20% of the initially available silanol groups. Aggregation happened during the hydrolysis of  $\text{SiCl}_4$  and during the surface treatment (because of the bifunctionality of  $(\text{CH}_3)_2\text{SiCl}_2$ ), and resulted in ramified (or fractal) clusters of several hundred Ångstroms in dimension.

## 3. Effect of Adsorption and Surface Treatment

Surface silanol groups are known to adsorb many substances. Adsorbed molecules diffuse much more slowly than the unadsorbed ones inside a porous medium. This “sticking” effect can be dominant in some cases where drastic decrease in diffusion rate was found, and gives rise to

discrepancy in reported diffusion study regarding the mechanisms of diffusion hindrance caused by the porous medium. See section D of chapter IV for more discussion.

Bishop has examined adsorption of polystyrene molecules by the pore walls of controlled pore glasses using light scattering technique, and found the diffusion was further hindered due to the presence of adsorption[20]. We examined the adsorption of labeled polystyrene on the surface of fumed silica using UV-Visible spectrometry. Silica R972 was mixed in the solution of labeled polystyrene, and the mixture is stored at room temperature overnight. It was then washed with the solvent (fluorobenzene). The washing was done by shaking the mixture, centrifugation, and removing the supernatant solution. This process was repeated until the supernatant solution gave no detectable absorption at the wavelength of approximately 440nm at which the attached azobenzene segment absorbs light. The suspension of silica was examined by an IBM Model 9420 UV-Visible spectrophotometer. A noticeable absorption peak at 440nm wavelength was observed indicating the presence of labeled polymer on the surface of R972, since at that time there was no dye molecules in the solution.

Diffusion in a porous medium of R972 was measured. It was found that the diffusion was drastically slowed even at a very low silica concentration (see Chapter V). In order to study the hindrance mechanisms other than adsorption, we performed chemical surface treatment on all the porous materials studied, to minimize adsorption of the polymer. The proctocols of treatment for these two types of silicas are slightly different,

due to the difference in their physical forms, but the principle is the same: to replace the active surface silanol groups by alkyl groups[97,98]. In our work, this is realized by capping the surface hydroxyl groups with trimethylsilane ( $-\text{Si}(\text{CH}_3)_3$ ) groups. Detailed procedures for silanizing the porous glass and fumed silica are as follows.

The glass surfaces were silanized by reaction of surface activated and thoroughly dried porous glasses with a large excess of chlorotrimethylsilane in toluene solution. The surface treatment of the porous glasses consisted several steps as follows.

The porous glass beads were heated overnight at  $90^\circ\text{C}$  in concentrated  $\text{HNO}_3$  and rinsed thoroughly with deionized water until neutral, to remove organic impurities. Beads were then soaked overnight at room temperature in concentrated  $\text{HCl}$  and rinsed until neutral to remove metal ions. The cleaned glass was dried at  $90^\circ\text{C}$  for 24 hours.

A Schlenk tube was used for the silanization reaction. The porous glass beads were dried for 4 hours at  $210^\circ\text{C}$  under vacuum, and then allowed to cool to room temperature under vacuum. The silanization solution was added to the Schlenk tube while sparging through the sidearm with prepurified nitrogen. The Schlenk tube was then capped under nitrogen flow and sealed for the duration of the reaction. Two kinds of silanization solution were used: 2M trichloromethylsilane (Aldrich) in toluene with a reaction time of 3 days at  $95^\circ\text{C}$ ; and 2M hexamethyl disilazane with a reaction time of 7 days at  $100^\circ\text{C}$ . Either of these two reagents worked satisfactorily. The reaction was stopped by addition of dry distilled methanol, which was also used to wash the glass beads until the

filtrate was neutral. Samples were then dried at 50°C overnight, and finally dried for 1 hour at 170°C under vacuum prior to use. The final heat treatment serves to further convert the silanized layer.

The fumed silica, Aerosil R972, was partially treated by the manufacturer to attain hydrophobicity which is desirable for some applications. We found the residual silanol density is still high enough to trap the labeled polystyrene (see Chapter V). We therefore performed further surface treatment on silica R972 to quench thoroughly the surface hydroxyls.

The silica was vacuum dried and later heated to 210°C for 4 hours to activate the surface, and then allowed to cool to room temperature in vacuum. Dry distilled toluene was added, and the mixture was degassed in an ultrasonic bath. The silanizing reagent hexamethyl disilazane was added under sparging nitrogen to make a concentration of 1M. The reaction time was 7 days at 100°C. At the end, the reaction was stopped by adding dry distilled methanol, and the methanol was later washed out by fluorobenzene. The washing process was the same as mentioned above, i.e., using centrifugation to separate out the washing liquid. The silica thus treated, referred to as R972-M later in the paper, was found to have negligible adsorption of labeled polystyrene, as detected by UV-Visible spectrometry.

The treated fumed silica was not dried, as drying can induce partial consolidation, resulting in a foamy and fragile material which is macroscopically nonuniform and which can not be dispersed in solution to make a uniform suspension or a gel. All the silica particles after treatment



were stocked in the mixture with fluorobenzene, which was later mixed with the labeled polymer of interest to form a silica gel of a silica suspension. The highest attainable silica concentration is limited by the highest silica concentration of the precipitated layer formed in the centrifugation.

### E. Apparatus and Experimental Procedures

#### **1. DLS Experiments and Data Analysis**

A silanized glass bead (1-2mm diameter in size) was mounted inside a dust-free sample cell (10 × 75 mm test tube) and the polystyrene solution was added to the cell containing the glass bead through a teflon membrane filter (Millipore). Sufficient time was allowed for the diffusion coefficient to become stable, typically several days. This time period is for the system to approach macroscopic equilibrium. We note that measured diffusion coefficients have remained stable for over one year. The glass and the solution had very similar refractive indices to minimize multiple scattering, as such, the diffusion of polymer within the porous glass fragment can be directly probed.

Dynamic light scattering measurements were made using a 50 mW Spectra-Physics model 125 He-Ne laser as the light source. The cell holder assembly (designed by Bishop[20]) was constructed with seven windows at scattering angles: 15°, 25°, 35°, 65°, 90°, 115°, and 155°, with axes tilted 5° from the horizontal to diminish stray light. The intensity of the scattered

light was detected by a photomultiplier tube which is connected to a pulse amplitude discriminator.

The photon-count autocorrelation function was measured with either of the two digital correlators: (a) Langley-Ford model 1096 digital correlator (Coulter Electronics) which had 256 contiguous and linear channels plus 16 channels delayed by  $1024 \times$  sample time for measuring the ACF baseline; and (b) the correlator from a N4-SD Particle Analyzer (Coulter Electronics) which had 80 nonlinearly spaced channels. In the second correlator the points at which the correlation function was measured were spaced approximately logarithmically in time. The time represented by each channel doubles for each successive group of 8 channels. Thus, the 80 channel correlator spans a total range of delay equal to the minimum sample time (used in the first channels) multiplied by a factor of 3072. It should be noted that in this instrument the sixteen initial channels are dedicated to the minimum sample time and the final 16 to the maximum sample time. This feature was important as it made possible the measurement of an appropriate last channel baseline for measuring the macroscopic diffusion coefficient while simultaneously monitoring the diffusion process at short time scales with sufficient resolution.

The diffusion coefficients of the polystyrene fractions in unbounded solution ( $D_0$ ) were normally obtained using a homodyne arrangement. The extraction of  $D_0$  from measured autocorrelation function was based on equations (2.8) and (2.17). In the homodyne arrangement, the calculation of diffusion coefficient should follow

$$D = \frac{\langle \Gamma \rangle}{2q^2} \quad (2.34)$$

where  $\langle \Gamma \rangle$  is the decay rate of the intensity ACF in the form of  $\exp(-\Gamma t)$ .

Diffusion within a porous glass bead was monitored using the heterodyne method. The light scattered by the macromolecules was mixed with light statically scattered by the glass matrix which served as a strong local oscillator with an intensity about 50 times that of polymer scattering. The data analysis for the heterodyne method is based on equations (2.11) and (2.17).

A least squares fit of  $\log G^{(2)}(t)$  to a second order cumulant expansion[99] was applied where

$$\log \frac{G^{(2)}(t_i) - B}{G^{(2)}(t_0) - B} = a + bt_i + ct_i^2 \quad (2.35)$$

with  $t_0$  the delay time of the first data channel used in the fit,  $t_i$  the delay time for each channel. The coherence factor  $f_c$ , the average intensity ACF decay rate  $\langle \Gamma \rangle$ , and the variance of the decay rate distribution  $\mu_2$  were derived from the fitting parameters  $a$ ,  $b$  and  $c$  respectively. Information about the polydispersity of the diffusion rate can be obtained from the normalized variance:

$$V \equiv \frac{\mu_2}{\langle \Gamma \rangle^2} \quad (2.36)$$

For the heterodyne arrangement the measured photon-count ACF  $G^{(2)}(t)$  is related to the normalized scattered electric field ACF  $g^{(1)}(\mathbf{q}, t)$  by equation (2.11). For translational diffusion of non-interacting particles over distances large compared to the pore size,  $\langle \Gamma \rangle$  is proportional to  $q^2$ .

The slope of  $\langle \Gamma \rangle$  versus  $q^2$  defined the macroscopic diffusion coefficient  $D$  of polymer in pores, i.e.,

$$D = \frac{\langle \Gamma \rangle}{q^2} \quad (2.37)$$

A correct determination of the ACF baseline was essential to the data extraction, especially for heterodyne measurements for which the entire decaying signal amplitude was about 2% of the baseline height, i.e.  $G^{(2)}(t=0) \approx 1.02B$ . Therefore, even an error of 0.2% in the baseline would have been unacceptable. As a criterion, a given ACF was judged to be unacceptable when there is no good agreement between the flat region of the decaying curve and the delayed last channels on the Model 1096 correlator, or when there is not a flat last channels region on the N4 correlator. The last channels baseline  $B = G^{(2)}(t \rightarrow \infty)$  was used satisfactorily for low and medium  $\lambda_H$  measurements. For high  $\lambda_H$  measurements, for which a sample time of the order of  $100\mu s$  had to be used, an acceptable baseline was more difficult to acquire probably because of factors such as laser intensity variation, relative movements of beam and sample, etc. This problem was addressed by performing the second cumulants fit with an adjustable baseline to minimize the sum of the squared residuals. If the difference in the measured diffusion coefficient using the last channel baseline and the adjustable baseline was greater than 10%, that run was rejected.

A regularized inverse Laplace transform of  $\log G^{(2)}(t)$  was also performed using Provencher's CONTIN program[100] to calculate the ACF decay rate distribution and thus the diffusion rate distribution. The

diffusion coefficients obtained from CONTIN were usually within 5% of those from the second cumulants fit.

## 2. FRS Experiments and Data Analysis

Chapter V will report the diffusion study on dye-labeled polystyrene chains in the porous media of fumed silica using the forced Rayleigh scattering spectrometer. The sample preparation and FRS measurement procedures are presented here.

A silica suspension was made by mixing a labeled polystyrene solution with surface-treated fumed silica on a Vortex-Genie Test Tube Mixer (Fisher). If the silica concentration is above the critical gelation concentration, the silica suspension will gradually transform into a gel without external perturbation. This gelation process took several hours to several days depending on the silica concentration. Our criterion on the formation of a "gel" is not a rigorous one, since it is not necessary in this work. We simply tilt the sample cell containing the mixture of silica and polymer solution to an angle of about 60 degrees. If we observe no appreciable flow over a time period of one minute, we say it has gelled. For the silica with different surface chemistry, i.e. R972 with hydroxyl groups and R972-M without, the silica concentration necessary to induce gelation is quite different. The critical silica volume fraction is approximately 2.5% for R972 and 6% for R972-M, indicating that the surface hydroxyl groups play a very important role in silica gelation, probably through hydrogen bonding. When the silica fraction is below the critical concentration, a visually uniform suspension is formed after

mixing, but the silica particles in this kind of dilute suspension will precipitate and form two distinguishable layers several weeks later. Both the silica suspension and the silica gel are generally referred to as porous medium of fumed silica in this dissertation.

The FRS setup is shown in Figure 2.2. The “writing beam” from a 5W Ar<sup>+</sup> laser (Spectra Physics, Model 2020) was split into two beams of equal intensity by a beam splitter, which were later converged on the sample by a 6-inch wide off-axis parabolic mirror; the focal length of this mirror is 40.125 inches. A linear fringe pattern of alternate bright and dark lines was created from interference of the two crossing coherent writing beams, in a way as shown in Figure 2.3. This optical grating induced a periodic concentration distribution of photochemically excited azobenzene groups attached to the polystyrene chains. The fringe spacing  $d$  can be calculated using equation (2.20). The wavelength of the writing laser is  $\lambda_0 = 455\text{nm}$ , which is the excitation line closest to the position of maximum absorption of the attached dye molecules. The output power of the writing beam was 0.003 to 0.06 W. The use of higher power will saturate the attached chromophores and will result in a fringe pattern with lower contrast in index of refraction. A higher writing power can also induce unexpected photochemical reactions such as dimerization that complicate the transient scattering intensity. In our experiments, the fringe spacing  $d$  could be varied from 4 to 25  $\mu\text{m}$  by adjusting the distance between the two parallel beams impinging on the parabolic mirror. A mechanical shutter in front of the Ar<sup>+</sup> laser controlled the width of the writing pulse that is typically 1 ms. The reading beam was from a 1.5mW He-Ne laser (Spectra Physics

Model 102-3,  $\lambda_R = 632.8$  nm), whose power was attenuated to below 0.1 mW to reduce possible perturbation on the modulated sample. The use of higher reading beam power can shorten the life time of the excited states, by hastening the thermal *cis* to *trans* transition. The reading beam was projected to the induced fringe of photoexcited molecules at an angle satisfying Bragg's condition (equation 2.25). The position of the reading beam has to be adjusted each time the fringe spacing changes, i.e., each time the distance between the two writing beams changes. The diffraction intensity was detected with a photomultiplier tube, whose output (after being integrated by  $1\text{M}\Omega$  resistance and the approximately 150 pF capacitance of the cable) was acquired by a digital storage oscilloscope (Nicolet 310). The data were then transferred to a Zenith Z-386 Data Station via an RS232 cable.

The whole measurement process of forced Rayleigh scattering was automated and controlled by the computer and a Four Channel Digital Delay/Pulse Generator (Model DG535, Stanford Research Systems). The flow diagram of the FRS measurement is shown in Figure 2.4. Two UniBlitz Model 100-2B shutters (Vincent Associates, New Jersey) were used to control the width of the writing pulse and the detection of the diffracted reading beam. These shutters are opened by a 5V DC voltage and closed when the voltage is below the threshold. Appendix B describes more technical details for the FRS apparatus.

The transient voltage that is proportional to the transient intensity of the diffracted light was measured by the digital oscilloscope. The characteristic decay time  $\tau$  of the transient diffraction intensity  $I(t)$  was

obtained by fitting  $I(t)$  to equation (2.24) by a nonlinear least square fit. We used the algorithm developed by Marquardt, [101, 102] which combined the best features of gradient search and the method of linearizing the fitting function [101].

For single mode diffusion processes, the characteristic decay time  $\tau$  versus the squared scattering wavevector ( $q^2$ ) of the spatial modulation should follow equation (2.28), from which the diffusion coefficient can be obtained. From the curve fitting, it was found that in our system  $\tau_{\text{life}}$  of the excited dye molecules was very long (typically larger than 100s) compared to the diffusion process, i.e.,  $1/\tau_{\text{life}}$  is negligible.



**Table 2.1**  
Characteristics of polystyrene samples

Code	Source <sup>a</sup>	$M_p \times 10^{-3}$ <sup>b</sup>	$D_0 \times 10^7$ (cm <sup>2</sup> /s) <sup>c</sup>	$R_H$ (Å) <sup>d</sup>
P 2	SPP	2.5	32.2	12.9
P 4	SPP	4	26.3	15.8
P 13	PC	13	15.0	27.7
P 17	PC	17	13.4	30.9
P 24	PC	24	11.5	36.0
P 35	PC	35	10.3	40.2
P 47	PC	47	8.15	50.8
P 50	PC	50	7.88	52.6
P 68	PL	68	6.74	61.4
P 89	PC	89	5.73	72.3
P100	PC	100	5.43	76.3
P127	PL	127	4.61	89.8
P170	PC	170	3.93	105
P198	PC	198	3.58	116
P350	PC	350	2.50	166
P575	PC	575	2.02	205
P949	PC	949	1.55	267
P1030	PL	1030	1.48	280
P1400	PL	1400	1.26	329
P2050	PL	2050	1.07	387

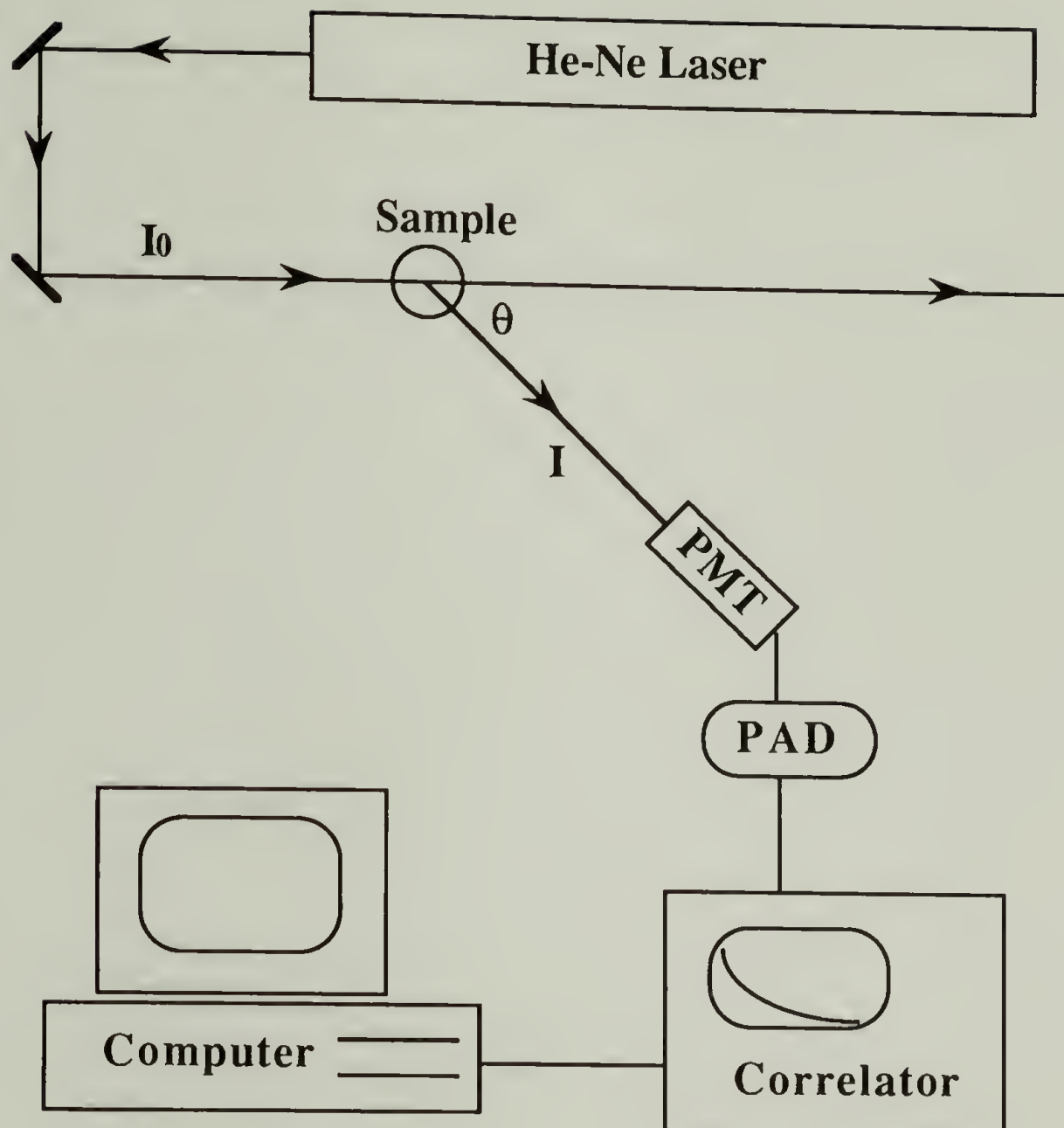
- a. PC: Pressure Chemical Co.; PL: Polymer Laboratories; SPP: Scientific Polymer Products
- b.  $M_p$ : peak molecular weight by size exclusion chromatography.
- c.  $D_0$ : diffusion coefficient measured in free solution at concentration  $C^*/8$  at 37.8°C.
- d.  $R_H$ : hydrodynamic radius calculated from  $D_0$  using eq. (2.29).

Table 2.2

Characteristics of the porous glass samples<sup>a</sup>

	G75	G275	R893	Vycor
$R_p$ , Pore Radius <sup>b</sup> (Å)	75	275	893	20
$v$ , Pore Volume <sup>c</sup> (cm <sup>3</sup> /g)	1.0	1.3	1.2	0.18
$\phi$ , Porosity (%)	0.69	0.74	0.72	0.28
$s$ , Surface Area <sup>d</sup> (m <sup>2</sup> /g)	276	105	18	200

- a. All data supplied by the manufacturer: Shell Development Co. for G75 and G275, and Electro-Nucleonics for R893.
- b. Nominal radius from mercury porosimetry
- c. Measured by mercury porosimetry
- d. Measured by BET nitrogen adsorption



**Figure 2.1** Dynamic light scattering spectrometer. PMT stands for the photomultiplier tube, and PAD stands for the pulse amplitude discriminator.

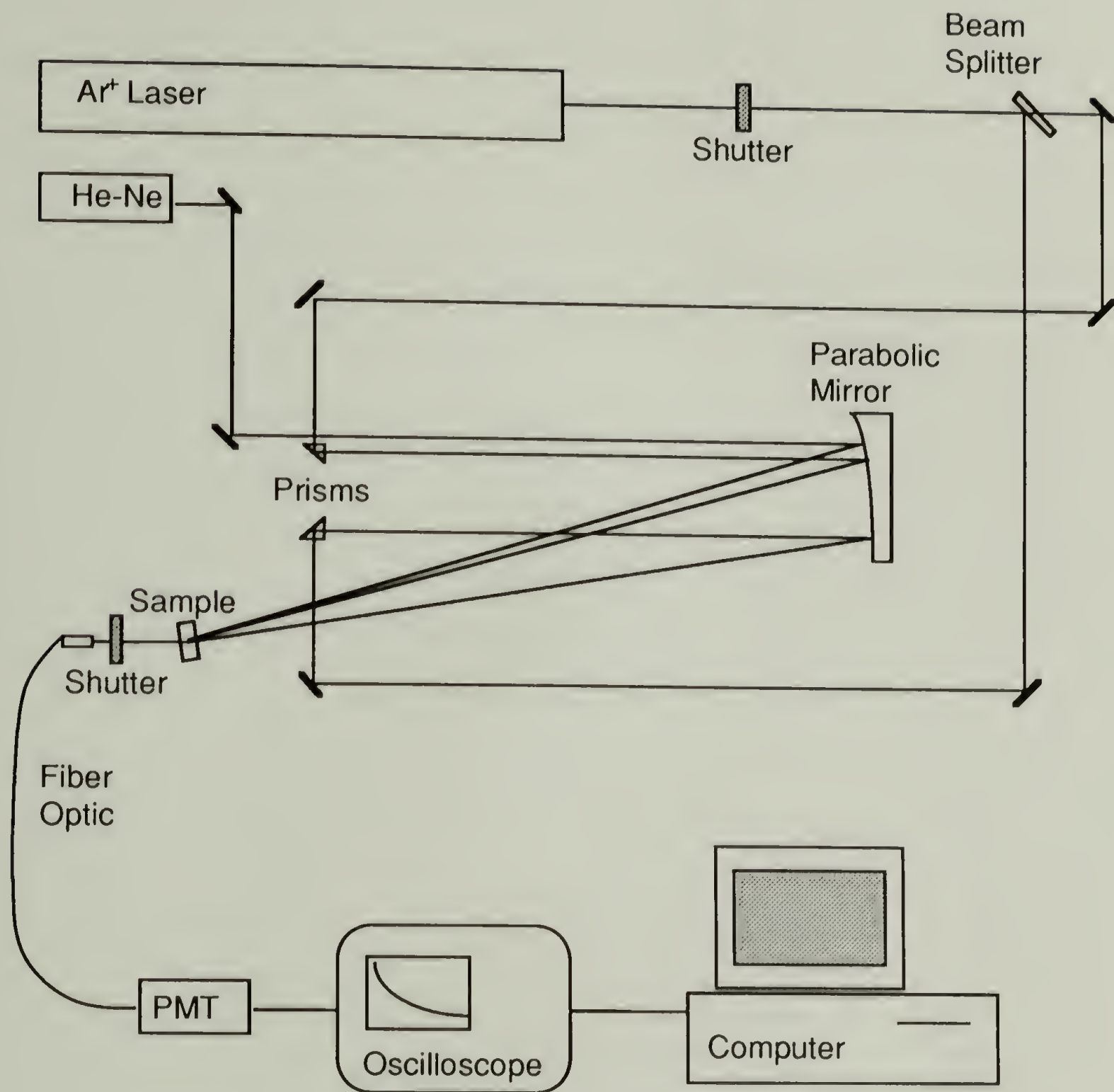
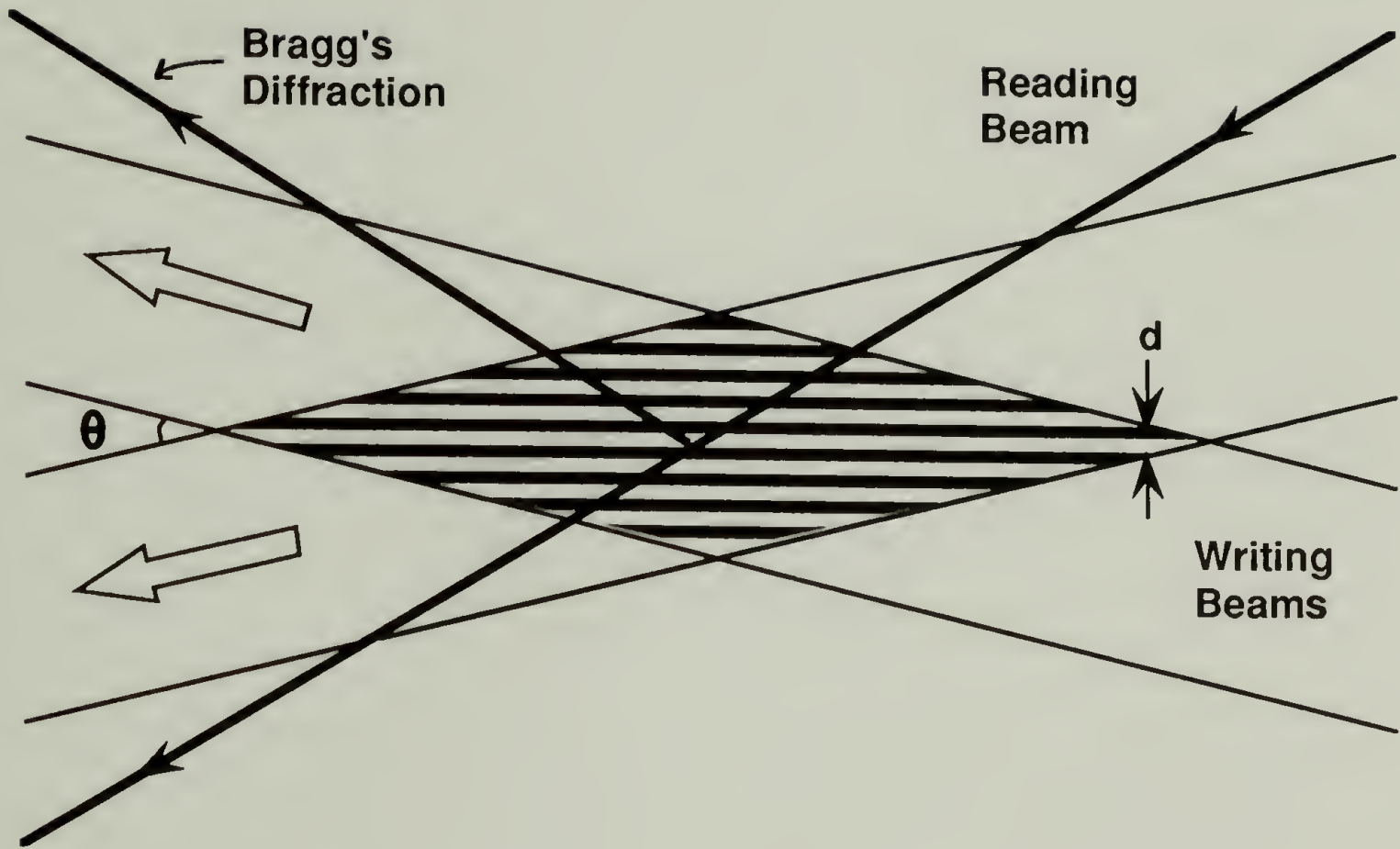
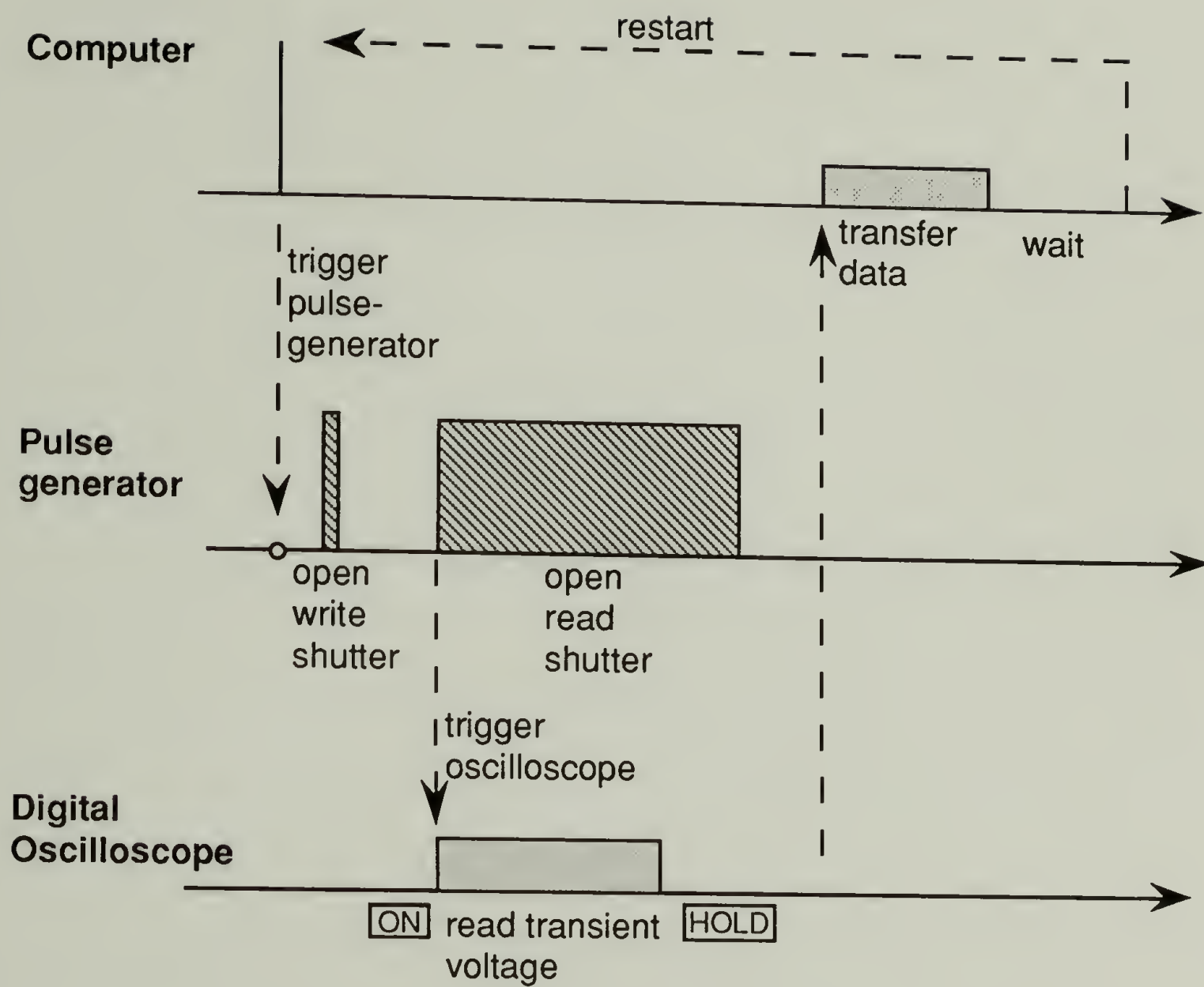


Figure 2.2 Forced Rayleigh scattering spectrometer.



**Figure 2.3** The spatially periodic interference pattern in the sample created by the two writing beams crossing at an angle  $\theta$ . The incident reading beam ( $\lambda=632.8\text{nm}$ ) satisfies the Bragg condition. The diffraction intensity is detected by a photomultiplier tube.



**Figure 2.4** Timing diagram of the forced Rayleigh scattering measurements.

## CHAPTER III

# TIME SCALE DEPENDENCE OF DIFFUSION IN POROUS MATERIALS

### A. Background

Many factors, for example hydrodynamic interaction, geometric obstruction from the solid phase, and chain conformation adjustment hinder the diffusion of a polymer molecule or other species inside porous media. Each factor manifests its effects to a different extent at different length scales [19,20], so that the apparent diffusion coefficient (defined by equation 3.5 below) depends upon the length scale, or equivalently the time scale, of observation. For a polymer molecule diffusing within a single pore, the hindrance is mainly due to the hydrodynamic interactions between the polymer and the pore walls, whereas transport over large distances also involves the geometric characteristics (i.e. tortuosity) of the porous materials. In the work presented in this chapter, the polymer diffusant was small compared to the pore dimension, so that the effect of conformational adjustment was not considered.

This laboratory has previously employed the technique of dynamic light scattering (DLS) for direct measurement of polymer diffusion in

porous glasses[19,20]. It was observed that the apparent diffusion coefficient varied with the scattering angle, or the wavevector  $q$ [19]. When  $1/q \gg R_p$ , i.e., when the wavelength of the concentration fluctuation being monitored was much larger than the pore size, the apparent diffusion coefficient asymptotically attained a constant value. Diffusion in this regime was referred to as macroscopic diffusion as the transport hindrance was averaged over a macroscopic region encompassing many pores. Previous results[19-21] emphasized the dependence of this macroscopic diffusion on the molecular weight and architecture of the polymer. In contrast to macroscopic diffusion, if the fluctuations probed are small compared to pore radius ( $1/q \ll R_p$ , described as single pore diffusion), the situation resembles that found in free solution except that polymers near a pore wall experience significant additional hydrodynamic drag. In this chapter we report the study of the transition region ( $1/q \approx R_p$ ) between single pore and macroscopic diffusion. In this region we observed a DLS autocorrelation function dominated by single pore diffusion at early times, crossing over to a relaxation characteristic of macroscopic diffusion at later times. This has not been previously studied, largely because existing correlators were not capable of measuring the details of the nonexponential autocorrelation function of the scattered light.

Instruments are now available in which the channels are allocated approximately logarithmically in time, enabling high resolution measurement of the rapid evolution of polymer displacement at short times,



simultaneously with slower macroscopic transport at longer times. In this part of the dissertation work we have used such a correlator (the correlator of an N4-SD Particle Analyzer, Coulter Electronics) to examine the correlation function of laser light scattered from polystyrene in 2-fluorotoluene solution filling the pore spaces in a single fragment of controlled pore size glass (R893). More details of the samples and the experiments are described in Chapter II.

Although many computer simulations of the dynamics of a macromolecule moving in spaces of restricted geometry have been performed[103-105], none of the situations which have been examined closely approximates the physical environment in which the molecules in the present experiment are found. We have therefore carried out diffusion calculations on a simple model designed to incorporate most of the relevant features of the system: a highly branched multiply connected network of roughly cylindrical pores. In particular, our model considers a hard sphere which diffuses within cylinders that are interconnected to form a three-dimensional cubic lattice (Figure 3.1). Many significant features of the calculated diffusion are in good agreement with the DLS measurements in porous glass.

### B. Computer Simulation

The model pore structure is shown in Figure 3.1. The diffusion within this porous medium is simulated by a restricted random walk process of a single diffusant. The random walk was repeated many times

and an average displacement at each step of the iterated process was calculated, from which an apparent diffusion coefficient was obtained. The following are the assumptions used in this computer simulation.

1) The model pore structure, represented schematically in Figure 3.1, is an infinite three dimensional cubic network of cylindrical pores with radius  $R_p$ . The distance between centers of two neighboring pores,  $C$ , combined with the pore radius, determines the intrinsic conductivity  $X$  of the material.

2) The polymer molecule, which has a much smaller size than  $R_p$ , is assumed to be hydrodynamically equivalent to a hard sphere of radius  $R_H$ . Previous results[19-21] show that hydrodynamic theories are valid when  $R_H < 0.3R_p$  which is obeyed in all our simulations.

3) Brownian motion inside the pores is simulated by a restricted random walk process. The direction of each step is equally probable in three dimensional space. The step length  $S$  depends on the radial and axial position of the polymer. For simplification we assumed there is no hindrance when a polymer molecule is within an intersection of cylindrical pores along the three axes (equation 3.1a). Between intersections, the step length is reduced due to the interaction between polymer and pore wall (equation 3.1b). Equation (3.1) shows the calculation of  $S$ ,

$$\left\{ \begin{array}{ll} S(\beta) = S_0 & \text{within an intersection} \end{array} \right. \quad (3.1a)$$

$$\left\{ \begin{array}{ll} S(\beta) = S_0 K^{-1}(\beta) & \text{between intersections} \end{array} \right. \quad (3.1b)$$

where  $\beta = r/R_p$  and  $r$  is the radial coordinate of the diffusing polymer with respect to the cylinder axis. The largest step length  $S_0$  which is set to be

inversely proportional to the polymer size, is based on the Stokes equation (equation 2.30). The inverse enhanced drag  $K^{-1}(\beta)$  is the ratio of friction coefficient in free solution to that at a specific position  $\beta$  within the pore; this ratio is also equal to the ratio of the local diffusivity in a pore to that in free solution. The results of Famularo and Hirschfeld[7,24,106] are used to calculate  $K^{-1}(\beta)$ :

$$K^{-1}(\beta) = 1 - \xi(\beta)\lambda \quad (3.2)$$

where  $\lambda = R_H/R_P$  and  $\xi(\beta)$  is given by

$$\begin{cases} \xi(\beta) = 2.09 & (\beta < 0.6) \\ \xi(\beta) = \frac{9}{16(1-\beta)} + 1.9(1-\beta) & (0.6 < \beta < 1) \end{cases} \quad (3.3)$$

The function  $K^{-1}(\beta)$  from equations (3.2) and (3.3) is shown in Figure 3.2. The trend is that a step is shorter when the diffusant is larger or when the position is closer to the pore wall, corresponding to larger local friction due to the hydrodynamic interactions with the pore walls. It is noted here that the expression from the results of Famularo and Hirschfeld (equations 3.2 and 3.3) is not valid when the diffusant is very close to the wall (e.g.  $\beta = 1-\lambda$ ), as the predicted  $K^{-1}(\beta)$  does not diminish to zero. Nonetheless, this error does not significantly affect our simulation results, because the calculated diffusion coefficient is an average in which the weight of the positions very close to the pore wall is relatively small.

4) The starting position of a polymer diffusant in a random walk is equally probable over all accessible volume.

5) A trial step ending in the solid phase is discarded and a new trial step is randomly regenerated until a step is found which ends within a pore space. A discarded step does not count as a step in the random walk, i.e., it does not consume time.

In this Monte Carlo simulation, random walks, typically having 500 steps, were repeated at least  $10^5$  times. The average displacement at each step of the iterated progress was taken to be the ensemble average. The diffusivity  $D_0$  in unbounded solution was obtained from a simulation assuming a free random walk process with a step length  $S_0$  for every step. The hindrance factor  $D/D_0$  versus relative size ratio  $\lambda$  was plotted and a value of tortuosity  $X$  was obtained by extrapolating to  $\lambda = 0$ . When the size ratio  $\lambda$  is small, the normalized hindrance factor  $D/(D_0X)$  is a measure of  $f(\lambda)$ , the ratio of polymer diffusivity inside a single pore to that in free solution. The plot of  $D/(D_0X)$  versus  $\lambda$  from the simulated diffusion in a model pore structure can be well fitted by the numerical expression for  $f(\lambda)$  developed by Brenner and Gaydos[25] which was used to interpret previous experimental results[19-21].

### C. Results and Discussion

The diffusion of polymer chains in the controlled pore glasses was monitored by dynamic light scattering using a heterodyne arrangement in which the statically scattered light from the glass matrix served as the local oscillator. The normalized electric field autocorrelation function  $g^{(1)}(t)$  which is directly related to molecular dynamics, was obtained from the

measured light intensity ACF using equation (2.11). In the dilute solutions studied the polymer molecules are non-interacting and statistically independent, hence  $g^{(1)}(t)$  is related to the time-dependent mean-square displacement of macromolecules (equation 2.15)[44]. For simplicity, the scattered field ACF is denoted by  $g(t)$  from this point, and equation (2.15) can be rewritten as:

$$\ln g(t) = - \frac{q^2 \langle R^2(t) \rangle}{6} \quad (3.4)$$

The apparent diffusion coefficient (which may be a function of time),  $D_{app}(t)$ , is defined as:

$$D_{app}(t) = \frac{1}{6} \frac{d}{dt} \langle R^2(t) \rangle \quad (3.5)$$

which can be calculated from  $g(t)$ .

The normalized electric field ACF of a polystyrene fraction (MW = 50,000) in glass R893, shown in Figure 3.3(a), was measured at an intermediate value of  $qR_p = 0.8$ , suitable for studying diffusion in the transition region. The total delay time spanned a range large enough for the decay to be complete, thus assuring an accurate measured baseline. Figure 3.3(b) is a semilogarithmic plot of the first millisecond of the same correlation function. All data points fall onto a straight line, except for the initial portion, which is shown in expanded form in Figure 3.3(c). It is clear in Figure 3.3(c) that the ACF decay changes from a faster rate at small time to a slower and constant rate at larger time, indicating a dependence of diffusion behavior on the time scale of observation.

The apparent diffusion coefficient,  $D_{app}(t)$ , is the negative slope (five point average) of the plot in Figure 3.3(b) divided by  $q^2$  (equations 3.4 and 3.5), and is shown in Figure 3.4. Initially, the value of  $D_{app}$  is close to the diffusion coefficient measured in free solution. At larger times,  $D_{app}$  drops to a smaller and constant value. The transition was observed only when the probing length scale of the DLS was comparable to the pore size, i.e., when  $1/q \approx R_p$ . We interpret this crossover behavior as follows.

For a polymer molecule within a single pore which is larger than the polymer dimension, diffusion is hindered mainly by hydrodynamic interactions between the polymer and the pore walls. At small time scales, the average time dependent root mean square displacement  $\langle R^2(t) \rangle^{1/2}$  is smaller than the pore dimension, and the ACF decay is, for the most part, due to polymer translation within a single pore. The  $D_{app}(t)$  observed at small  $t$  is therefore a manifestation of microscopic Brownian motion without fully experiencing geometric obstruction by the glass matrix. The apparent diffusion coefficient near  $t = 0$  could be viewed as resulting from the inverse enhance drag  $K^{-1}(\beta)$  (equations 3.2 and 3.3) averaged over all available positions within the pore, yielding a value close to, but smaller than  $D_0$ .

Transport over large distances involves the macroscopic characteristics or tortuosity of the porous material which accounts for the wandering paths through which a diffusant must move. The geometric obstruction is reflected in the ACF only at large time scales. At large  $t$ , when  $\langle R^2(t) \rangle^{1/2} \gg R_p$ , the movement of the polymer molecules again obeys the diffusion law,  $\langle R^2(t) \rangle = 6Dt$ , where  $D$  denotes the macroscopic

diffusion coefficient. The constant value of  $D_{app}$  in Figure 3.4 at large  $t$  represents macroscopic hindered diffusion, the process by which polymer molecules move over distances much larger than that of the pore size. On this distance scale microscopic heterogeneity is averaged out and the apparent diffusion coefficient is constant, indicative of macroscopic uniformity of the pore structure.

The time at the midpoint  $[(D(t \rightarrow 0) + D(t \rightarrow \infty))/2]$  of the transition in Figure 3.4,  $t_1$ , was used to characterize the crossover from single-pore to macroscopic diffusion. This is possibly not the best choice among many ways of characterizing this type of crossover. Other time characteristics, such as the crossing point of the initial slope and the slope at much larger times in Figure 3.3(b) and (c), or the inflection point can also be used in good stead. The midpoint was chosen mainly because of less error in extracting its value given the noise in the crossover regime. On the other hand, a different choice of time to characterize the crossover does not affect the trend of the crossover time as a function of parameters such as pore radius and polymer size.

It was found that within the range of scattering angles over which a crossover could be observed, the crossover time for a given polymer-porous glass system was independent of the scattering angle. This excludes two other possibilities that can also give rise to the observed change in the ACF decay rate: (a) observation at the same time some particles undergoing free diffusion and some other particles undergoing hindered diffusion; (b) homodyne contribution to the autocorrelation function, i.e., the neglected term  $\langle |E_S(0)|^2 |E_S(t)|^2 \rangle$  from equation (2.9), which can give a decay mode in

$G^{(2)}(t)$  twice as fast as  $g^{(1)}(t)$ . If (a) or (b) is what we saw, the autocorrelation function at different angles should fall onto a universal curve if plotted against  $q^2t$ . By contradiction reasoning, we know that the crossover is not due to possibility (a) or (b) since  $t_1$  is independent of  $q$ , rather than inversely proportional to  $q^2$ . The exclusion of (a) and (b) is expected as a result of the taken experimental measures. To eliminate possibility (a), the scattering volume is limited completely *within* the porous fragment. To eliminate possibility (b), the intensity of the local oscillator (the static scattering from the glass matrix) is stronger than the scattering from the diffusing polymer by a factor of 50, such that the homodyne contribution is negligible. Realistically, the crossover time is determined by the real transport process, independent of the observation.

In Figure 3.3, the situation  $\langle R^2(t) \rangle^{1/2} \approx R_p = 893 \text{ \AA}$  is equivalent to  $\ln g(t) \approx 0.1$ . The position of the data point corresponding to this situation is shown in Figure 3.4. At the time when  $\langle R^2(t) \rangle^{1/2} \approx R_p$ ,  $D_{app}(t)$  begins to attain a lower and constant value, and macroscopic diffusion emerges. Therefore, the time preceding macroscopic diffusion, i.e., before the polymers fully experience geometric obstruction from the glass matrix, is roughly the time required for a polymer molecule to traverse a single pore.

Results of the computer simulation study are shown in Figure 3.5 through 3.7. The mean square displacement  $\langle R^2(t) \rangle$  as a function of time, or step number of the restricted random walk, is plotted in Figure 3.5. At the large step numbers  $\langle R^2(t) \rangle$  increases more slowly and the curve asymptotically approaches a constant slope. The apparent diffusion coefficient,  $D_{app}(t)$ , obtained from the slope in Figure 3.5 by using



equation (3.5), is shown in Figure 3.6. Similar to the DLS experimental data, there is a crossover from a larger  $D_{app}(t)$  at small step number (attributed to single pore diffusion), to a smaller and asymptotically constant  $D_{app}(t)$  at large step numbers (attributed to macroscopic diffusion). For this system, the time, or step number, at which  $\langle R^2(t) \rangle^{1/2} \approx R_p$  is shown in Figure 3.6. We can see that macroscopic diffusion behavior emerged after the displacement of the polymer taking a random walk is approximately equal to the pore size, similar to what we found in the DLS measurements.

Figure 3.3(c) (from DLS experiment) and Figure 3.5 (from computer simulation) are related by equations (3.4) and (3.5); in both figures the slope is proportional to the diffusion rate. Figure 3.4 (from DLS) and Figure 3.6 (from simulation) are also directly comparable. Qualitative agreement is found in that both techniques show the crossover behavior from rapid single pore diffusion to slower macroscopic diffusion at a time when the root mean squared displacement approximately equals the pore radius. We note here that the time scales in Figures 3.4 (semilogarithmic) and 3.6 (linear) are different. This is because in the DLS experiments the autocorrelation function was measured at times approximately logarithmically spaced, while in the computer simulation, the time period for each step is the same. If a logarithmic time scale is to be used in a plot like Figure 3.6, many more steps are needed to demonstrate the crossover trend, which necessitate a formidable amount of computation time.

The midpoint of the transition of the simulated apparent diffusion versus step number is taken to be the crossover time again. The dependence

of the crossover time  $t_1$  on polymer and pore radius is given in Figures 3.7 and 3.8. It was found in the computer simulations (Figure 3.7) that  $t_1$  is essentially proportional to  $R_H$  and to  $R_P$  ( $t \propto R_H \times R_P$ ) over the range of the simulation. The experimental results from DLS for  $t_1$  versus  $R_H$  (Figure 3.8) while not as extensive, suggest that the data can be fitted with a straight line having a nonzero intercept. The finite intercept, as opposed to the zero intercept in Figure 3.7 from computer simulation, represents a realistic situation: a point diffusant ( $R_H \rightarrow 0$ ) moves at a finite diffusion rate (in spite of the Stokes-Einstein relation) and requires a finite time period to move a distance larger than the pore radius. The zero intercept in Figure 3.7 is an artifact of simulation, arising because the step length diverges as  $R_H$  approaches zero. The experimental finding that the crossover time is linearly related to the polymer size indicates that the diffusivity on the smaller time scale within a single pore does resemble the diffusivity in free solution in terms of the inverse proportionality between the diffusivity and the diffusant size in Stokes-Einstein relation.

Baumgärtner and Muthukumar have studied polymer dynamics in totally random porous media using Monte Carlo simulations[104]. Their results showed three distinct regimes for the time evolution of  $\langle R^2(t) \rangle$ . In the early and late stages the displacement obeyed diffusion law ( $\langle R^2(t) \rangle \propto t$ ), and a transition regime was found in intermediate stages. In the short time regime, they found that the diffusion followed the Rouse theory ( $D(t) \propto N^{-1}$ ) where  $N$  is the degree of polymerization. In the late stages of diffusion,  $D(t)$  was found to depend on  $N$  more strongly as  $N^{-w}$ ,  $w$  being dependent on the porosity of the model. For the porosity in the range of

0.5 to 0.9, they found  $w$  to range from 3.2 to 1.37. In our experiments for both DLS and computer simulation, the short time regime of Fickian diffusion was not observed because of the position dependence of hydrodynamic friction inside the pores. Fickian diffusion is observed if the simulated step length is assumed to be the same at all available positions, i.e.,  $K^{-1}(\beta)=1$ . The hindrance at short time and length is reflected in our computer simulation in that the friction coefficient is a function of both confinement ratio ( $\lambda$ ) and radial position ( $\beta$ ).

The crossover time  $t_1$  for constant  $R_H$  and  $R_P$  from the computer simulations is insensitive to the interpore spacing  $C$  of the model pore structure, which means that our calculated values of  $t_1$  are independent of the porosity of the porous material. However, the crossover is dependent on the initial spatial distribution of the polymer concentration inside the pores. A well measured ACF combined with information from computer simulation should furnish some insight into the spatial distribution of the polymer concentration within the pores. This task is difficult for the systems studied here because the dimensions of the polymers and the pores are not unambiguously defined. However, for such systems as starburst-dendritic macromolecules[86] in thick track-etched membranes[107] extraction of more information is possible.

#### D. Conclusions

The dependence on the time scale of the diffusion behavior of polymers inside controlled pore silica glasses was studied using dynamic light scattering and computer simulation. A crossover from rapid decay at short times to a lower constant apparent diffusion coefficient at larger times was observed at a fixed light scattering angle. The crossover time  $t_1$  was found to be independent of the scattering wavevector  $q$ . For times  $t \ll t_1$ , the apparent diffusion coefficient is a measure of the diffusivity within a single pore where hindrance is due primarily to hydrodynamic interactions with the pore walls. For  $t \gg t_1$ , we observe macroscopic diffusion which is influenced by hindrance arising not only from hydrodynamic interaction, but also from obstruction because of the geometric structure of the pore space, i.e., the tortuosity of the porous material. The time period before the polymer attains macroscopic diffusion behavior is roughly the time required for polymer to diffuse a distance equal to the pore size. By moving over distances large compared to the pore size, the polymer movement averages over the local nonuniformity of pores and solid matrix in the glass and attains the macroscopic features. The crossover behavior observed by DLS is in qualitative agreement with that calculated in a computer simulation. The crossover time was found to be linearly related to the polymer size in both DLS measurements and computer simulation.

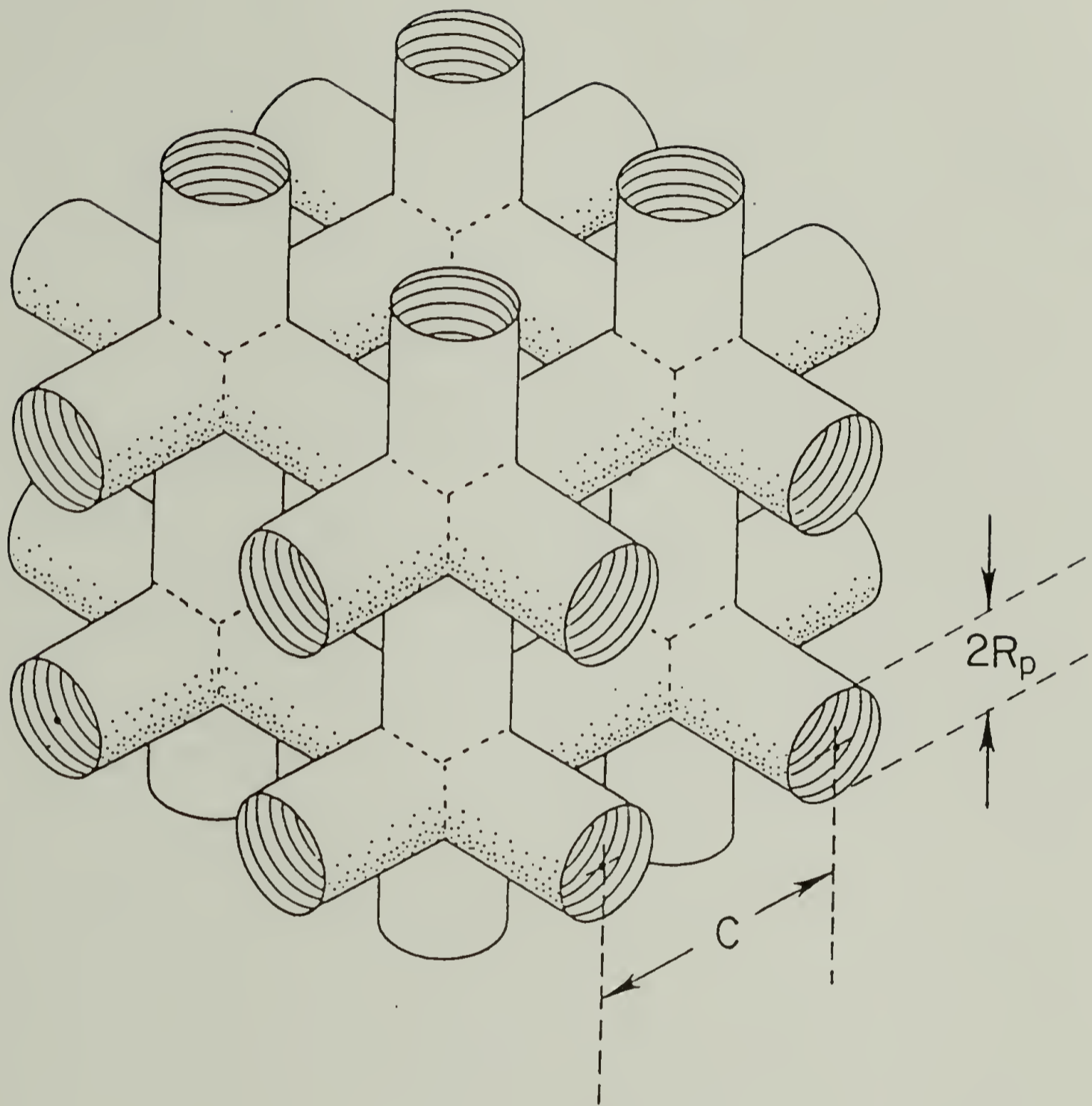


**Figure 3.1** Model pore structure used in the computer simulation.  $R_p$  is the pore radius,  $C$  is the center-to-center distance between neighboring pores.

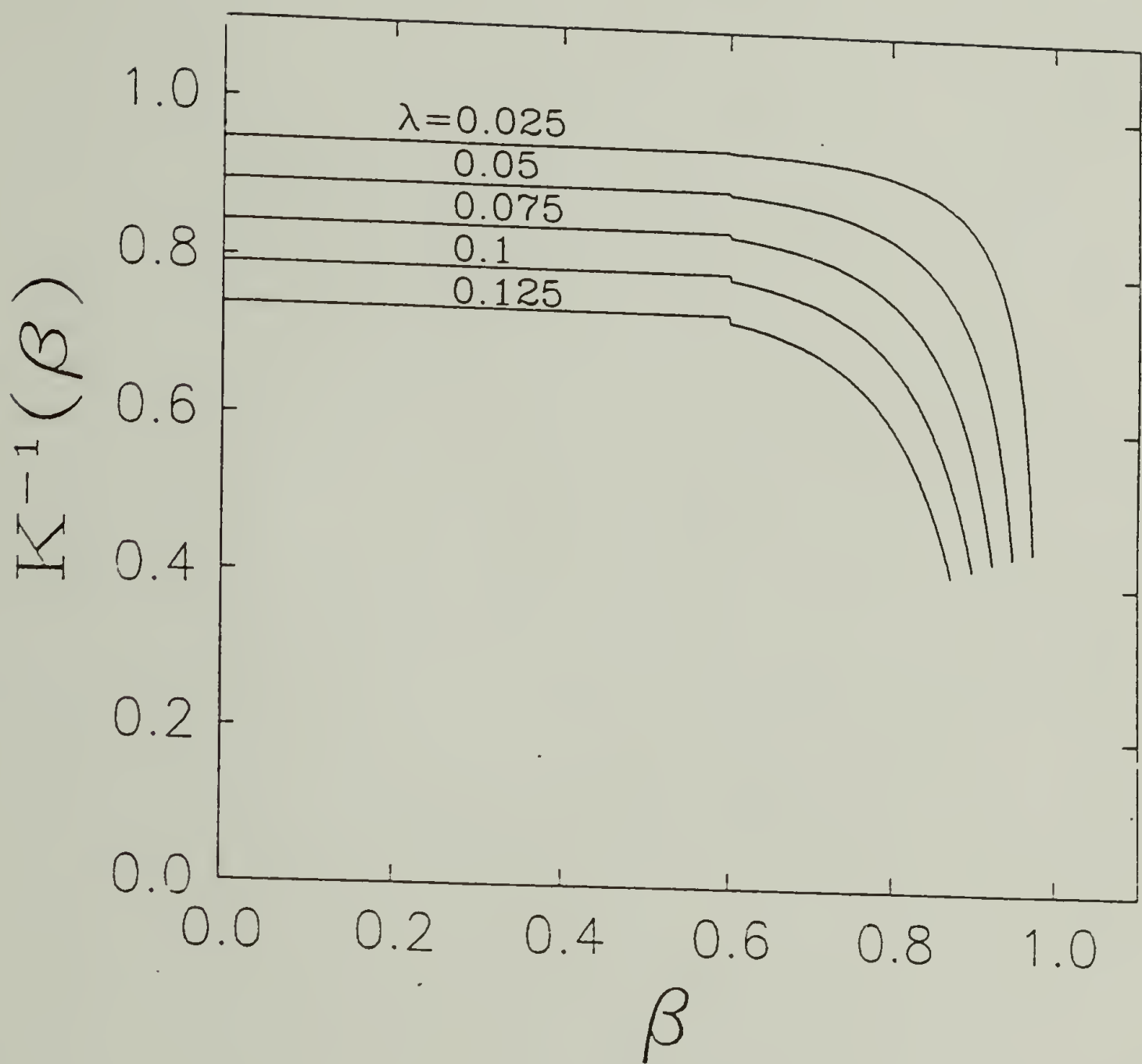


**Figure 3.2** The inverse friction ratio  $K^{-1}(\beta)$  used in the computer simulation. Here  $\beta = r/R_p$  is the radial position of the diffusant. The solid curves for various size ratio  $\lambda$  are calculated using equations (3.2) and (3.3).

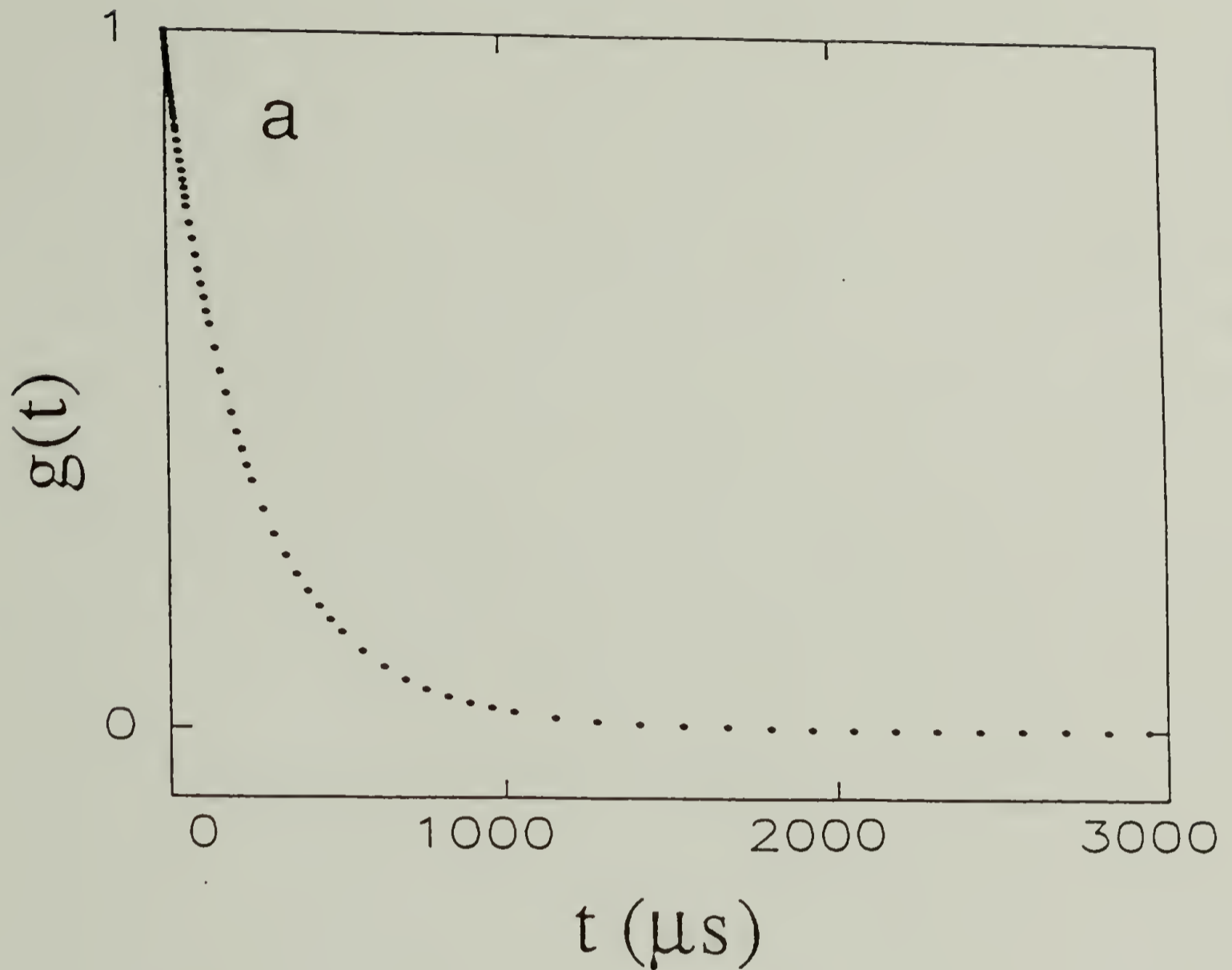


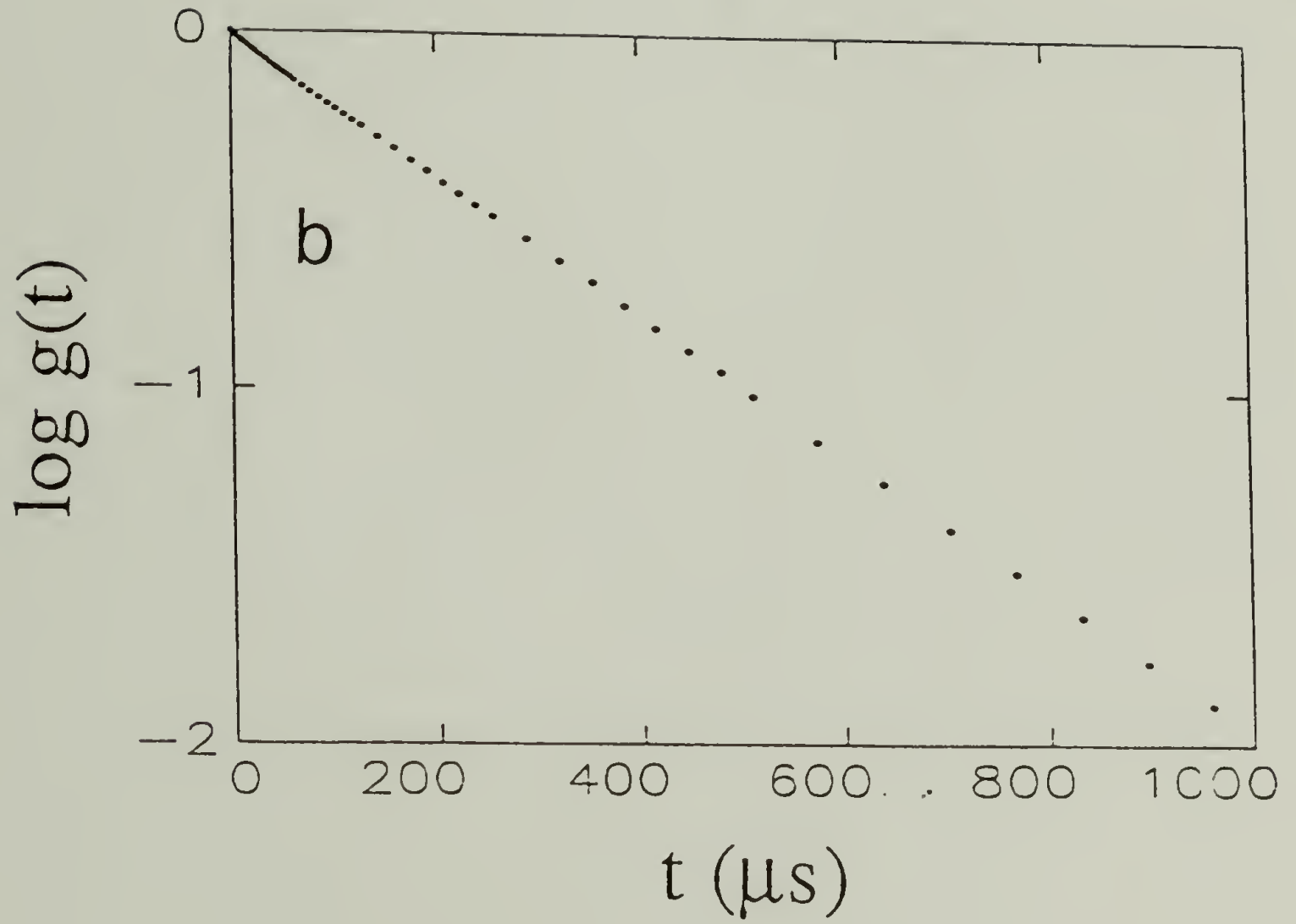
**Figure 3.3** Field autocorrelation function  $g(t)$  (normalized after baseline subtraction) measured by dynamic light scattering from a solution of polystyrene ( $M=50,000$ ,  $R_H=52 \text{ \AA}$ ) in the controlled pore silica glass R893 ( $R_P=893 \text{ \AA}$ ). Scattering angle was  $35^\circ$  ( $qR_P = 0.8$ ).

(a) Linear plot of  $g(t)$ .

(b) Semilogarithmic plot of the first millisecond of the ACF shown in Figure 3.3(a).

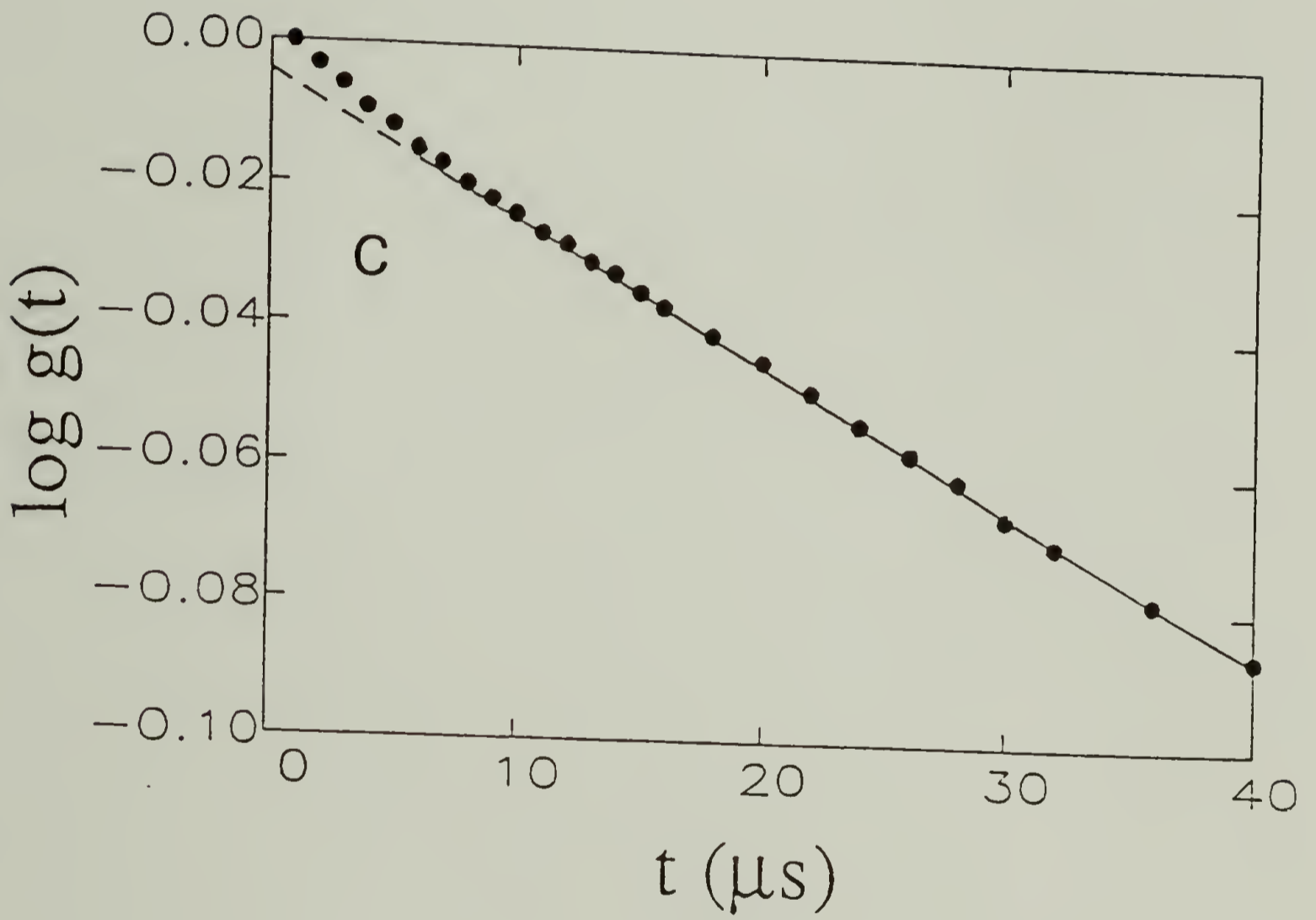
(c) Expanded view of the initial portion of the ACF in Figure 3.3(b).

(to be continued on the next page)



(to be continued on the next page)





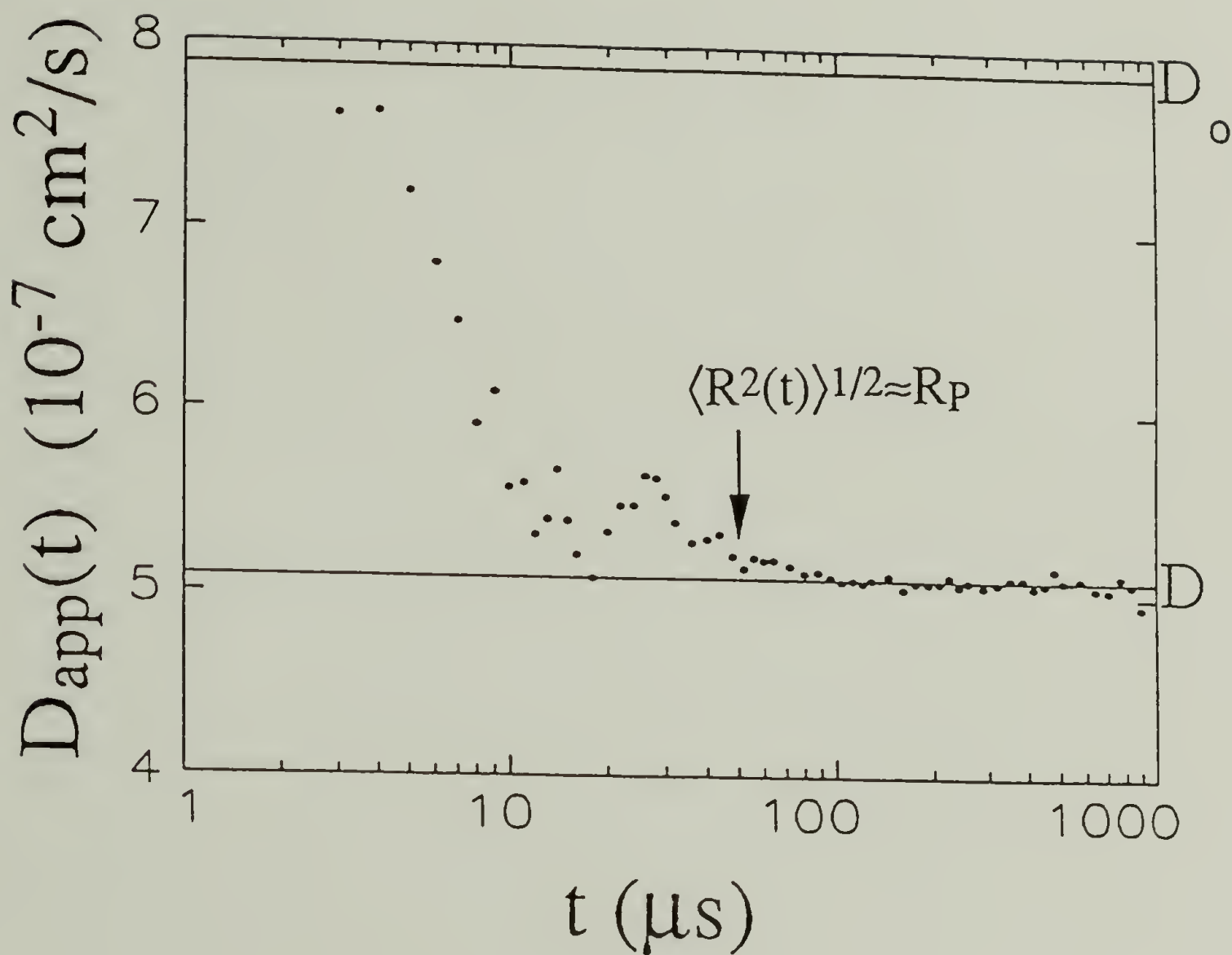


Figure 3.4 The apparent diffusion coefficient as a function of time, proportional to the slope of the ACF in Figure 3.3(b) and (c).  $D_0$  and  $D$  are the unbounded solution and the macroscopic diffusion coefficient, respectively. The point at which  $\langle R^2(t) \rangle^{1/2} \approx R_P$  is pointed out in the figure.

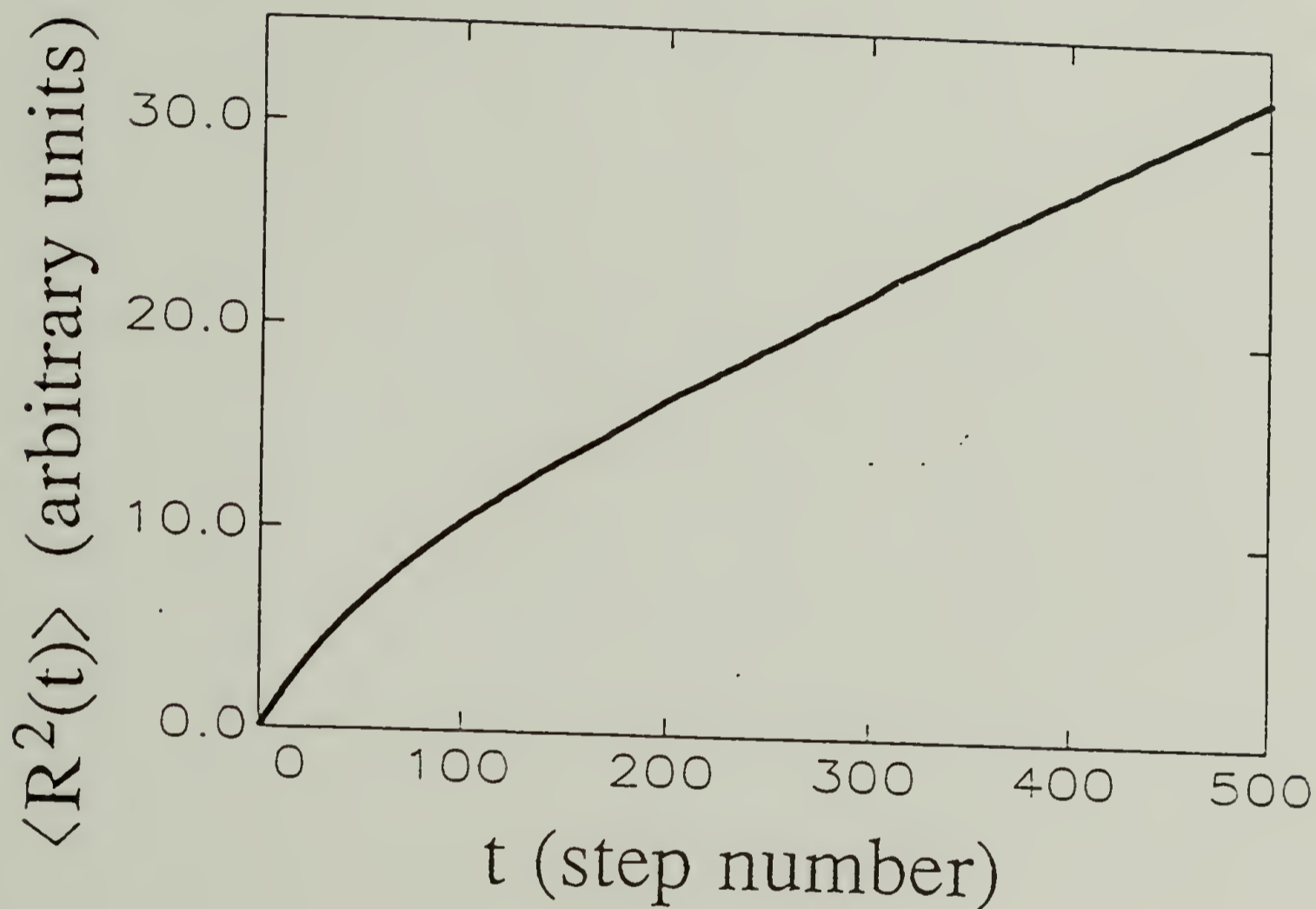
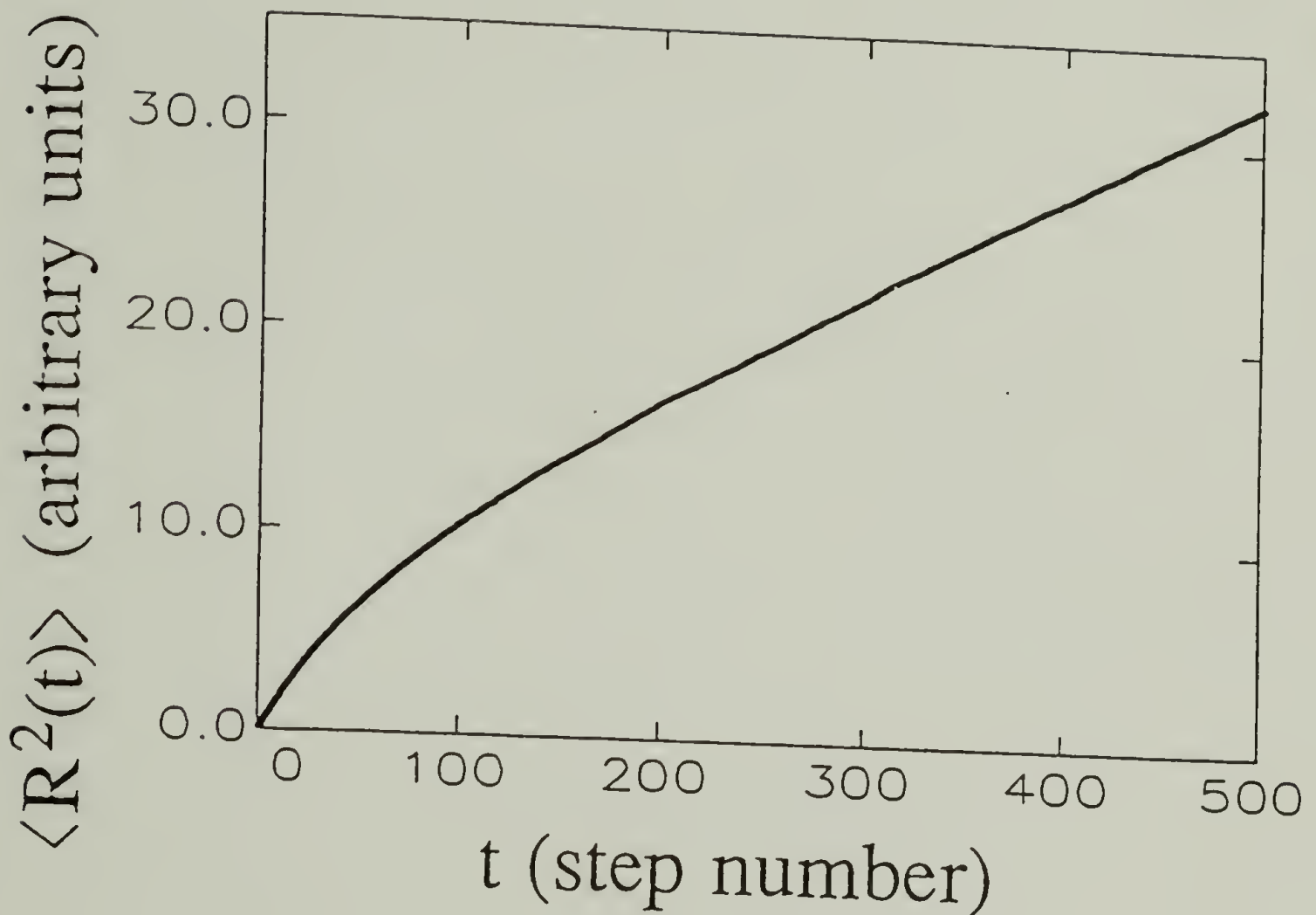


Figure 3.5 Mean square displacement  $\langle R^2(t) \rangle$  versus random walk step number (equivalent to time), obtained from computer simulation. This figure is for a model in which  $R_P=3$ ,  $R_H=0.3$ ,  $C=20$  and  $S_0=0.5$  (all in the same arbitrary units).



**Figure 3.5** Mean square displacement  $\langle R^2(t) \rangle$  versus random walk step number (equivalent to time), obtained from computer simulation. This figure is for a model in which  $R_P=3$ ,  $R_H=0.3$ ,  $C=20$  and  $S_0=0.5$  (all in the same arbitrary units).

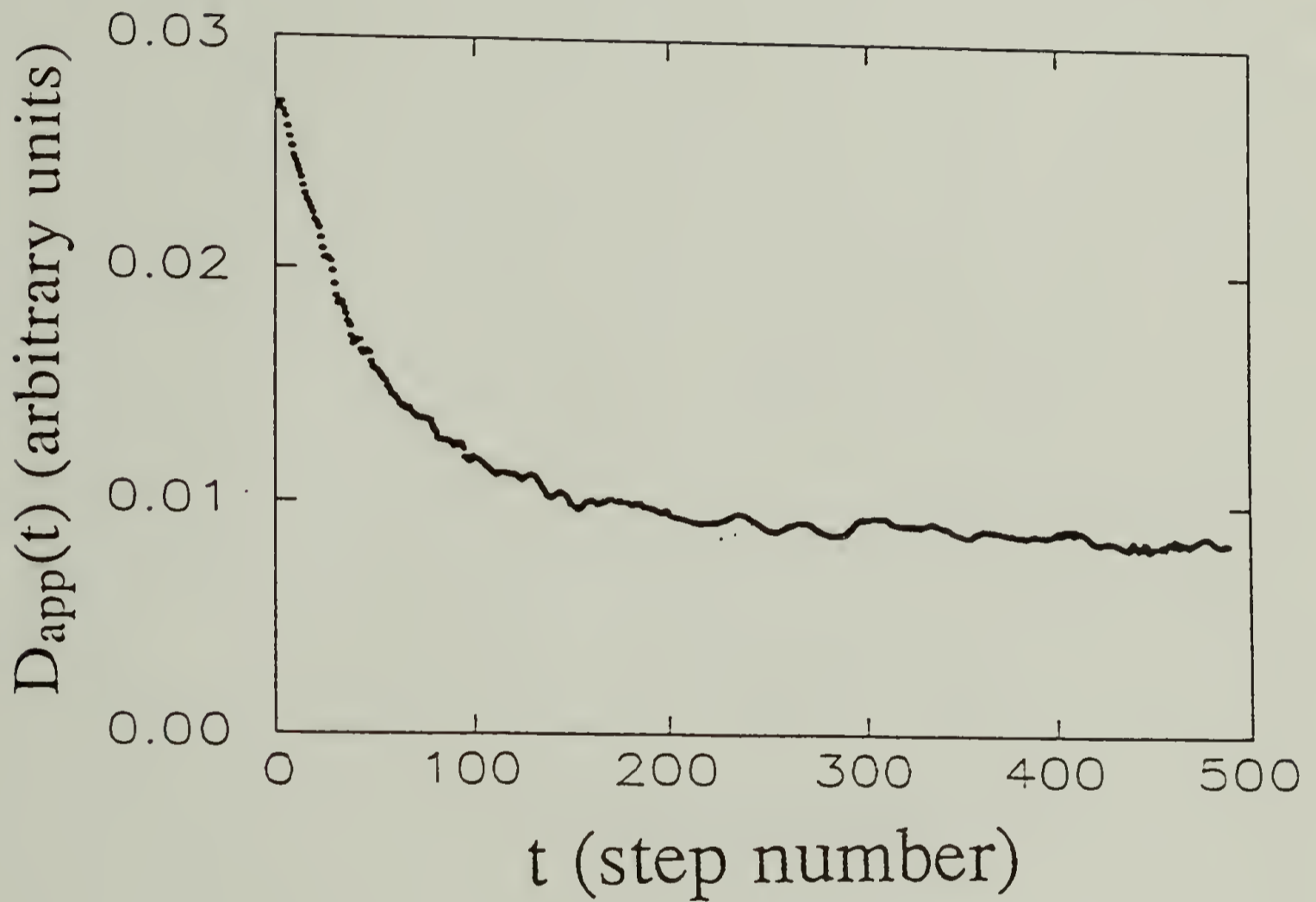


Figure 3.6 Computer simulation calculation of the apparent diffusion coefficient obtained from the slope of the curve in Figure 3.5. The point at which  $\langle R^2(t) \rangle^{1/2} \approx R_p$  is also pointed out in the figure.

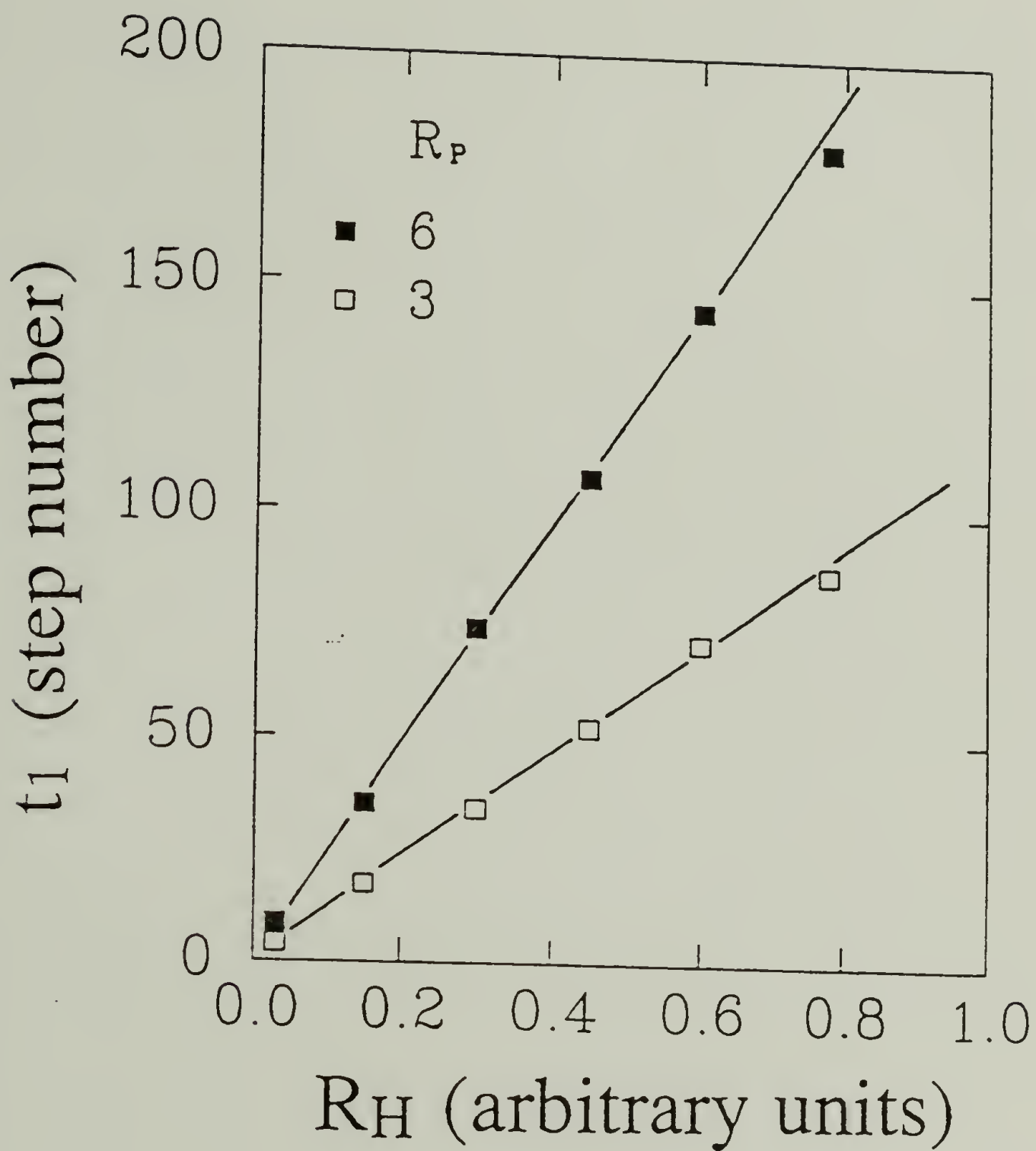


Figure 3.7 Dependence of the crossover time on polymer radius  $R_H$  and pore radius  $R_P$ , from computer simulation.  $R_H$  and  $R_P$  are measured in the same arbitrary units. It can be seen that  $t_1$  is essentially proportional to  $R_H \times R_P$ .

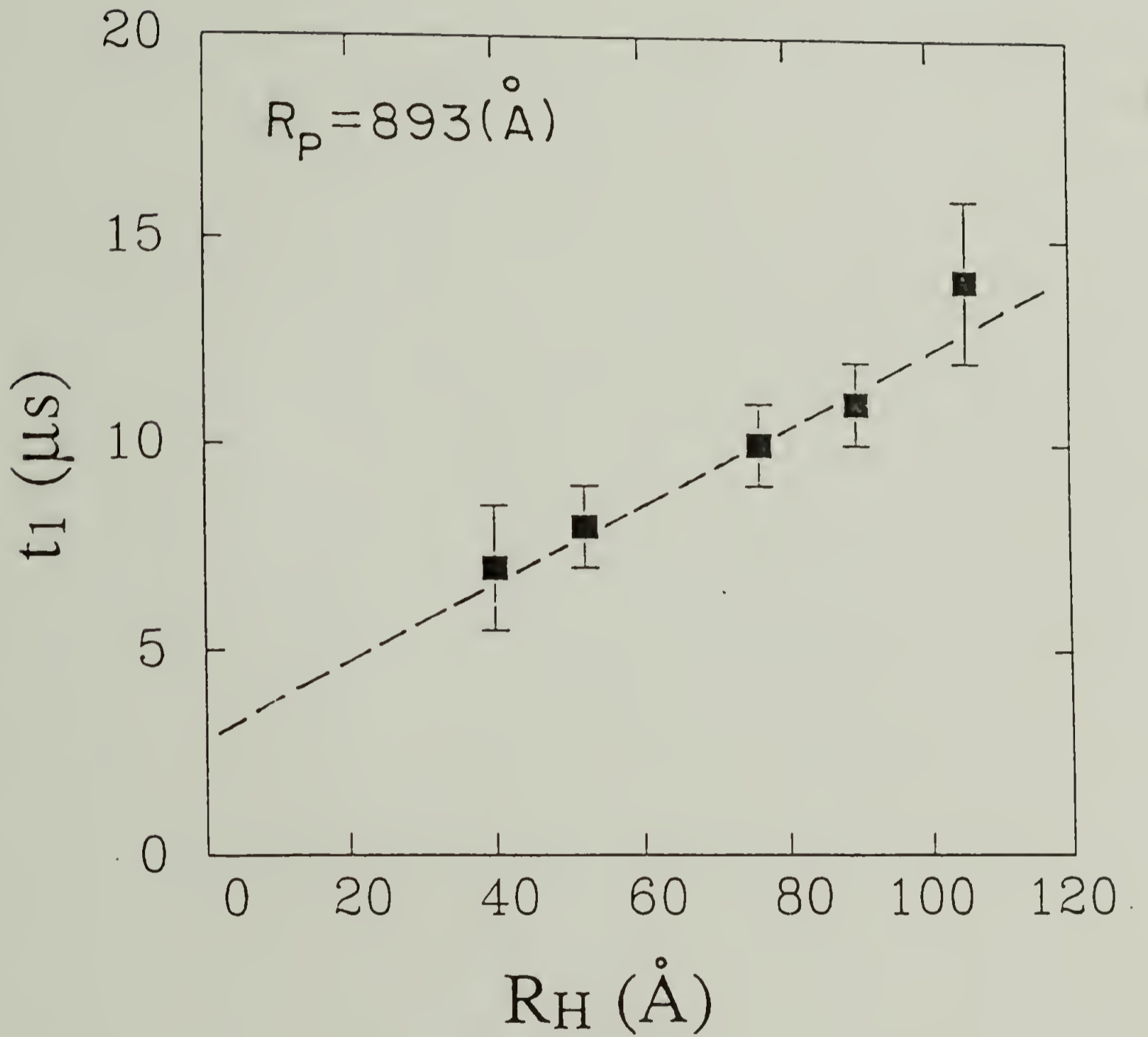


Figure 3.8 Dependence of the crossover time  $t_1$  on polymer radius  $R_H$ , measured using DLS. Polystyrene solutions ( $M=3.5 \times 10^3$  to  $1.7 \times 10^5$ ) in porous glass R893 ( $R_p=893 \text{\AA}$ ).

## CHAPTER IV

# MACROSCOPIC DIFFUSION OF POLYMERS IN POROUS GLASSES

### A. Background

The diffusion of polymers or other species in porous materials has attracted great interest from different disciplines because of its importance in processes such as chromatography, catalysis, enhanced oil recovery and membrane separation. In almost all these processes, it is the macroscopic diffusion that is ultimately related to the outcome or the productivity. Therefore, the understanding of macroscopic diffusion behavior is of most interest.

Polymer molecules, such as linear polystyrene chains, diffuse more slowly in a porous medium than in solution, due to the presence of an obstructing solid phase and hydrodynamic interactions between the polymer and the pore walls. Inside the pore spaces of porous glass, a diffusing polymer molecule experiences hydrodynamic drag from the pore walls while it moves inside the tortuous paths. When the size of the macromolecule is comparable to that of the pores, a change in conformation greatly affects diffusion behavior. The hindrance factors including tortuosity, hydrodynamic drag and conformational entropy change were investigated to reveal the individual mechanisms, and their dependence on



the structure and dimension of the polymer diffusant and of the pore spaces.

The pioneering study of the diffusion of polystyrene chains inside pore spaces of porous glasses using the technique of dynamic light scattering was done by Bishop et al. [19,20] They investigated molecular weight dependence of translational diffusion of polystyrene in three different glasses each with different pore radius and porosity. In interpreting their results, they assumed that the macroscopic diffusion coefficient  $D$ , measured over distances large compared to the pore radius (i.e.  $qR_p \ll 1$ ) is given by:

$$D/D_0 = Xf(\lambda_H) \quad (4.1)$$

$D/D_0$  is the hindrance factor for macroscopic diffusion, and  $X$  is the intrinsic conductivity of the porous material [6,108]. The parameter  $f(\lambda_H)$  is the size dependent ratio of diffusivity within the pore space to that in the unbounded solution. Conceptually, this assumption is that the total hindrance is a product of the hindrance due to the tortuosity and the hindrance due to hydrodynamic interactions. The separation of structural and hydrodynamic effects (equation 4.1) is only valid when all the pores are well connected and when the pore size distribution is narrow [20].

These conditions were met in the controlled pore glasses. For  $\lambda_H \rightarrow 0$ , the factor  $f(\lambda_H) \rightarrow 1$ , thus a measured value of  $X$  can be obtained by extrapolating the data of  $D/D_0$  versus  $\lambda_H$  to the limit  $\lambda_H = 0$ . The intrinsic conductivity  $X$ , which is the inverse of the tortuosity, is characteristic of the material and is thus independent of the polymer diffusant. Universal

behavior was found for  $D/(D_0X)$  versus  $\lambda_H$  for polystyrene in all three glasses which had different porosities and pore sizes.

When the confinement is relatively weak the hydrodynamic interactions dominate the diffusion behavior. There are a number of theories quantitatively predicting the hindrance due to hydrodynamic interactions as a function of diffusant-to-pore size ratio  $\lambda$ . Our experimental results in this regime are compared to two relevant theories: the Brenner-Gaydos theory[25] and the Davidson-Deen theory[9,15].

Brenner and Gaydos (BG) developed a hydrodynamic theory for diffusion of a hard sphere inside a cylindrical pore, which predicts that[25]

$$f(\lambda_S) = \frac{1 + (9/8) \lambda_S \ln \lambda_S - 1.539 \lambda_S}{(1 - \lambda_S)^2} \quad (4.2)$$

where  $\lambda_S = R_S/R_P$ , and  $R_S$  is the radius of a rigid spherical diffusant.

Bishop et al. [19,20] compared the measured diffusion coefficients of polymers in porous glasses to the BG prediction. A scaling factor  $\kappa$  was introduced by Bishop to correlate  $\lambda_S$  and  $\lambda_H$ ,

$$\lambda_S = \kappa \lambda_H \quad (4.3)$$

Though the incorporation of  $\kappa$  as a fitting parameter into the BG theory lead to better fit of the reported experimental results, the nature of parameter  $\kappa$  was not unambiguous. Bishop suggested several possible reasons that may cause the deviation of  $\kappa$  from unity, among which are the most important ones: (1) underestimation of the pore radius by mercury

intrusion porosimetry[93]; and (2) inequality of  $R_H$  and  $R_S$  for flexible polymers.

Following the work of Bishop, Easwar et al.[21] measured diffusion of linear, 4-arm, and 8-arm polyisoprenes in porous glasses. These authors concluded that  $\kappa$  indeed depends upon the structure of the polymer and that the underestimation of  $R_p$  is insignificant. They found that for the same  $\lambda_H$ , the polymer molecule with more arms (linear polymer can be viewed as having 2 arms) diffuses more slowly. It is logical to extend the diffusion study to more compact, less permeable polymer molecules. The recently developed starburst-dendritic macromolecules[86] are suited for this purpose. Section C of Chapter II can be referred to for more information about the polymer samples.

Davidson and Deen recently developed a hydrodynamic theory to predict the inverse enhanced drag  $K^{-1}(\lambda_H)$ , which is the ratio of the friction coefficient in free solution to that inside the pores, for a *flexible* polymer chain inside cylindrical pores. These authors modeled a random coil macromolecule as a porous body, whose average shape and solvent permeability were affected by confinement in a pore. The calculated values of  $K^{-1}$  for different  $\lambda_H$  at different permeabilities were tabulated and plotted in reference 15. They found that for random coil macromolecules the hydrodynamic behavior of the polymer is mainly determined by  $\lambda_H$  and the effect of the permeability is relatively weak, and thus  $K^{-1}(\lambda_H)$  was calculated approximately as a function of  $\lambda_H$  only. Under the centerline approximation[8], the diffusivity ratio  $f(\lambda_H)$  is the same as  $K^{-1}(\lambda_H)$ , such that the final numerical expression is[9]

$$f(\lambda_H) \approx K^{-1}(\lambda_H) \approx 1 - 2.848\lambda_H + 3.269\lambda_H^2 - 1.361\lambda_H^3 \quad (4.4)$$

Equation (4.4) was claimed valid for  $\lambda_H \leq 0.8$ .

Section B of this chapter reports the results of our investigation on the diffusion hindrance due to hydrodynamic interactions and its dependence of the molecular architecture. A better understanding on the effect of hydrodynamic interactions, which dominated the polymer diffusion at low size ratio  $\lambda_H$ , was obtained from the diffusion study of a dendritic and a linear polymer in CPGs. Several comparisons were made to achieve the conclusions of this section; these comparisons were: (1) between the experimentally measured diffusion coefficients of two polymers with drastically different structural architectures — linear polystyrene and starburst-dendritic polyamidoamine; (2) between the diffusion behavior of the dendritic polymer and that predicted by a hydrodynamic theory for hard sphere diffusion in cylindrical pores[25]; and (3) between the molecular weight dependence of hindered diffusion of polystyrene and that predicted by the recently developed hydrodynamic theory for a flexible polymer chain in a cylindrical pore[9,15].

Another part of the work in this chapter, which is presented in Section C, is the study of diffusion of strongly confined polystyrene chains. Easwar[21] extended the diffusion measurement of polystyrene in porous glasses from  $\lambda_H = 0.47$  in Bishop's work to a higher  $\lambda_H$  regime ( $\lambda_H \leq 0.74$ ). In this work I extended diffusion measurements to new regimes of much higher confinement of linear polystyrene in controlled

pore glasses. I have used several dimensional ratios of the polymer and the pores up to a ratio of  $\lambda_H = 1.4$ .

Our measured diffusion results for polystyrene chains at large  $\lambda_H$  were compared to the "elongated cigar" model, which is a scaling analysis of dynamics of polymer chains trapped in small cylinders. This model satisfactorily explained diffusion behavior of strongly confined flexible polymer in the almost cylindrical pores of track-etched membranes[13,14].

In the present work the dynamic behavior at large  $\lambda_H$  was also studied in light of the recently developed theory for the entropy barrier by Muthukumar et al.[31] They modeled the pore structure by an assembly of cavities of dimension  $L$ , connected to one another by bottlenecks or gates with cross-sectional and longitudinal dimensions  $C$  and  $d$ . A polymer chain with a degree of polymerization  $N$  translates inside pores thus defined with a diffusion coefficient  $D$ , where

$$D = X D_0 \exp(-\Delta F / k_B T) \quad (4.5)$$

with  $\Delta F$  the conformational free energy difference;  $X$ , as a modification to the original theory, is used in this case to relate the diffusivity of a chain within a pore space to the macroscopic diffusion coefficient. The fraction of monomer units in the bottleneck,  $\beta$  (noted as  $f$  in reference 31), was given by:

$$\left\{ \begin{array}{ll} \beta = 1 & dC^2 \gg V_P \\ \beta = \frac{QC^{1/v}}{NC} & dC^2 \leq V_P \end{array} \right. \quad (4.6)$$

where  $Q$  (not used in reference 31) is a prefactor determined by  $d$ , monomer unit length, etc.,  $\nu$  is the exponent relating the molecular weight to the polymer size ( $R \propto N^\nu$ ), and  $V_p$  is the volume occupied by the polymer. As  $N$  increases,  $\beta$  asymptotically approaches  $QN^{-1} C^{(1/\nu)-1}$ . By calculating  $\Delta F$  using appropriate weight factors, Muthukumar et al. finally obtained:

$$\frac{D}{XD_0} = \exp \left\{ -N \left[ \frac{\beta}{C^{1/\nu}} + \left( \frac{1-\beta}{Z} - 1 \right) \frac{1}{L^{1/\nu}} \right] \right\} \quad (4.7)$$

where  $Z$  is the average number of cavities which contain  $(1-\beta)N$  unconfined repeating units per gate. It will be shown that there is qualitative agreement between our experimental data and this theoretical prediction.

## B. Effect of Hydrodynamic Drag

### 1. Hindered Diffusion of Starburst-Dendritic Polyamidoamine

The condition  $qR_p \ll 1$  was satisfied for all measurements presented in this chapter. The wavelength ( $2\pi/q$ ) of the fluctuations whose relaxations were monitored by DLS was thus much larger than the pore size. The quantity  $qR_G$  was always in a regime ( $qR_G < 1$ ) suitable for measuring the translational diffusion coefficient of macroscopic diffusion, where  $R_G$  is the radius of gyration of the macromolecule in free solution. The translation of polymer molecules within porous glasses was studied on a time scale, the time for autocorrelation function evolution, at which

polymer chains move distances of many times the pore radius. The study on hindered polymer diffusion at short time scales and on the crossover from single pore diffusion to macroscopic diffusion was presented in Chapter III.

The experimental results of diffusion of dendritic polyamidoamine in porous glasses (G275 and R893) are given in Table 4.1, which lists the values for the hydrodynamic radius of polymers  $R_H$ , the size ratio of polymer to pore  $\lambda_H$ , the polymer diffusivity in free solution  $D_0$ , the macroscopic diffusion coefficient in pores  $D$ , the diffusivity ratio  $D/(XD_0)$ , and the temperature of these DLS measurements. Different temperatures were used because of the slight difference in the index of refraction of the glasses. The solvent for the dendritic polyamidoamines was transdecahydronaphthalene (Aldrich). (See Appendix A for some relevant properties of this solvent).

It was observed by Bishop that the normalized diffusivity ratio  $D/(XD_0)$  versus  $\lambda_H$  superimpose for diffusion of polymers with the same chemical structure diffusing in pores of different pore sizes but similar pore structures[19,20]. It was also observed by Easwar that polymers with different chemical or architectural structures do not have this behavior of superposition[21]. In other words the difference in the behavior of diffusivity ratio versus the size ratio reflects the dependence of diffusion on chemical or architectural structures of the polymer.

The normalized diffusivity ratio  $D/(XD_0)$  versus the size ratio  $\lambda_H$  for the dendritic polyamidoamines is shown in Figure 4.1. The data of diffusion of linear polystyrenes in the same glasses were also plotted in the same figure. The filled triangles were results measured by myself and the

empty triangles were the results obtained by Bishop[19]. The intrinsic conductivity values are:  $X = 0.78$  for R893 (obtained by Bishop), and  $X = 0.89$  for G275 (see Section C of this chapter). These values were based on measured diffusion of polystyrenes in porous glasses. They are used to interpret the diffusion results of the dendritic polyamidoamine, because the intrinsic conductivity is a characteristic of the material independent of the type of diffusant. The diffusivity inside the pores is significantly reduced relative to the unbounded solution, which is generally consistent with most other reported works. We note that  $D/(XD_0)$  of the dendritic polymer decreases with increasing  $\lambda_H$  faster than that of the linear polymer chains. In other words, at the same  $\lambda_H$  the dendritic polymer has a smaller  $D/(XD_0)$  than linear chains, and the larger the  $\lambda_H$  the larger the difference in  $D/(XD_0)$  between the linear flexible macromolecules and the dendritic macromolecules.

The difference in diffusion of linear polystyrene and starburst polyamidoamine can be conceptually understood by taking into account the compressibility of the entire polymer molecule. Inside the volume occupied by the polymer molecule, the dendritic polymer has much less space than the linear polymer. So the conformation adjustment is more difficult for the dendritic polymer, and thus it has much less compressibility. As a result, once inside the confining pores, the dendritic polymer has a larger effective size than the linear polymer with a same free solution hydrodynamic radius. In this eventuality, the hindrance for the larger effective size diffusant is stronger. This view is consistent with other published results[12,21].



Since the dendritic polymer bears more similarity to the hard sphere model, the diffusion results for dendritic polyamidoamines are directly compared to the BG theory[25], by assuming  $R_H$  correctly measures the effective radius in not only free solution but also the confined spaces, i.e.,  $R_H = R_S$ . The curve in Figure 4.1 represents the prediction of Brenner and Gaydos, which was calculated from equations (4.1) and (4.2). We found that the function based on the BG prediction fits the diffusion results of starburst-dendritic polyamidoamine in pores reasonably well (given the experimental uncertainty) *without* any fitting parameter.

The quantitative agreement between BG and our experimental results proved direct applicability of BG (at small size ratio  $\lambda_H$ ) to non-ideal pores such as those of controlled pore glass, if the pores are well connected and have a narrowly distributed pore radius  $R_P$ . This agreement also implies that the nominal pore radius  $R_P$ , measured by mercury intrusion porosimetry under the assumption of cylindrical pore geometry, is a reasonably good measure of the pore dimension that is effectively connected to the transport processes.

Following the methodology of Bishop et al.[19], we also incorporated the scaling parameter  $\kappa$  into the BG theory by equation (4.3) to fit the data of diffusion of dendritic polymer in pores. A least-square fit yielded  $\kappa(\text{dendritic}) = 0.97 \pm 0.06$ . This value is compared to that of the linear polystyrene ( $\kappa(\text{linear PS}) = 0.76 \pm 0.02$ )[19], linear polyisoprene ( $\kappa(\text{linear PI}) = 0.45$ ), 4-arm star-branched polyisoprene ( $\kappa(4\text{-arm}) = 0.83 \pm 0.09$ ) and 8-arm star-branched polyisoprene ( $\kappa(8\text{-arm}) = 0.94 \pm 0.09$ )[21]. Obviously the parameter  $\kappa$ , which correlates the effective

hard sphere radius in free solution ( $R_H$ ) to that in restricted spaces ( $R_S$ ), increases with higher compactness of the diffusant. In spite that  $\kappa(\text{dendritic})$  is close to unity, we should keep in mind that after all the pores are not straight cylinders. It is noted that  $\kappa(\text{dendritic})$  and  $\kappa(8\text{-arm})$  are not significantly different. This is consistent with the observation of Bohrer et al. [12] who found that the 8-arm, 12-arm and 18-arm star polymers had almost the same reduced diffusivity in pores of track-etched membranes, if they have the same hydrodynamic radius.

To summarize the study on the diffusion of dendritic polyamidoamines, we found that dendritic polymer molecules diffuse more slowly than linear polymer molecules with the same  $\lambda_H$ . For this relatively rigid polymer, the hydrodynamic radius  $R_H$  in free solution is very close to the effective radius  $R_S$  in constraining pores, whereas for flexible polymers  $R_H$  and  $R_S$  are generally different. A least square fit using eqs. (4.2) and (4.3) yielded  $\kappa(\text{dendritic}) = 0.97 \pm 0.06$ . The comparison of this  $\kappa(\text{dendritic})$  value against  $\kappa(4\text{-arm})$  and  $\kappa(8\text{-arm})$  shows that the scaling parameter  $\kappa$ , which correlates  $R_H$  to  $R_S$ , increases and approaches an asymptotic value close to unity, with higher compactness of the polymer.

## 2. Hindered Diffusion of Linear Polystyrene at Small $\lambda_H$

The Fickian diffusion law in which displacement is proportional to  $t^{1/2}$  was always observed at condition  $qR_p \ll 1$ . This is true even for very strongly confined polystyrene chains with  $\lambda_H > 1$  in the glasses with small pore radii (G75 and G275). This is shown by the linear relation of  $\log G^{(2)}(t)$  versus  $t$  as exemplified by Figure 4.2.

Some data were also analyzed by inverse Laplace transform, using Provencher's CONTIN program[100], to solve the decay rate distribution  $G(\Gamma)$ . Starting from equation (2.11), this method solves the following equation for  $G(\Gamma)$ :

$$\frac{G^{(2)}(t)}{B} - 1 = \int_0^{\infty} G(\Gamma) \exp(-\Gamma t) d\Gamma \quad (4.8)$$

The ACF decay rate spectrum based on the scattered intensity for the same data in Figure 4.2 is shown in Figure 4.3. This ACF decay rate distribution, equivalent to diffusion rate distribution, is broader than that of macroscopic diffusion at low size ratios, but narrower than that of diffusion in the single pore diffusion region ( $qR_p > 1$ ) and the transition region ( $qR_p \approx 1$ ).

A less accurate measure of the polydispersity of diffusion rate distribution was provided by the least squares fit to equation(2.35). The normalized variance  $V$  (equation 2.36), referred to as polydispersity, was obtained from the results of the fitting. For diffusion in free solution,  $V \approx 0.02$  corresponding to the slight polydispersity of the polymer molecular weights. For the diffusion in the porous glasses, typically  $V \approx 0.1$  for the porous glasses G75 at all  $\lambda_H$  values and G275 at  $\lambda_H < 0.5$ ;  $V \approx 0.2$  for G275 at  $\lambda_H > 0.5$ . Considering the nonuniformity of the pores and the small but still significant molecular weight polydispersity which tends to broaden the diffusion rate distribution more strongly than in free solution because of the increasing molecular weight dependence[109], it seemed justified to treat diffusion within the pores in terms of a single mode

process and therefore to use second cummulant fitting as the main data analysis method. All the measured diffusion coefficients in this chapter were based on this analysis method.

The hindrance factor  $D/D_0$  versus the size ratio  $\lambda_H$  for the polymer in the glass G275 is shown in Figure 4.4;  $D/D_0$  decreases monotonically with  $\lambda_H$  as expected. The intrinsic conductivity[6, 108] of the porous glass G275 was obtained by extrapolating the data points to  $\lambda_H = 0$ . It was found that  $X = 0.89$ , in agreement with what one would expect for this type of glass. Pismen[110] proposed a formula (equation 4.9) to calculate tortuosity (T) for diffusion in a porous solid composed of random structural pore elements chaotically connected with one another, his results was,

$$X = \frac{1}{T} = 1 - \frac{2}{3} (1+\phi)(1-\phi)^{2/3} \quad (4.9)$$

The calculated inverse tortuosity (using equation 4.9) for G275 (porosity  $\phi = 0.74$ ) is  $X = 0.85$ .

The broken line in Figure 4.4 represents the function obtained by combining equation (4.1) and Davidson's prediction[9, 15], equation (4.4). The experimental data were in good agreement with this hydrodynamic theory up to  $\lambda_H \approx 0.3$ . This is noteworthy in several respects. First, no adjustable fitting parameter such as  $\kappa$  was necessary. Second, equation (4.4), for the hydrodynamic effect, was directly tested. In Davidson's study, the product of  $\phi K^{-1}$  was measured and compared to the theory, it being noted that the partition coefficient  $\phi$  itself is often complicated by other factors such as specific interaction between the polymer and the pore

wall[9]. Although equation (4.4) was expected to be valid up to  $\lambda_H \approx 0.8$ , agreement with the data clearly deteriorates for  $\lambda_H > 0.3$ .

### C. Diffusion of Polymer Chains under Strong Confinement

Diffusion in the strong confinement regime is of great interest, both theoretically and practically. Many unique features of polymer are reflected in this regime, thus distinguishing polymers from small molecule diffusants. By using controlled pore glasses with small pore radii we were able to perform light scattering measurements at very high  $\lambda_H$ , which had previously been unattainable. We have achieved measurements of diffusion coefficients at size ratios as high as  $\lambda_H = 1.4$ .

At  $\lambda_H > 1$ , the scattering from within the glass fragment gave a well defined autocorrelation function indicating a finite polymer concentration inside the pores. This is somewhat surprising in view of the existing theories[111,112] and a Monte Carlo simulation[113] which indicate that equilibrium partitioning coefficients are expected to become negligible as  $\lambda_H$  approaches 1. Apparently polymer chains can enter the pores to a reasonable extent notwithstanding their deformation by the pore walls. This evidence of compression of a polymer molecule by the pore walls also lends support to the interpretation in Section B of this chapter, in which the dependence of diffusion on molecular architecture was attributed to the difference in compressibility.

The molecular weight dependence of diffusion is shown in Figure 4.5. When  $\lambda_H$  is close to zero, the hydrodynamic interactions between the

polymer and the pore wall vanishes, so that the diffusion behavior in free solution given by  $D \propto M^{-\nu}$ , is retained as was demonstrated previously [19]. Within the range,  $0.2 < \lambda_H < 0.5$ , the slope is nearly equal to  $-1$  for both glasses thus resembling Rouse behavior[29,114,115]. The Oseen tensor[114] which describes the flow perturbation and the hydrodynamic interaction vanishes at distances large compared the pore dimension, and long range monomer-monomer interactions (which result in an excluded volume effect in free solution) are, for the most part, screened by the pore walls. Though this regime is not wide enough to exhibit distinct Rouse molecular weight dependence, the straight line of slope  $-1$  in Figure 4.5 is intended to show the trend of the data in the intermediate  $\lambda_H$  region. The diffusion behavior in the entire  $\lambda_H$  range should rather be viewed as a continuously evolving process influenced by several factors each manifesting itself to a different extent depending on the degree of confinement.

The scaling theories of Brochard and de Gennes et al.[27-30] which explained membrane transport phenomena successfully were examined for their applicability to polymer diffusion in non-ideal pores. By modeling a flexible polymer chain trapped in a cylindrical pore as an "elongated cigar" with elementary units of the same size as the pore diameter, de Gennes et al. made the scaling prediction

$$D/D_0 \sim \lambda_H^{-2/3} \quad (4.10)$$

Figure 4.6 is a logarithmic plot of hindrance factor  $D/D_0$  versus the size ratio  $\lambda_H$ . The lower left box shows the data points encompassed in the

dashed box in an expanded form. It can be seen that the size ratio dependence  $\lambda_H^{-2/3}$  does not persist through high confinements; instead deviation occurs at  $\lambda_H \approx 0.6$ . Obviously, our results do not support the application of the “elongated cigar” model to pores with non-ideal geometry at very high confinements.

When  $\lambda_H > 0.6$ ,  $D/D_0$  decreases with  $\lambda_H$  more quickly than  $D/D_0 \propto \lambda_H^{-2/3}$ . From the empirical relation between the radius of gyration and the hydrodynamic radius of polystyrene:  $R_G \approx 1.45R_H$ [116],  $\lambda_H \approx 0.6$  is equivalent to  $\lambda_G = R_G/R_P \approx 0.9$ . Therefore, the beginning of the stronger molecular weight dependence is related to the situation in which the dimension of the polymer is approximately the same as the cross sectional pore size. When the polymer equivalent diameter is larger, its conformation must adjust to suit the local pore structure as it moves within the pore space. The sections of the pores in which the entropy of the polymer chain must decrease, e.g. narrow necks, strongly hinder chain motion. This is a major cause of the stronger dependence of  $D$  on molecular weight in the regime  $\lambda_H > 0.6$  for the porous glasses. For uniformly cylindrical pores, there is no entropy change requirement.

Figure 4.7 is a possible schematic of the structure of the controlled pore glasses used in these experiments. The important features[117] which are incorporated in the diagram are: 1) the pores are highly connected; 2) microscopic non-uniformity of the local pore dimension exists as a result of the manufacturing process; 3) the smallest openings in the pore space (shaded areas) are quite uniform in size. It is known that the pore size distribution obtained from mercury intrusion porosimetry reflects the radii

of the *restricted* passages, through which all volume is accessible[93,94]. Thus the narrower distribution of  $R_p$  measured by mercury intrusion in our samples suggest a relatively uniform size of minimum passage opening. The scanning electron micrographs in references 19 and 20 support this view. In comparing Figure 4.7 with the "cavity and bottleneck" model we can see that the scaling model for the entropy barrier[31] is appropriate in describing the conformational change accompanying diffusion of strongly confined polymer chains in pores; the parameter  $C$  is identified with  $R_p$ .

Figure 4.8 shows plots of  $1/M \log(D/D_0)$  versus  $1/M$ , for glass G275 (in (a)) and G75 (in (b)), as suggested by equation (4.7) which reduces to

$$\frac{\ln(D/D_0)}{N} = \frac{\ln X}{N} + (C^{-1/\nu} - L^{-1/\nu}) \quad \text{if } \beta = 1 \quad (4.11)$$

or

$$\frac{\ln(D/D_0)}{N} = \frac{\ln X - Q/C}{N} + \left[ \frac{(1-\beta)}{Z} - 1 \right] L^{-1/\nu} \quad \text{if } \beta = \frac{QC^{1/\nu}}{NC} \quad (4.12)$$

A tangent of more negative slope at the larger  $M$  (or  $N$ ) regime is consistent with the predictions of equations (4.11) and (4.12). A transition is thus implied, from a  $\beta = 1$  regime at small  $N$  in which an entire chain may be accommodated in a bottleneck, to a  $\beta < 1$  regime at large  $N$  in which only a fraction of the polymer chain can be contained. The transition in Figure 4.8 and the deviation from  $D/D_0 \propto \lambda_H^{-2/3}$  in Figure 4.6 occur at similar molecular weights which are equivalent to the situation  $R_G \approx R_p$ . These facts suggest that the stronger molecular weight dependence is due to the entropy barrier, and that the entropy barrier enters when the size of the



polymer is approximately the same as the cross-sectional size of the pores. Furthermore, the difference in slope between the extremes in the two regimes for G75 is larger than that for G275. In equations (4.11) and (4.12) this difference is represented by  $Q/C$ . The ratio of the differences in slope is similar to the inverse ratio of the pore sizes, suggesting that the term  $Q/C$  (or equivalently  $Q/R_P$ ) may indeed account for the observed transition.

The semi-quantitative agreement between the experimental data and the entropy barrier model indicates the importance or even the dominance of the entropy change on the dynamics of highly confined polymer chains in pores with non-uniform geometry. Since  $R_P$  measures the dimensions of narrow passages whose counterparts in the model are bottlenecks,  $\lambda_H$  does reflect the determining confinement at larger ratios of polymer to pore sizes. Consequently a low  $\lambda_H$  polydispersity (assured by a low polydispersity in  $R_P$  and molecular weight) ensures a low dispersion of the diffusion coefficients as observed in Figures 4.2 and 4.3.

We note that Muthukumar's scaling analysis for the entropy barrier, [31] from which equations (4.7), (4.11) and (4.12) were drawn, was based on a model of cavities connected by short bottlenecks. Realistically it is the variation in local pore size that gives rise to the entropy barrier. Useful information can be obtained from nuclear magnetic relaxation analysis which allows characterization of the true distribution in pore sizes[32].

#### D. Diffusion of Polystyrenes in Vycor Glass with Very Small Pores

Vycor glasses are commercial products of Corning Glass Works. It has many applications, especially for adsorption and separation of compounds, due to its thermal, mechanical and chemical stability. Diffusion of small molecules in Vycor porous glasses has been studied by different techniques, such as FRS[118], polarized picosecond transient grating experiment[119], PFGNMR[33], constant volume method[120], and tracer method[121]. Among these studies, the FRS diffusion measurement by Dozier et al.[118] is most directly comparable with our measurements of polystyrene diffusion in porous glasses by DLS, as the techniques in both studies are similar and the porous glass studied is the same (Vycor 7930). Those authors found that the diffusion of azobenzene molecules in Vycor glass was 2 orders of magnitude slower than in free solution, which was interpreted by a parallel-pore model and by a fractal pore structure model. Both these interpretations are doubtful. This was the major motivation of our study on diffusion in Vycor. We suspected that in Dozier's work surface adsorption could be dominant in reducing diffusivity inside the pores of Vycor, and therefore we treated the internal surfaces of Vycor to prevent adsorption. The surface treatment procedures are described in Section D of Chapter II.

The porous material used in this study is Vycor 7930 (Corning). It was made by a phase separation and leaching process[91,92]. It has a narrow pore size distribution with an average pore radius of 20Å. Its porosity is 28%, and its internal surface area is 200 m<sup>2</sup>/g. All these data

were provided by the manufacturer. The pore structures of CPG and Vycor are fundamentally the same, except that Vycor had not undergone a final controlled etching (by NaOH) to remove the silica deposits from SiO<sub>2</sub> initially present in the Na<sub>2</sub>O-B<sub>2</sub>O<sub>3</sub> rich phase[90-92], and thus Vycor has more surface irregularities than CPG. SANS and SAXS measurements showed power law between scattering intensity and squared wavevector, corresponding to a surface fractal dimension of 2.4, notwithstanding the controversial fractal properties of Vycor glass, while CPG has a surface fractal dimension of 2.2[122].

The decay rate ( $1/\tau$ ) of DLS autocorrelation function versus the squared wavevector  $q^2$  for a polystyrene fraction (MW=7,000) in Vycor glass is shown in Figure 4.9. The linear relation between  $1/\tau$  and  $q^2$  indicates that the macroscopic diffusion is governed by Fick's diffusion law. Figure 4.10 shows the hindrance factor  $D/D_0$  as a function of size ratio  $\lambda_H$ . The curve in Figure 4.10 is intended to show the trend of the data points.

Figure 4.10 was compared to the diffusion results in a similar porous material — controlled pore glass (CPG, Shell Development Co.) shown in Figure 4.4. We found general agreement between these two sets of results in terms of the magnitude and trend of decreasing  $D/D_0$  with  $\lambda_H$ . The polymer diffusion results for Vycor were not extensive, limited by the very small pore size and weak scattering from low molecular weight polymers. Nevertheless these results, in the range  $0.64 \leq \lambda_H \leq 1.35$ , demonstrate the same trend as observed for polystyrene diffusion in CPGs.

It is difficult to extract a value of intrinsic conductivity  $X$  [6,108,110] for this Vycor glass. A very rough estimate yields  $X = 0.3-0.7$ . We also used Equation (4.9) to calculate the tortuosity of the Vycor glass ( $\Phi = 0.28$ ) and the result was  $X = 0.48$ , in agreement with our experimental finding.

Our results are compared to the work of Dozier et al.[118] Those authors measured diffusion coefficient of an azobenzene molecule ( $R_H \approx 3\text{\AA}$ ) in the same Vycor glass using FRS, and they observed puzzlingly slow dynamics: diffusion in this porous glass was 2 orders of magnitude lower than that in free bulk solution. The smallest polystyrene fraction used in this study ( $MW = 2,500$ ,  $R_H = 12.8 \pm 0.2\text{\AA}$ ) has a value of  $D/D_0 = 0.105 \pm 0.006$ , though its size is much larger than azobenzene.

We suggest that the very strong hindrance to diffusion in Dozier's work be attributed to surface adsorption of molecules by glass surfaces. This "sticking" effect is not rare in our studies for porous materials with untreated surfaces. In DLS experiments, the adsorption of pure polystyrene on the surfaces of CPG and Vycor can be satisfactorily suppressed by silanizing the glass surfaces. But in FRS experiments, even the surface-treated Vycor still adsorbs dye-labeled polystyrene chains to some extent.

The attribution of the unusually slow diffusion in Dozier's work to adsorption effect is supported by the rotational relaxation measurement[119] of azobenzene in Vycor 7930 treated the same way as by Dozier et al. That measurement showed a drastic decrease in diffusion rate

even on a microscopic scale, which was interpreted in terms of “sticking” effects of pore walls.

### E. Conclusions

Macroscopic diffusion of starburst-dendritic polyamidoamine and linear polystyrene molecules within porous glasses (including CPG and Vycor) was studied directly by DLS, under macroscopic equilibrium. The Fickian diffusion law was observed for movement of all polymers in porous glasses up to very high confinements. The dependence of the macroscopic diffusion coefficient on molecular weight and polymer-to-pore size ratio was investigated.

At small  $\lambda_H$ , hydrodynamic interactions dominated the diffusion behavior. The study of the dependence of hydrodynamic interactions on the molecular architecture was extended to diffusion measurements of starburst-dendritic polyamidoamines in porous glasses. At the same  $\lambda_H$ , a dendritic polymer molecule diffuses more slowly than a linear polymer chain, which is attributed to less compressibility of the dendritic polymer because of its higher structural compactness. Within the range of size ratio studied,  $0.03 \leq \lambda_H \leq 0.23$ , the diffusion results were in quantitative agreement with the BG theory for hard sphere diffusion[25], with the assumed relation  $R_S = R_H$ . A least square fit to equations (4.1) and (4.2) yielded  $\kappa(\text{dendritic}) = 0.97 \pm 0.06$ , which was compared to the values of  $\kappa(4\text{-arm})$  and  $\kappa(8\text{-arm})$ ; the scaling parameter  $\kappa$  that correlates  $R_H$  to  $R_S$  increased with higher molecular compactness.

Diffusion of a very wide size range of polystyrenes in two controlled pore glasses with small pore radii has been studied. The diffusion measurement was extended to a regime of strong confinement, with  $\lambda_H$  as high as 1.4, permitting us to acquire more insight into transport of flexible polymers in tortuous pores which are parallel over small dimensions. At small  $\lambda_H$  when the diffusion behavior is controlled by hydrodynamic interactions, our results are in good agreement with the predictions based on the hydrodynamic theory of flexible chains. In the intermediate range,  $0.2 < \lambda_H < 0.5$ , the diffusion coefficient tends to be inversely proportional to molecular weight, a result stemming from the screening effect of the pore walls. Our results are also compared to the "elongated cigar" model[27-30] which predicts that  $D/D_0 \propto \lambda_H^{-2/3}$  for a good solvent in very high confinement regimes ( $\lambda_H > 2$ ). At  $\lambda_H > 0.6$ , we observed a size dependence stronger than  $D/D_0 \propto \lambda_H^{-2/3}$ , which is attributed to hindrance due to entropy changes. This makes the "elongated cigar" model inapplicable for high confinement situations in pores of variable cross section. We suggest that the variation in local pore size imposes restrictions on polymer conformations and thus requires conformational entropy adjustments for polymer movement, which greatly hinders diffusion. Our experimental data are consistent with a scaling model of these entropy barriers[31].

We also measured diffusion of polystyrenes in a Vycor glass, motivated by the doubtful results and interpretation of Dozier et al.[118]. The hindrance factor  $D/D_0$  as a function of size ratio  $\lambda_H$  is in agreement with our studies on diffusion in controlled pore glasses. The value of  $D/D_0$

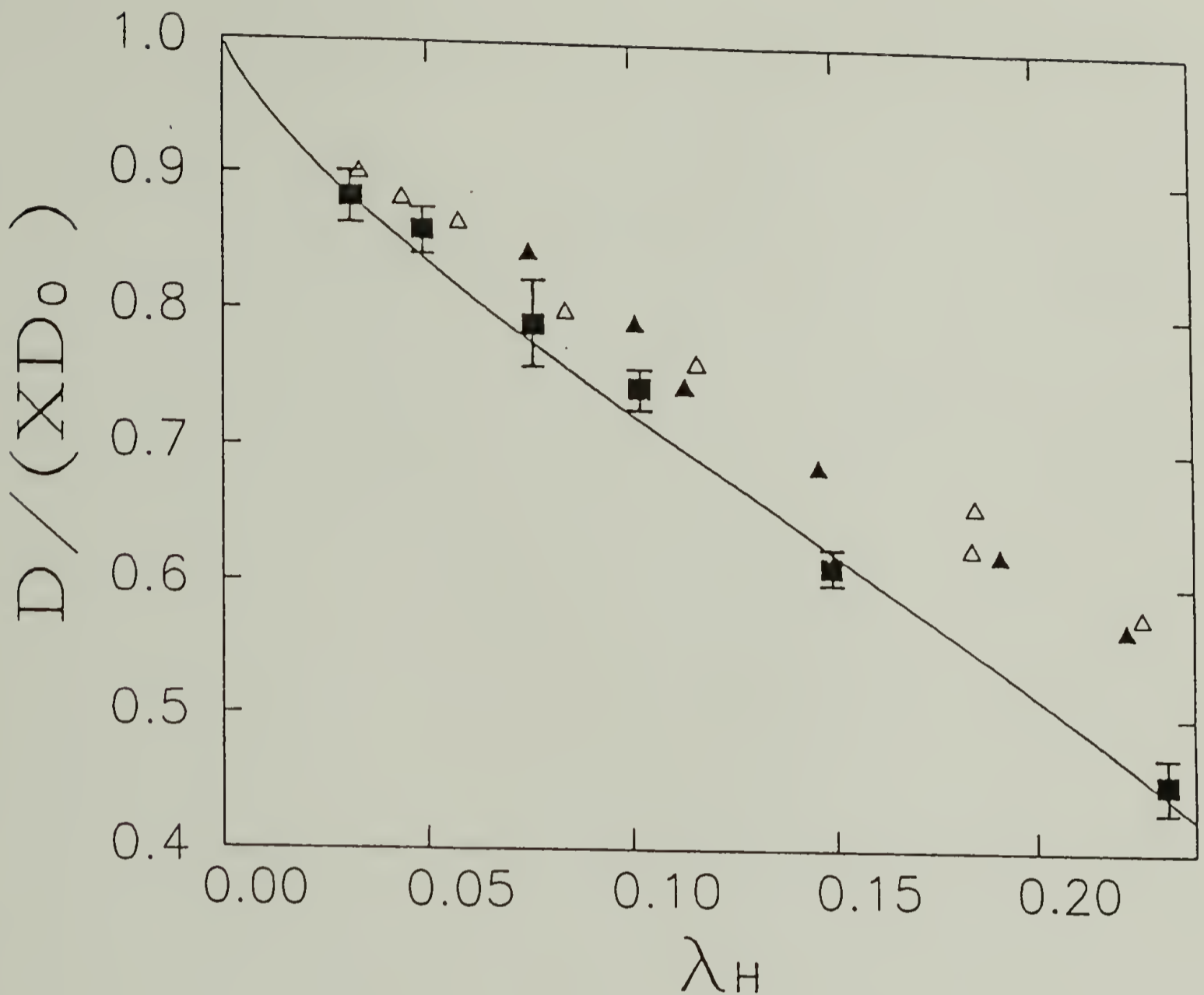
for the smallest polystyrene ( $R_H = 12.8 \pm 0.2 \text{ \AA}$ ) diffusing in Vycor is approximately 1 order of magnitude larger than that of a smaller diffusant (azobenzene,  $R_H \approx 3 \text{ \AA}$ ) in the same porous material reported by Dozier et al. We attribute the difference in diffusion between our measurements and Dozier's to "sticking" effects due to adsorption on the pore walls.

Table 4.1

Hydrodynamic radius( $R_H$ ), size ratio( $\lambda_H$ ), diffusivity in unbounded solution( $D_0$ ), macroscopic diffusion coefficient( $D$ ), and diffusivity ratio( $D/(D_0X)$ ) for starburst-dendritic polyamidoamine in porous glasses

Genera- tion	Glass	Temp (°C)	$R_H$ (Å)	$\lambda_H$	$D_0$ ( $10^{-7}\text{cm}^2\text{s}^{-1}$ )	$D$ ( $10^{-7}\text{cm}^2\text{s}^{-1}$ )	$D/(D_0X)$
5	R893	35	29	0.032	4.79	3.30	$0.883\pm 0.019$
7	R893	35	44	0.049	3.15	2.11	$0.859\pm 0.016$
10	R893	35	68	0.076	2.02	1.24	$0.790\pm 0.032$
5	G275	23	28	0.102	3.76	2.49	$0.744\pm 0.015$
7	G275	23	41	0.149	2.57	1.40	$0.612\pm 0.013$
10	G275	23	64	0.233	1.64	0.66	$0.451\pm 0.020$





**Figure 4.1** The ratio of the diffusivity,  $D/(XD_0)$ , for dendritic polyamidoamines in porous glasses R893 ( $R_p=893\text{\AA}$ ) and G275 ( $R_p=275\text{\AA}$ ) versus the size ratio  $\lambda_H$  (filled squares). These results are compared to the diffusion of linear polystyrene and a hydrodynamic theory. The filled triangles represent the hindered diffusion of polystyrene in R893, [19] and the empty triangles represent that in G275. The curve in the figure corresponds to the hydrodynamic theory by Brenner and Gaydos (equation 4.2). [25]

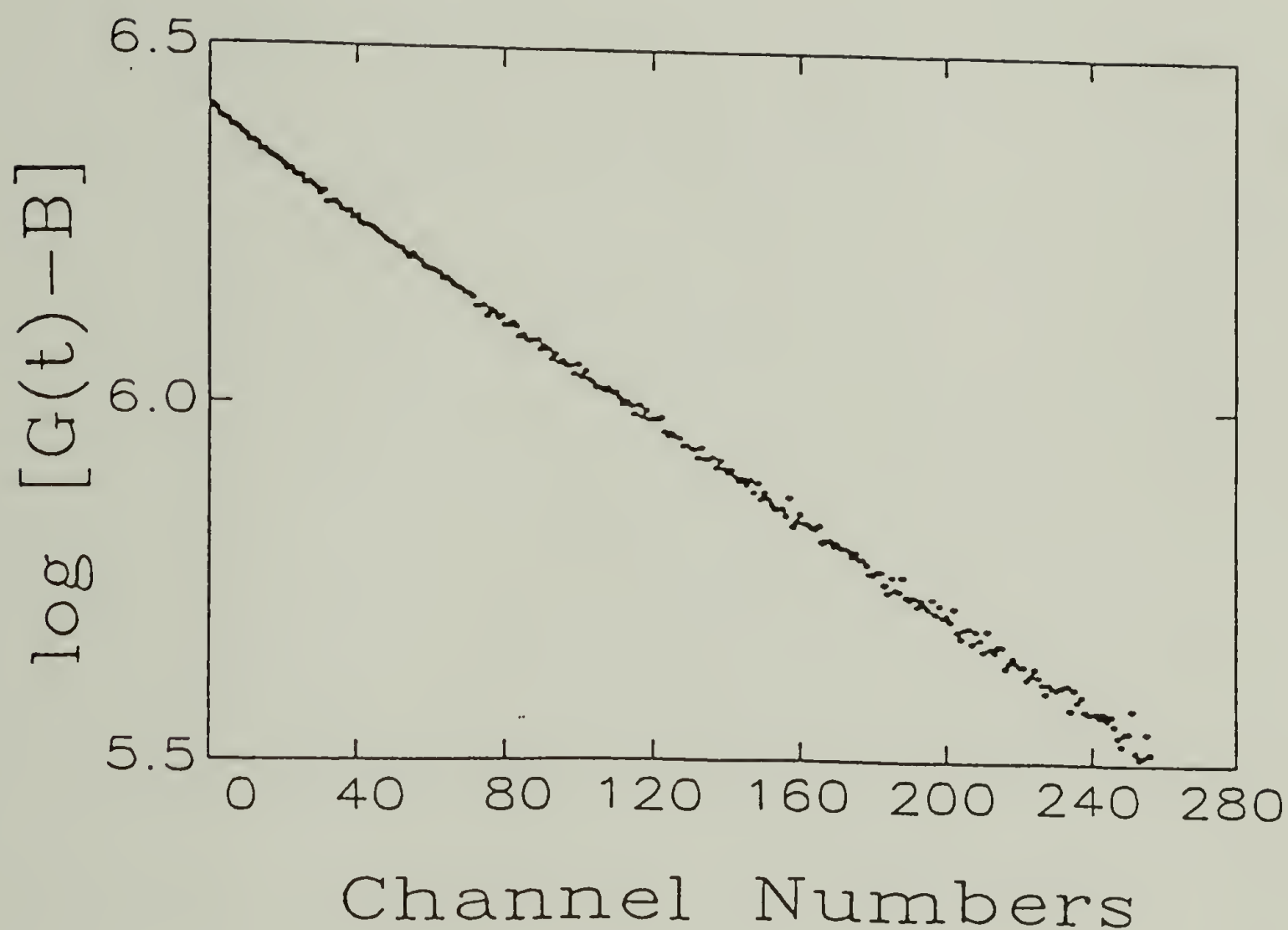


**Figure 4.2** Semilogarithmic plot of the intensity autocorrelation function for polystyrene P100 in glass G75 ( $\lambda_H = 1.01$ ) measured at a scattering angle of  $35^\circ$ . Each channel corresponds to a  $30 \mu\text{s}$  sample time. The last channel baseline (delayed by 1024 channels) was used.

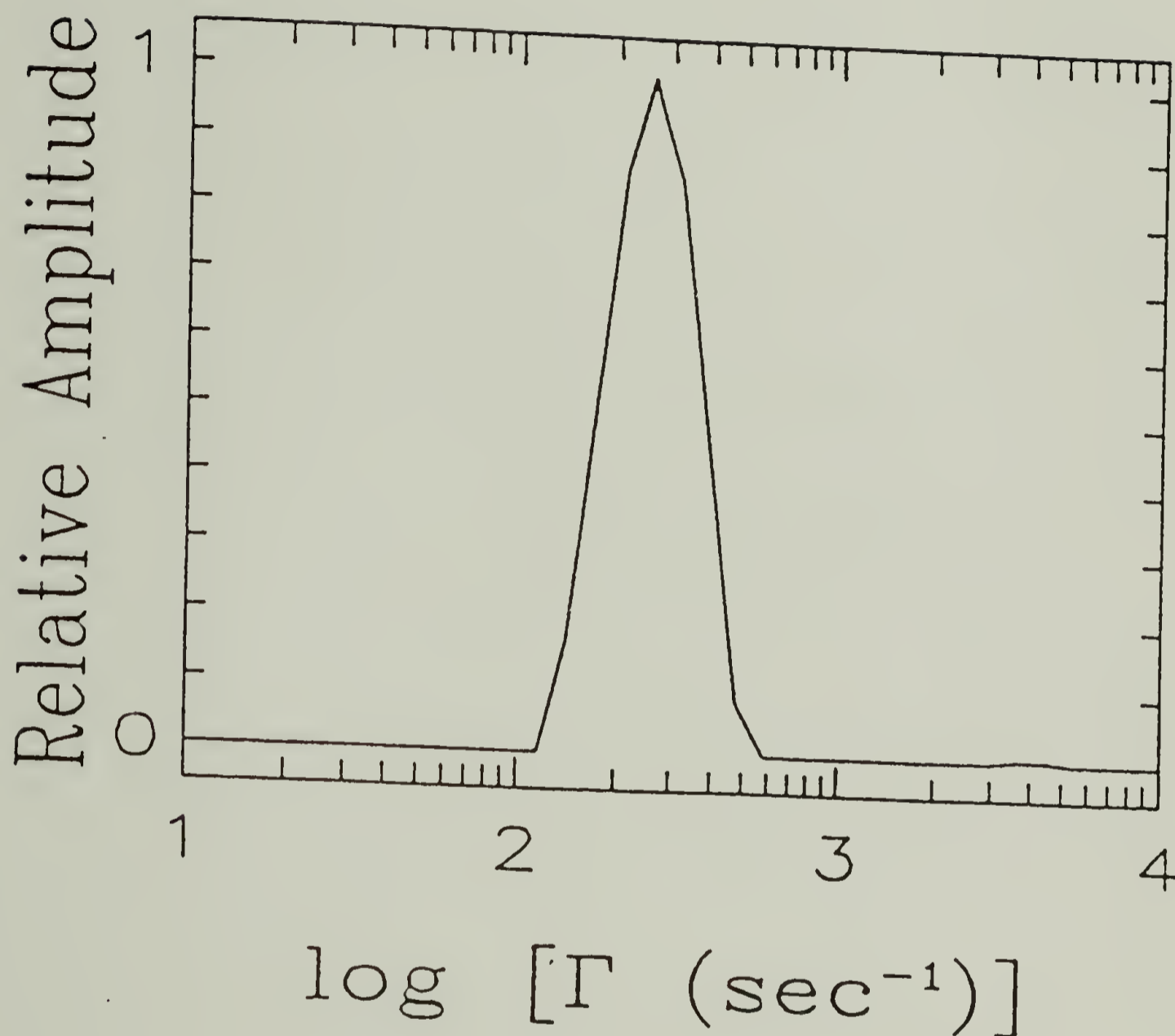
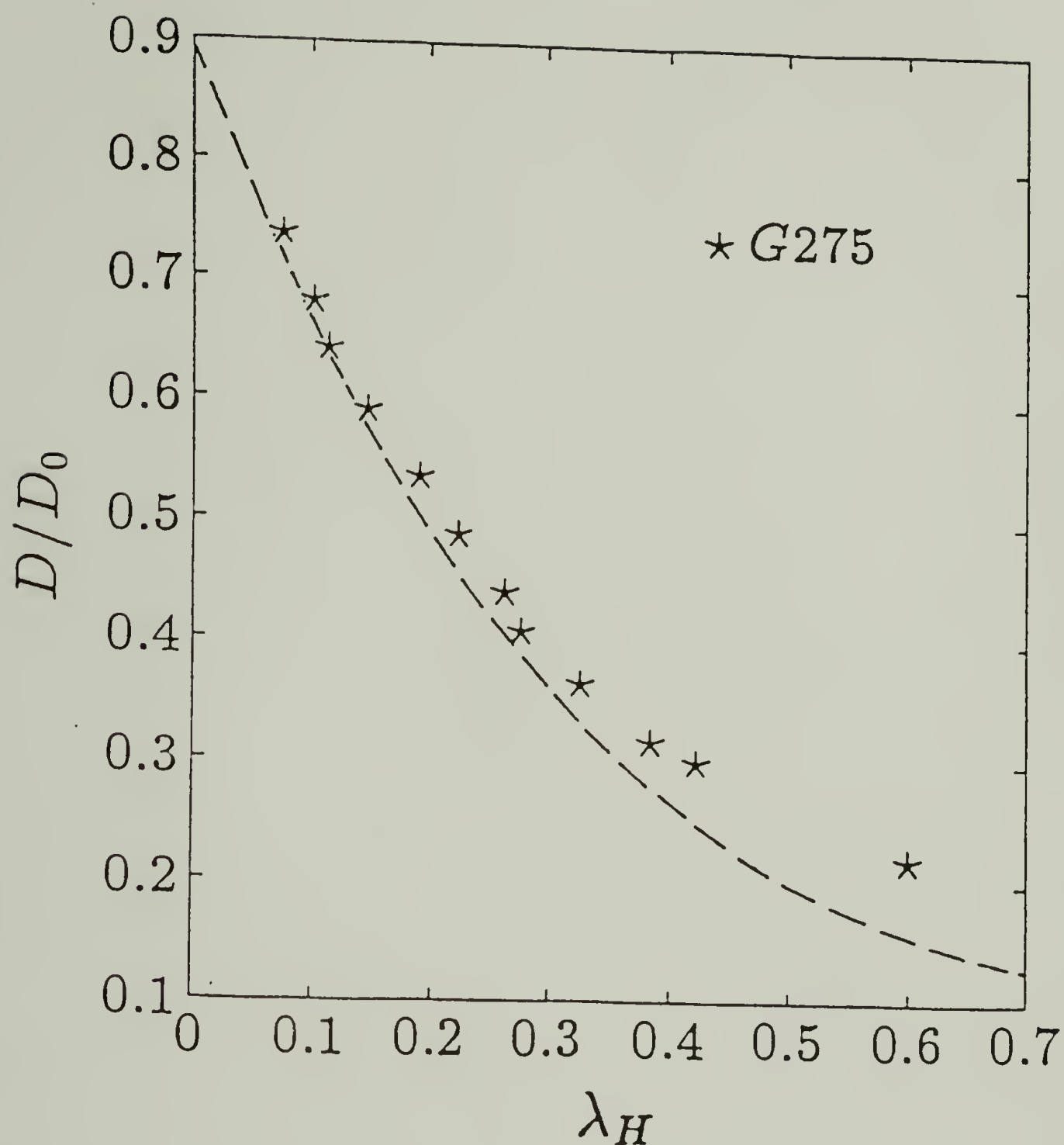
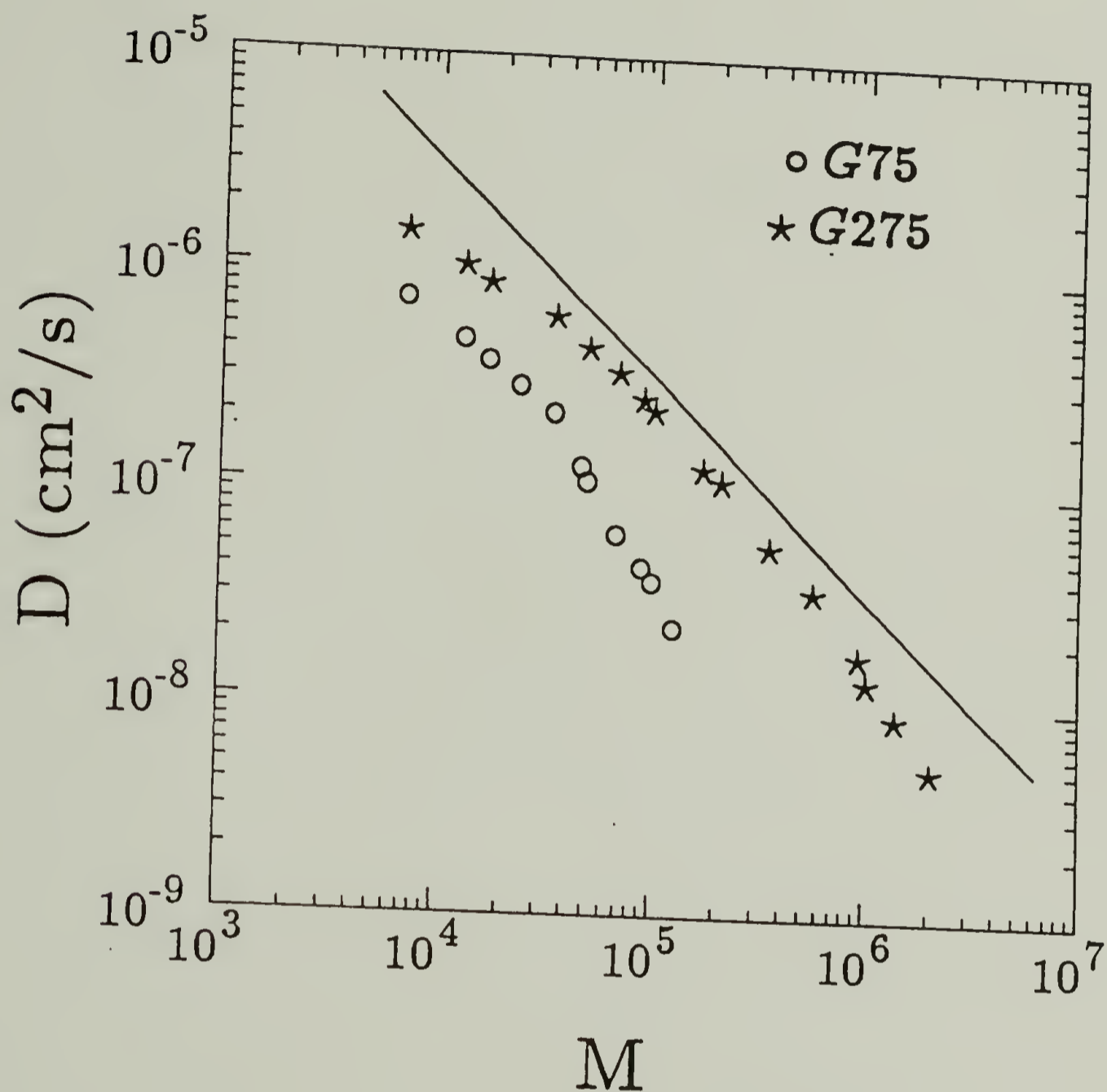


Figure 4.3 Autocorrelation decay rate spectrum based on scattered intensity, calculated from the ACF shown in Figure 4.2 using CONTIN program. [100] The macroscopic diffusion coefficient for this system is  $3.6 \times 10^{-8} \text{ cm}^2/\text{s}$ .



**Figure 4.4** Hindrance factor for macroscopic diffusion ( $D/D_0$ ) versus polymer to pore size ratio ( $\lambda_H$ ). These data are compared to the hydrodynamic theory of a flexible macromolecule in a cylindrical pore. The broken line represents the function  $D/D_0 = Xf(\lambda_H)$ , with  $X = 0.89$  and  $f(\lambda_H)$  from equation (4.4), the theoretical prediction of Davidson et al. [9, 15] Only the lower part of the  $\lambda_H$  range studied is shown here.



**Figure 4.5** Molecular weight dependence of the macroscopic diffusion coefficients of polystyrene fractions ( $7 \times 10^3 < M < 2.05 \times 10^6$ ) inside the porous glasses G75 and G275. The straight line has a slope of  $-1$ , which represents the Rouse molecular weight dependence.

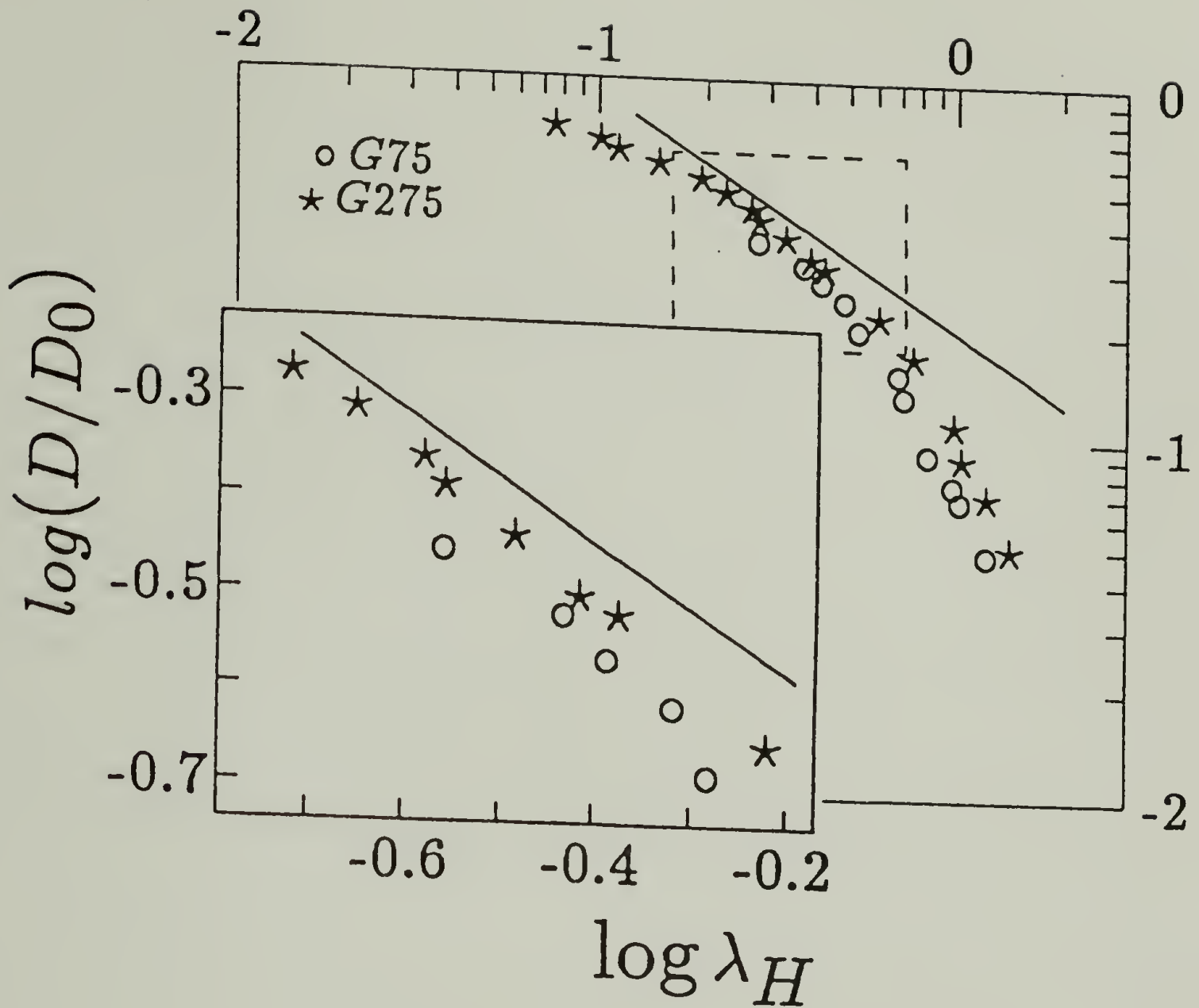


**Figure 4.6** Logarithmic plot of the hindrance factor ( $D/D_0$ ) versus size ratio ( $\lambda_H$ ). The straight lines have slopes of  $-2/3$  representing the scaling prediction of Brochard and de Gennes. [28] An expanded view of the region enclosed by the dashed lines is shown in the bottom left corner.

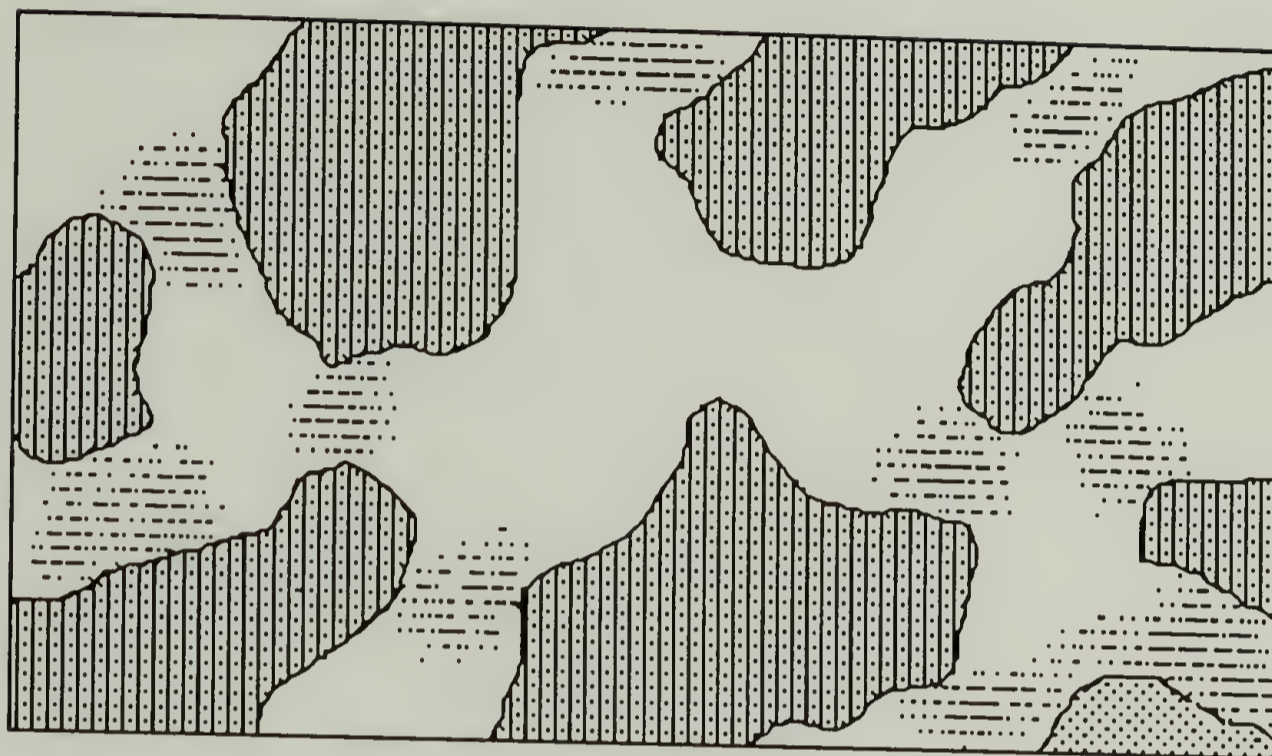


**Figure 4.7** A schematic representation of the pore structure. The areas with gridlines represent the glass matrix. The shaded areas inside the pores represent the narrowed passages which play an important role in determining the dynamic behavior of the polymer at large  $\lambda_H$ .

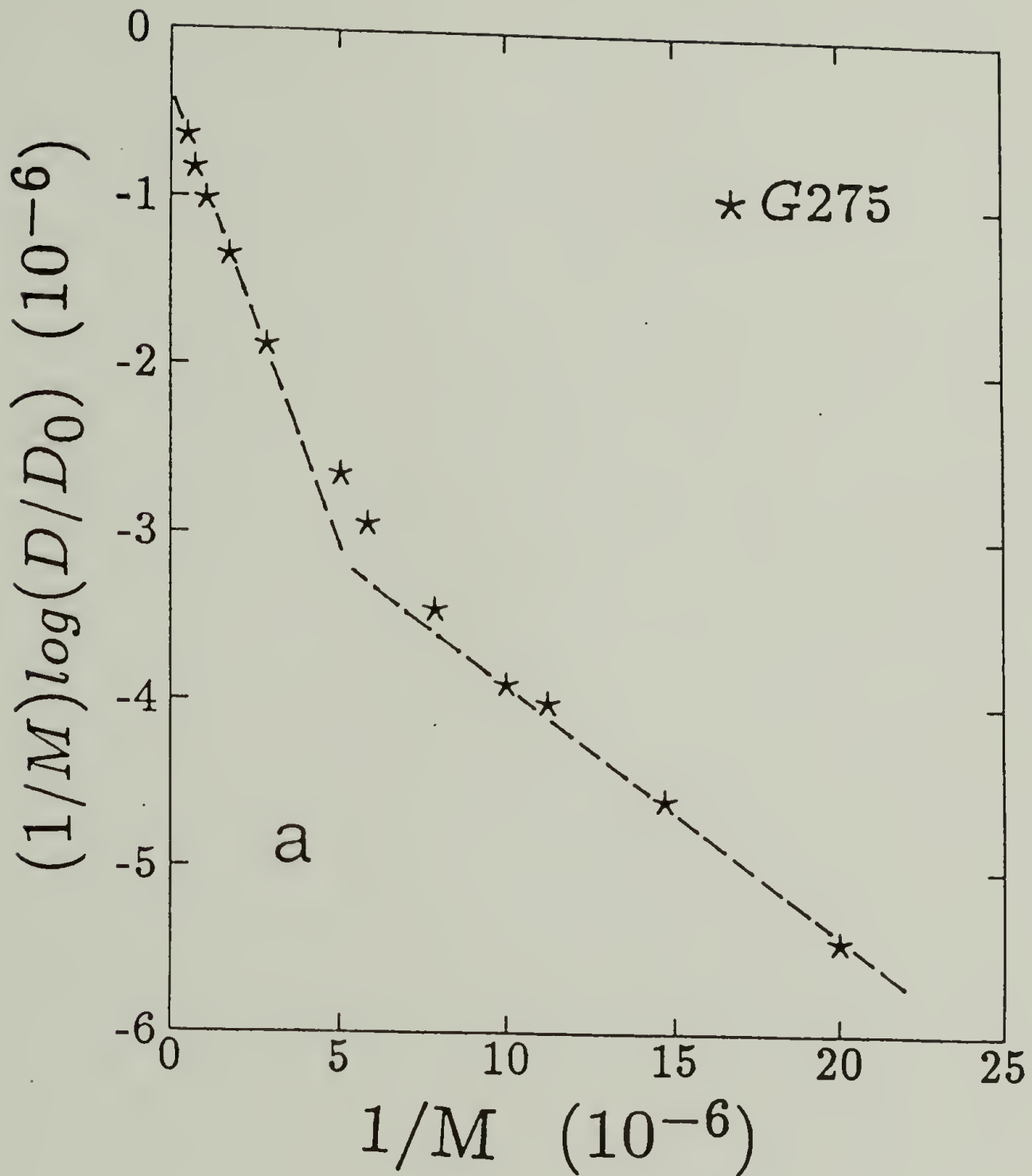
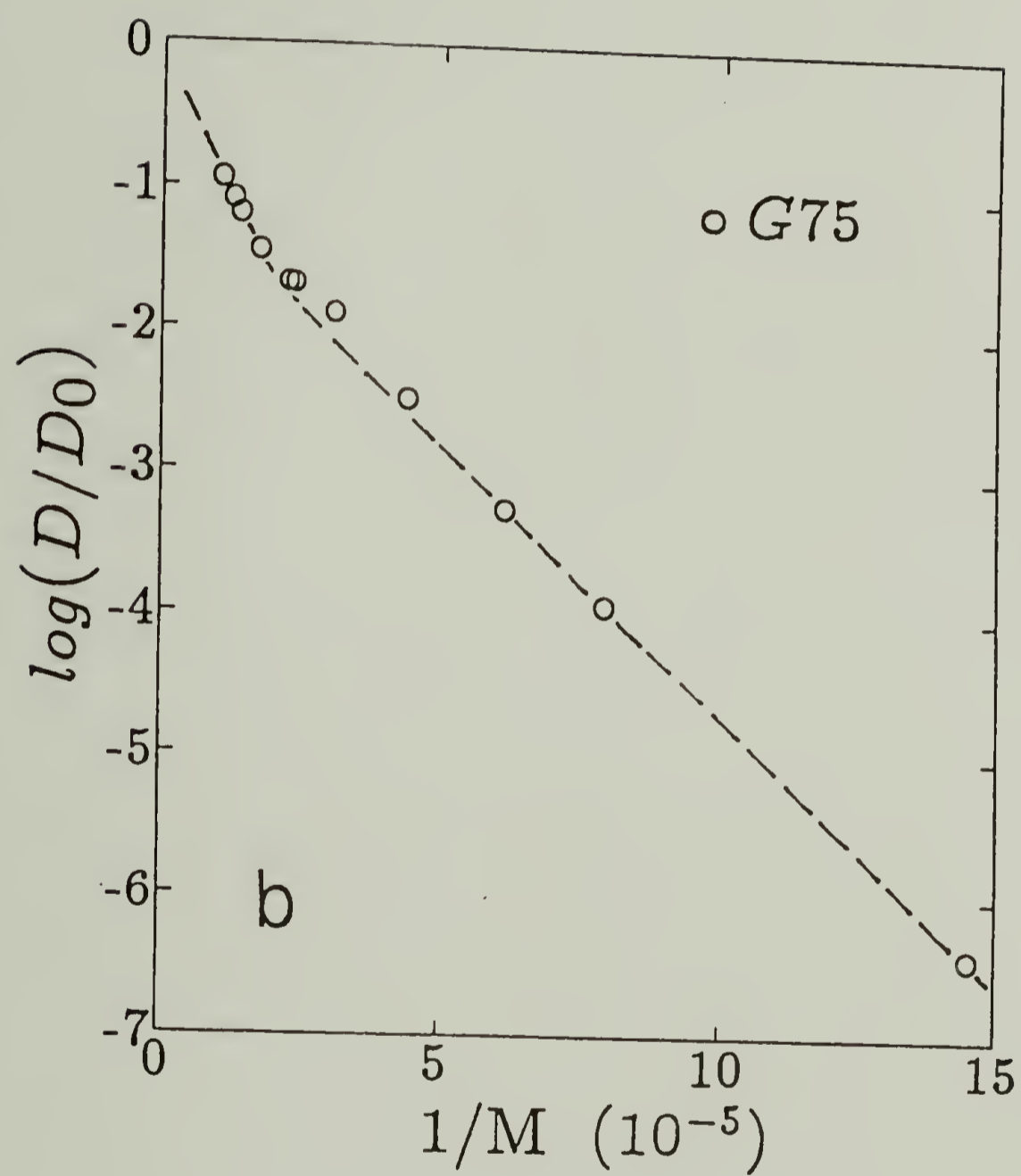
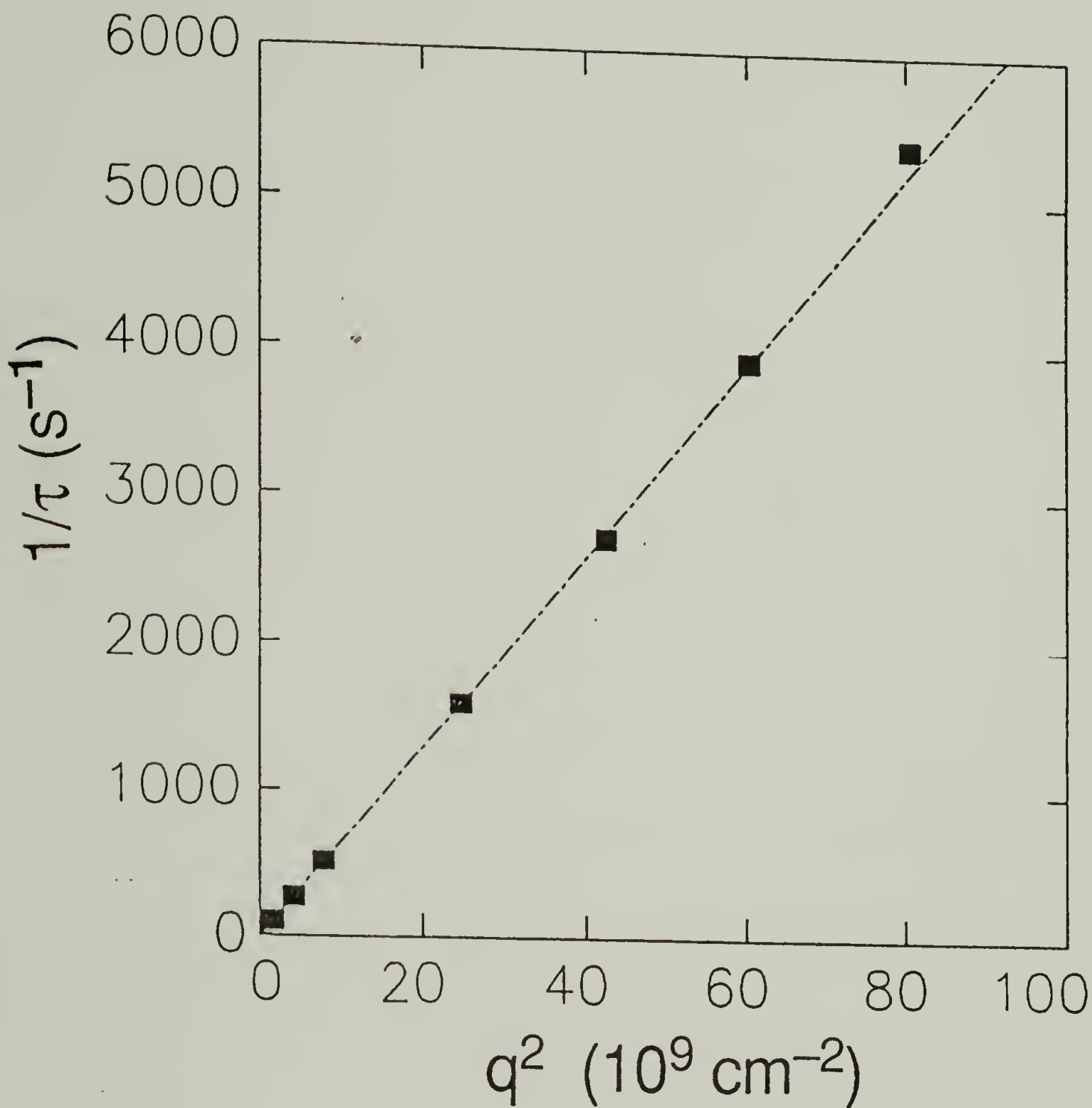


Figure 4.8 A comparison of the experimental data to the predictions of the entropy barrier theory, [31] a) glass G275; b) glass G75. The broken lines are tangent to the data points at the two extremes of the molecular weight range studied.

(to be continued on the next page)







**Figure 4.9** Decay rate of DLS autocorrelation function ( $1/\tau$ ) versus squared wavevector  $q^2$ , for polystyrene (MW=7,000) in Vycor glass. The straight line is a least square fit; the slope defines the macroscopic diffusion coefficient.

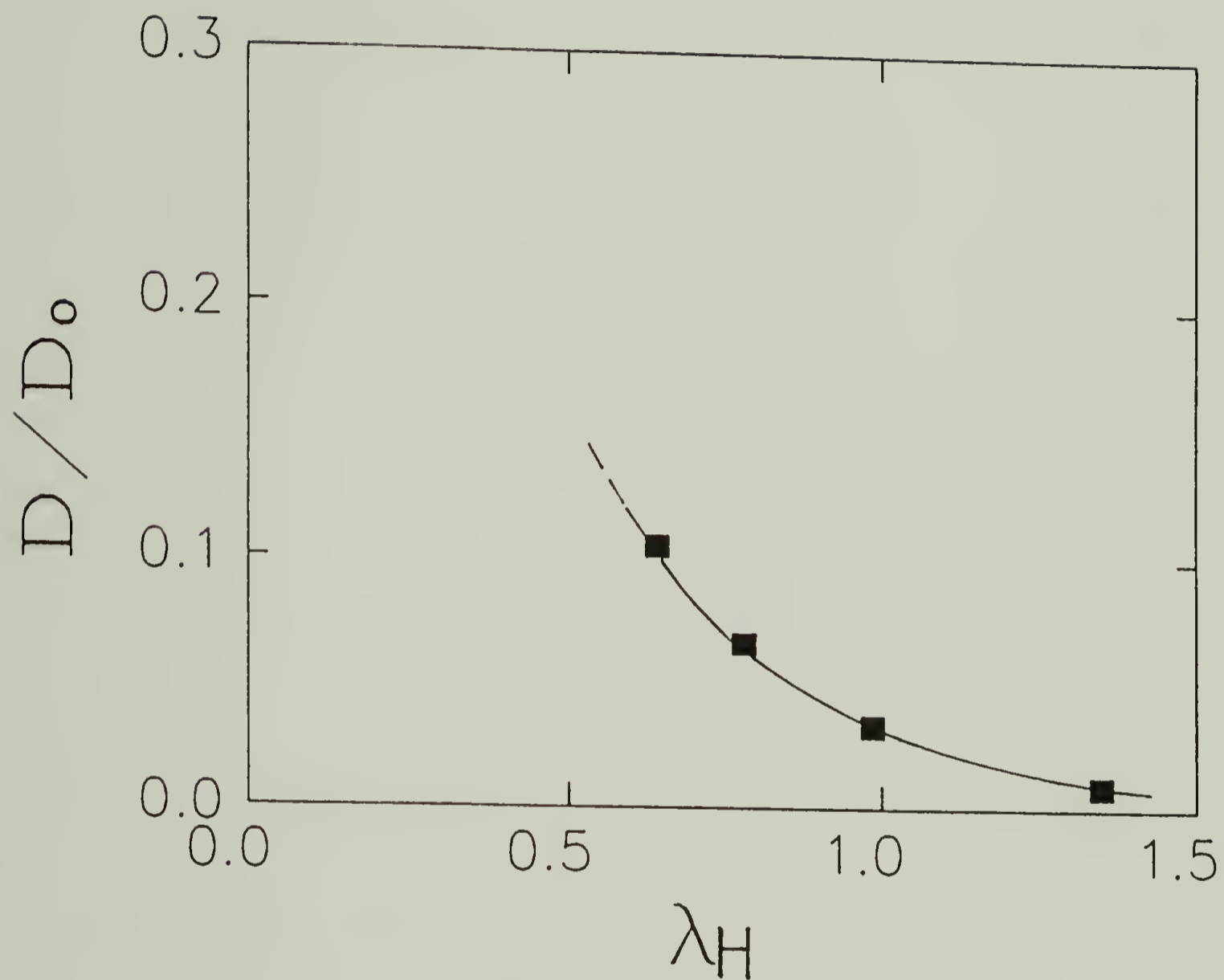


**Figure 4.10** Hindrance factor  $D/D_0$  as a function of size ratio  $\lambda_H$  for polystyrenes (MW=2,500 to 13,000) in Vycor ( $R_p=20\text{\AA}$ ). The curve shows the trend of the results. A rough estimate yields an intrinsic conductivity value of 0.3 to 0.7, see text.

## CHAPTER V

# DIFFUSION IN POROUS MEDIA FORMED FROM FUMED SILICA

### A. Background

The study of disordered material has become one of the liveliest current topics in the field of condensed matter physics[123]. Dynamics in disordered materials, including transport and relaxation, is one of the important subfields in this study. Knowledge in this subfield is of great importance to the understanding and control of industrial and natural processes ranging from oil recovery from rocks to blood transportation in arteries.

In this part of the work, we extended our diffusion study from polymer movement in roughly cylindrical pores in controlled pore size glasses to a totally random porous material. Silica again constitutes the obstructing solid phase in this part of the work, because silica is highly pure and can be easily index matched. In this study, we used fumed silica to form the porous medium. A more description of fumed silica were given in Chapter II.

When mixed with polymer solution, the silica particles can be in either of two forms, suspension or gel, which are not distinctively different. A suspension having a silica concentration greater than some

critical concentration will gradually transform into a gel in a time period of several hours or several days. Though a precise definition of "gel" is difficult, a gel characteristically consists of three dimensional microscopic networks which exist over macroscopic distances and which hold or entrap the liquid component. The preparation of silica gel in this work is simple: a fraction of fumed silica was mixed with a solution of labeled polystyrene, the mixture is stirred on a test tube mixer (Vortex-Genie, Fisher) to form a uniform suspension, and the suspension is left unperturbed until it is gelled.

Several other silica gel systems have recently been extensively used as experimental model systems for the study of the fractal nature of materials. A number of works have been published regarding the study of the fractal aspects of these silica gels and the relation between structure and the gelation conditions, using small angle scattering techniques such as SAXS and SANS[124-129]. The silica gels that have been studied can be roughly categorized into two groups: those formed by aggregation of colloidal silica such as Ludox (Du Pont)[124-127] and those from a sol-gel process[124, 128, 129]. The gel consisting of fumed silica can be viewed as similar to the gel from colloidal silica aggregation. Nevertheless, the differences are obvious: for fumed silica gels the basic units are ramified or fractal clusters and the gel linkage is physical and reversible, while in colloidal silica gels the basic units are spherical colloids and the gel linkage is a chemical bond.

The analytical technique employed in the study presented in this chapter is forced Rayleigh scattering, sometimes known by the more

accurate name holographic relaxation spectroscopy. It has been employed for the measurement of mass diffusion in both liquid and solid[51,60-78]. The principle and technique of FRS was discussed in Chapter II. For the study of transport in a porous medium, the FRS technique was used by Dozier et al.[118] to measure diffusion of a dye molecule (azobenzene) in porous Vycor glass.

There have been, to our knowledge, no published results concerning transport in silica gel, possibly because the abundant hydroxyl groups at the silica surfaces strongly adsorb diffusants and thus cause great complication. This problem is addressed by chemically treating the silica surface, i. e., replacing the surface hydroxyl groups by alkyls. Fumed silica is chosen in this work because it offers the advantage of stability in a powder form that facilitates the chemical treatment.

## B. Results and Discussions

The FRS signal from the diffusion of a labeled polystyrene ( $MW = 1.13 \times 10^6$ ) in a silica gel consisting of R972-M ( $\Phi=7.1\%$ ) is shown in Figure 5.1. The measured transient voltage  $V(t)$  is proportional to the transient diffracted optical intensity  $I(t)$  diffracted from the sample. The FRS signal had reached a maximum when the writing beams were turned off, and an exponential decay followed immediately. The amplitude of the initial diffracted intensity was about the same as that from the free solution under the same conditions. A non-linear least square fit[101,102] of  $V(t)$  to

equation (2.27) is quite good and displays a random distribution of residuals, which are plotted in Figure 5.2.

Contrary to the normal FRS signal from the gel of R972-M, the FRS signal from the silica gel of unmodified R972 usually showed an abnormal slow rise in diffracted intensity after the exposure of chromophores to the writing beams. Figure 5.3, an FRS signal from the labeled polystyrene ( $MW = 1.13 \times 10^6$ ) in the gel of R972 ( $\Phi = 2.6\%$ ) shows this typical abnormality. The maximum diffracted intensity was 5 to 10 times larger than that from the labeled polymer in free solution. We relate this peculiar behavior to the adsorption of the polymer by the silica surface, though we do not understand the underlying mechanisms in detail. The data points, except those previous to the inflection point, were fitted to equation (2.27). Figure 5.4 plots the residuals of this fit. The fit is not as satisfactory as for the gel of R972-M, due to the slow initial rise in diffraction intensity and a slow decrease in baseline at the later stage. The latter probably arises from the slow movement of a small portion of polymer molecules that were "stuck" to the surface.

The decay rates  $1/\tau$  obtained at different scattering wavevectors are plotted in Figure 5.5, for labeled polystyrene ( $MW = 1.13 \times 10^6$ ) in three different systems: (a) free solution, (b) R972-M silica gel, and (c) R972 silica gel. The FRS measurements in the gels were carried out several days after the gel preparation, so that the measured decay rates were stable with time. The difference in the diffusion behavior in porous media with different surface chemistry is discussed below.

For the R972-M gel, proportionality exists between decay rate ( $1/\tau$ ) and squared wavevector  $q^2$ . Thus the diffusion law governs the transport process in the R972-M gel as well as in free solution. The data points in Figure 5.5 for free solution and the silica gel of R972-M were fitted to equation (2.28). The dashed line and the dotted line represent the fitted linear functions (equation 2.28). The diffusion coefficients  $D_0$  (in free solution) and  $D$  (in R972-M gel) were obtained from the slope of  $1/\tau$  versus  $q^2$ . The linear relation of  $1/\tau$  versus  $q^2$  also indicates that the diffusion coefficient is independent of the length scale of observation, which is in the range of 4 to 25  $\mu\text{m}$  in our experiments. This means that the pore structure is uniform over this range of length scale being probed, as opposed to fractal pores in which the mean square displacement of a diffusant is not proportional to the time of movement [130-133]. It was found that the intercept of the fitted straight line, which is equal to  $1/\tau_{\text{life}}$  in equation (2.28), is very small. In other words, the life time of the excited state of the chromophores attached to the polystyrene chains is very long compared to the time scale of the diffusion process being studied.

The data for the R972 gel showed an obvious curvature. The straight lines, which are approximately tangential to the data points at the higher and lower  $q^2$ , are drawn to demonstrate the trend. The curvature in  $1/\tau$  versus  $q^2$ , which is not seen in R972-M gel, is related to adsorption of the polymer chains by the silica. It may also be partly due to larger error in the curve fitting which can be seen in the plot of residuals (Figure 5.4). In this work, a quantitative interpretation of the hindered diffusion largely due to adsorption in R972 gel is not feasible. Yet we still depict our observation



qualitatively. An apparent phenomenological diffusion coefficient  $D_a$  was obtained from a single angle measurement at  $q^2 = 4.74 \times 10^7 \text{ cm}^{-2}$  (corresponding to a prism spacing of 2 inches) using  $D_a = 1/(\tau q^2)$ .

The polymer diffusion inside a silica gel or a silica suspension is hindered compared to that in a unbounded solution. The hindrance factor  $D/D_0$  is plotted in Figure 5.6 as a function of silica volume fraction  $\Phi$ . The general trend is that the value of  $D/D_0$  decreases with the increasing  $\Phi$ , indicating a stronger hindrance at higher solid fraction. In the low silica concentration ( $\Phi < 6\%$ ) regime, the silica suspension will not gel, and the diffusion coefficient was measured before the separation of the dilute silica suspension into two layers (due to precipitation). In the higher silica concentration ( $\Phi > 6\%$ ) regime, the diffusion coefficients were measured after the gels had formed. Two labeled polystyrene samples with different molecular weights ( $MW = 4.8 \times 10^4$  and  $1.13 \times 10^6$ ) were used in this study. We observed little difference in hindrance between these two polymer sizes within experimental error. This implies that the polymer molecules are still much smaller than the pore dimensions. In other words, both these polystyrene molecules can still be approximated by point particles. The use of even higher molecular weight polymer, though desirable, is limited by increasing difficulty in the synthesis process.

The labeled polystyrene molecules diffuse in a porous medium of R972-M much faster than those in a porous medium of R972 (see Figure 5.7) where adsorption severely reduces the freedom of the polymer. The weak hindrance in R972-M is also dependent on  $\Phi$ . These indicate that the effect of adsorption is negligible in R972-M, and that the hindrance can be

attributed, for the most parts, to the steric obstruction and hydrodynamic interactions with the silica surfaces. There exist many theories that take into account these two factors and predict the relation between the hindrance factor  $D/D_0$  and porosity for different porous systems [6, 36, 110, 134]. Our experimental results are compared to a hydrodynamic theory developed by Neale and Nader (NN)[36] for a much simpler model system — a homogeneous swarm of spherical particles. This model, though simple, bears some similarity to the complex random porous medium of ramified fumed silica particles in our experiments. Based on a non-rigorous assumption that each particle sees other parts of the material as a uniform fluid, this model predicted that,

$$D/D_0 = 2(1-\Phi)/(2+\Phi) \quad (5.1)$$

We clarify here that in the notation of Neale and Nader,  $\Phi$  was used differently as porosity. In this dissertation,  $\phi$  is used to denote porosity. Equation (5.1), independent of the size distribution of the spheres, was in satisfactory agreement with experimental data for diffusion in a wide range of porous media throughout the whole porosity range[36-38]. The solid line in Figure 5.6 was calculated from equation (5.1). It is observed that our results in the low  $\Phi$  regime are in reasonable agreement with the NN theory (equation 5.1) within experimental error. The silica suspensions can be viewed, not strictly, as a collection of spherical primary units, though these units aggregated into ramified clusters during the hydrolysis and chemical surface treatment. At low solid volume fraction  $\Phi$  (or high porosity), the hindered diffusion in a fumed silica suspension is similar to

that in an unconsolidated homogeneous swarm of spherical particles. In the gelled systems, the formation of three dimensional networks further violates the implied assumption of the NN model, which requires different particles in the swarm to be independent of one another in the sense that their regions of hydrodynamic influence must not overlap. We observe that at higher  $\Phi$  (or lower porosity), the hindered diffusion tend to be slower than that predicted by the NN theory. This deviation is greater at higher silica concentration. We emphasize here that the NN model is not parallel to our experimental system. Therefore this comparison (as well as another comparison in the ensuing paragraph) is intended only to put our work in the context of other studies on the hindered transport in a random porous medium.

Next, our results are compared to a theory developed by Prager[85] for a homogeneous and isotropic suspension of solid particles of arbitrary shape. The main assumptions in the NN model that requires independence of hydrodynamic influence region was relaxed, and the principle of minimum entropy production[135] was applied to obtain bounds on the hindered diffusion rate:

$$D/D_0 < (1-\Phi)(1-\Phi/3) \quad (5.2)$$

Again,  $\Phi$  here is silica volume fraction, instead of porosity. The dashed curve in Figure 5.6 corresponds to Prager's theory (equation 5.2). Our experimental results basically satisfy the inequality relation predicted by Prager.

The ratio of diffusion coefficient  $D_a/D_0$  for labeled polystyrene (MW =  $1.13 \times 10^6$ ) in a porous medium of silica R972 is plotted against silica volume fraction  $\Phi$  in Figure 5.7; where  $D_a$  is the phenomenological diffusion coefficient defined previously. The diffusion is drastically hindered. For a polymer molecule in a suspension with silica volume fraction of about 1%, the apparent diffusion coefficient is smaller than that in free solution by over 60%. The value of  $D_a/D_0$  is only slightly dependent upon silica fraction  $\Phi$ . At the two lower silica concentrations, the silica suspension will not gel, and the hindrance in these two suspensions is similar to that in the gels. Apparently adsorption plays a dominant role in slowing down the polymer diffusion and even at low concentration the silica surface area is not completely covered by the adsorbed polymer molecules. The measured diffusion coefficient in R972 gel does decrease by a small amount as  $\Phi$  increases. There can be three possibilities to account for this small decrease: (1) increased ratio of surface to pore volume results in a higher probability for the labeled polymer molecule to be adsorbed, (2) steric obstruction increases slightly due to a higher solid fraction, and (3) greater silica concentration causes more static scattering and stray light resulting in a poorer FRS signal ratio and a higher baseline value, which could result in poor quality data analysis.

Though the labeling ratio (the density of the chromophore) does not affect the diffusion rate in a porous medium of R972-M, it does have an effect on the diffusion coefficient for the dye-labeled polystyrene in a porous medium of R972. For the polymer samples with the same molecular weight, a higher labeling ratio usually resulted in a slightly slower diffusion. Thus comparison between different polymer sizes is not made,

as we did not have a quantitative control of the labeling ratio in the labeling reactions. As a rough generalization of our observation, for most molecular weights and most labeling ratios we have studied, the value of  $D_a/D_0$  is between 0.2 to 0.4 in a volume fraction range of  $\Phi = 1 \sim 5 \%$ .

The silica gels in this work can be reckoned as physical gels that are reversible in nature, since there is no chemical bonding involved in the gelation. We monitored the development of hindrance during the formation of silica gels. At the beginning, the mixture of silica and polymer solution was heavily shaken on a Vortex-Genie Test Tube Mixer to destroy existing interconnection of the silica particles. FRS measurements were then conducted to obtain the changing diffusion coefficient at different times during the gelation process. We observed little difference within experimental error between a "fresh" gel and a gel reformed from a "destroyed" one.

The diffusion coefficient for polystyrene ( $MW = 1.13 \times 10^6$ ) inside a gel of R972-M ( $\Phi = 7.1\%$ ) as a function of gelation time is shown in Figure 5.8. There is a small difference in diffusion rate between the silica suspension immediately after the mixing and the gel formed later. The diffusion within the gel attained a stable value in approximately 5 hours. This time period is comparable to that needed for the gelation. The small difference in the diffusion rate at early and late stages may be attributed to the interconnection of silica particles into networks, which were not present in the initial suspension. It is also possible that immediately after violent mixing, turbulence and convection may speed up the smearing of the fringe pattern of excited dye molecules (created in the exposure to the

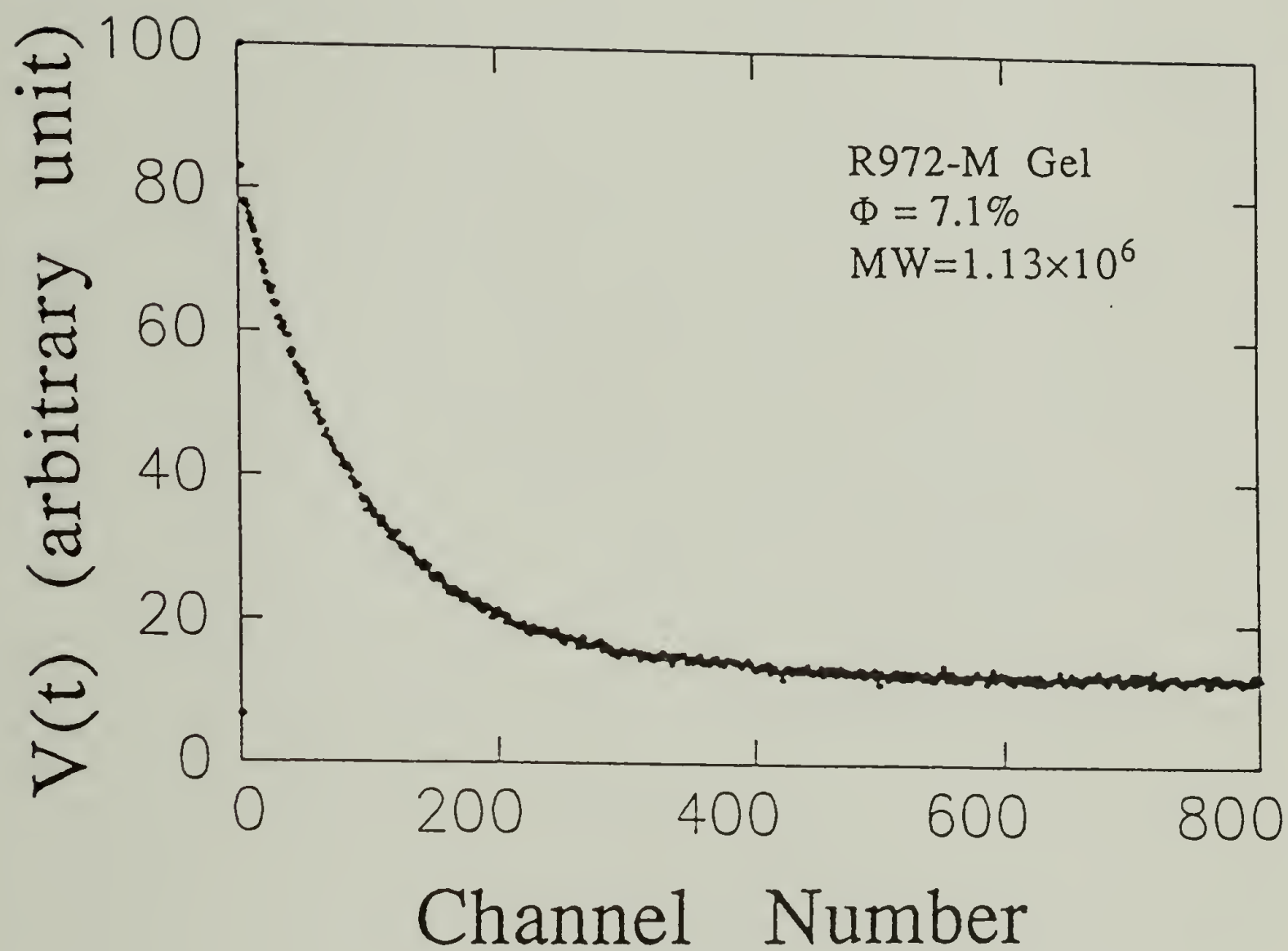
optical grating), and this could be inappropriately interpreted as faster diffusion. In the gel the three dimensional networks retard such turbulence and convection.

Figure 5.9 shows the diffusion coefficient as a function of gelation time for a R972 gel ( $\Phi = 2.6\%$ ). The diffusion reached a stable value in a very short time period (about 20 minutes), compared to several hours needed for the gelation. In other words, the mixture was still visually liquid when the strong hindrance built up. In a silica gel of R972, the hindrance is mainly due to surface adsorption of the polymer molecules. So it is rationalized that the time period to develop this strong hindrance is approximately the time period for the polymer chains to approach the solid surface and to be physically adsorbed, since those chemically adsorbed molecules would not come off the silica surface even under violent shaking.

Dynamic light scattering spectroscopy was also attempted in the study of polymer diffusion in silica gels. It was not possible to extract diffusion coefficients from the measured autocorrelation functions which were greatly complicated by the intensity fluctuation due to the oscillatory movement of the silica particles. This intensity fluctuation is mixed with that due to the polymer movement. It is noted that even a pure silica gel (without polymer) gives a significant decay in the ACF, in contrast to consolidated porous materials such as porous glasses which yield constant ACFs.

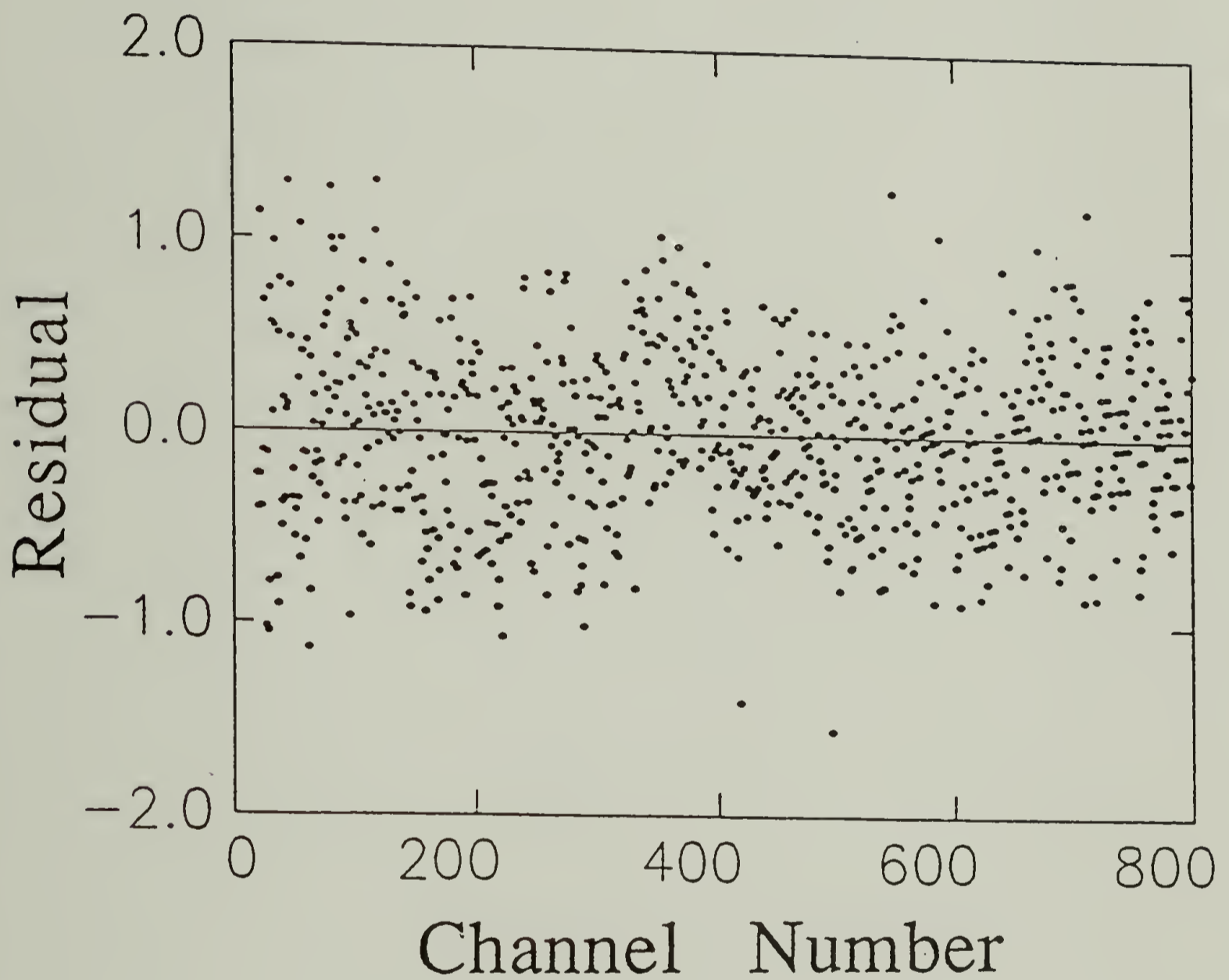
### C. Conclusions

We have used the technique of FRS to study the diffusion of dye-labeled linear polystyrene inside a porous medium of fumed silica. For silica R972 which has a finite surface silanol density, adsorption of polymer by the silica surface dominates the diffusion behavior. The diffusion in a porous medium of R972, which is not normal Brownian motion, shows a strong hindrance even in a silica suspension with low silica concentrations. This hindrance has a very weak dependence on silica volume fraction  $\Phi$ . For silica R972-M, adsorption is almost absent as a result of further surface treatment. In this system, the diffusion is of Brownian motion type, and the weak hindrance to polymer diffusion is attributed to geometric obstruction and hydrodynamic interactions with the silica surfaces. The change of diffusion coefficient during gelation is also monitored for both types of silica gels. The time needed for the diffusion rate to stabilize is commensurate with the mechanisms that is responsible for the diffusion behavior.

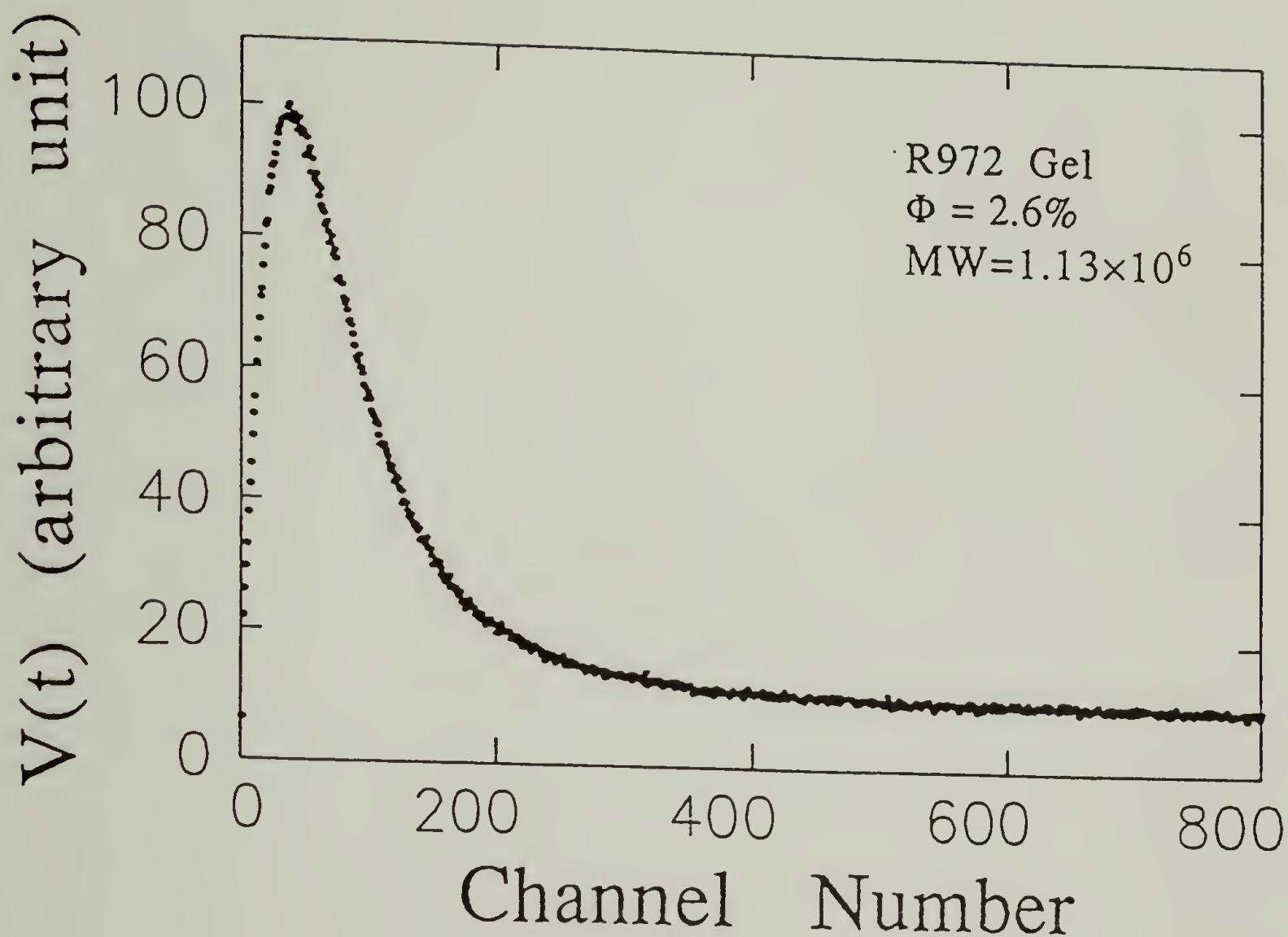


**Figure 5.1** Transient diffraction intensity  $V(t)$  for a dye-labeled polystyrene ( $MW = 1.13 \times 10^6$ ) in a silica gel composed of R972-M which has negligible adsorption of the polymer. This FRS signal is normal.

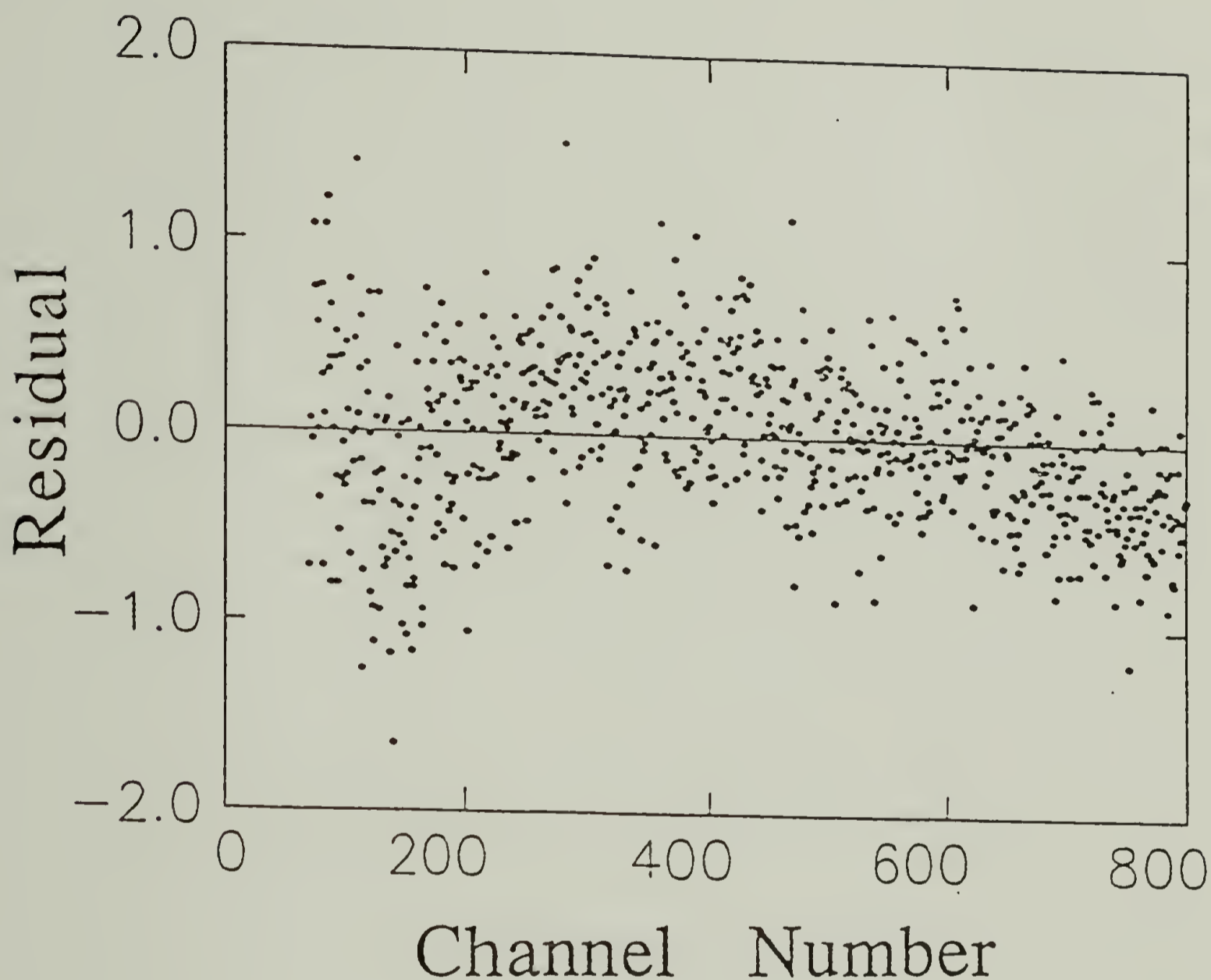




**Figure 5.2** A plot of the residuals (in the same arbitrary units as in Figure 5.1) of a non-linear least square fit of the data points in Figure 5.1 to equation (2.27). These residuals are very close to being random.

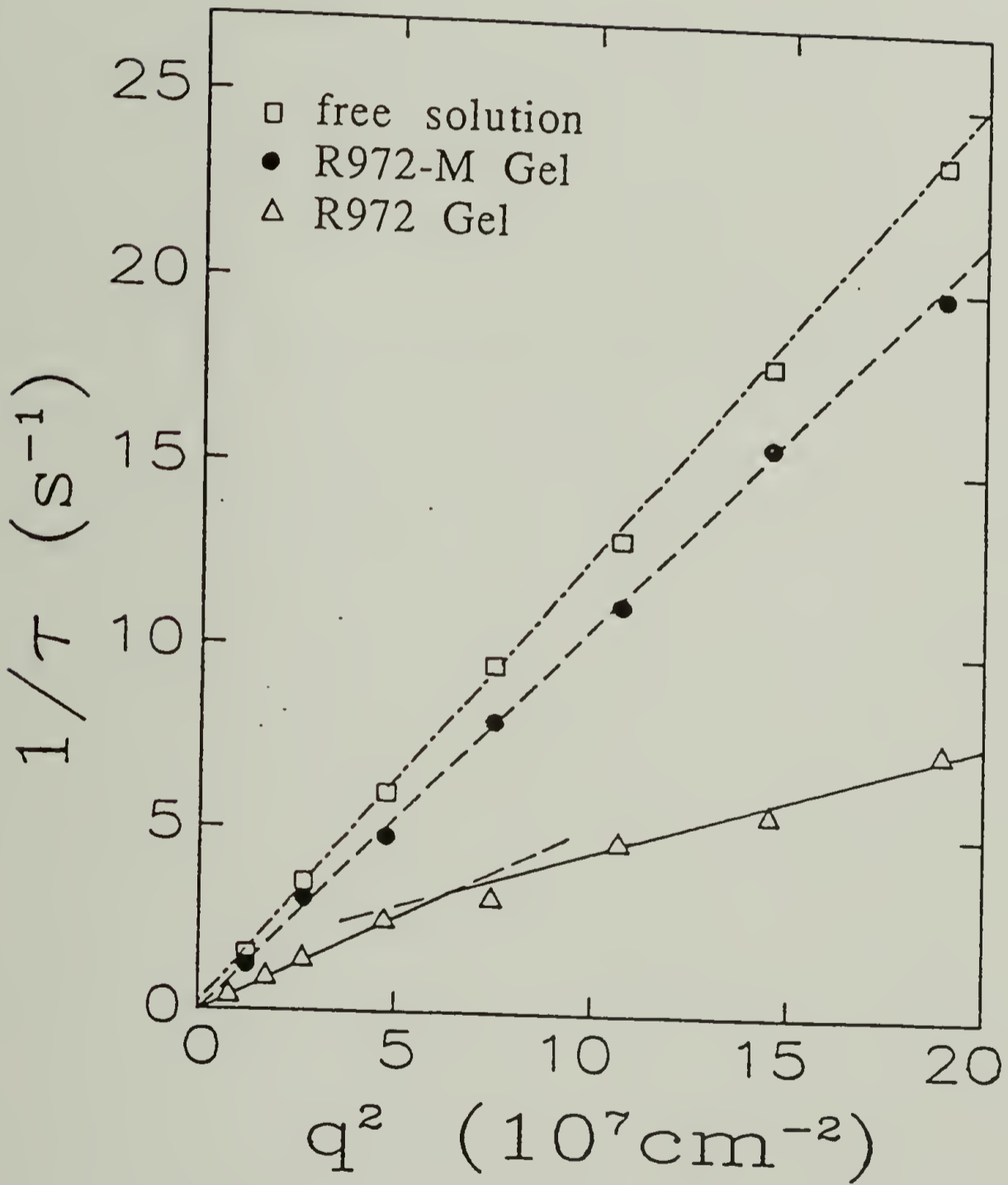


**Figure 5.3** Transient diffraction intensity  $V(t)$  for a dye-labeled polystyrene ( $MW = 1.13 \times 10^6$ ) in a silica gel of R972 which has a finite surface silanol density resulting in surface adsorption. This FRS signal is abnormal as there is a slow rise in the diffraction intensity after the exposure of the chromophores to the writing beams.



**Figure 5.4** A plot of the residuals (in the same arbitrary units as in Figure 5.3) of a non-linear least square fit of the data points in Figure 5.4 to equation (2.27). The first point of fitting is approximately the inflection point. There is a systematic error in this fit largely because of the initial slow rise in diffracted intensity and the very slow decrease in baseline.

**Figure 5.5** The decay rate  $1/\tau$  of the intensity diffracted from the transient grating of photo-excited dye attached to polystyrene ( $MW = 1.13 \times 10^6$ ) as a function of the squared wavevector  $q^2$  in three different systems: (a) unbounded solution ( $\square$ ), (b) silica gel of R972-M ( $\bullet$ ), and (c) silica gel of R972 ( $\Delta$ ). Linear relationship exists in both the unbounded solution and the R972-M gel indicating normal diffusion, while an obvious curvature is observed in the R972 gel. The slope of  $1/\tau$  versus  $q^2$  defines the diffusion coefficient for systems (a) and (b). The result of  $1/\tau$  divided by  $q^2$  at  $q^2 = 4.74 \times 10^7 \text{cm}^{-2}$  is used as the apparent diffusion coefficient  $D_a$  to describe the observation in the porous media of R972 in Figure 5.7.



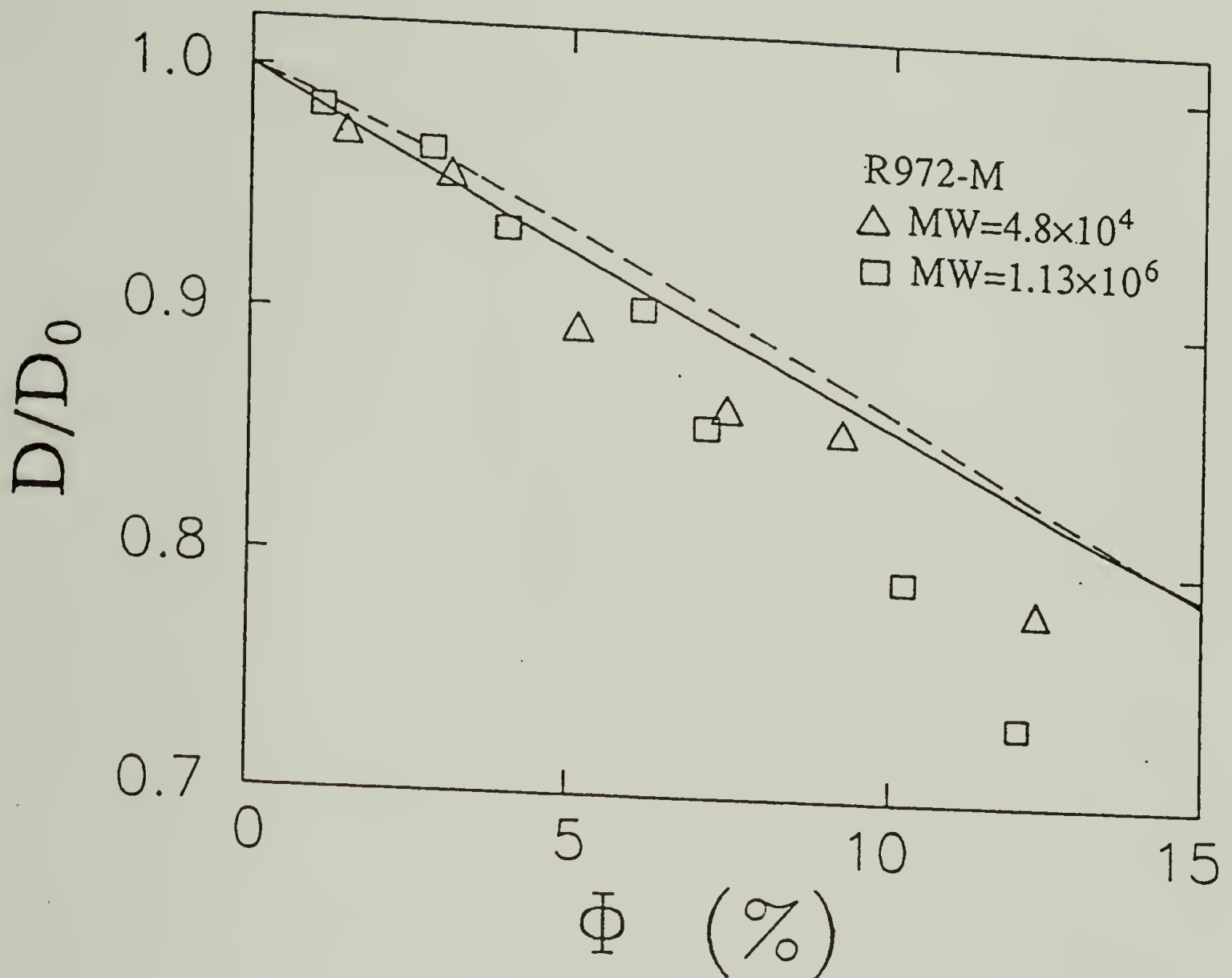


Figure 5.6 Hindrance factor  $D/D_0$  versus silica volume fraction  $\Phi$  for two polystyrene samples ( $MW = 4.8 \times 10^4$  and  $1.13 \times 10^6$ ) in R972-M gels. The weak hindrance is attributed to geometric obstruction. The solid curve represents the theory of Neale and Nader[36] (equation 5.1) for diffusion in a homogeneous, isotropic swarm of spheres. The dashed curve corresponds to the bound predicted by Prager[85] (equation 5.2) for a homogeneous, isotropic suspension of solid particles of arbitrary shape.

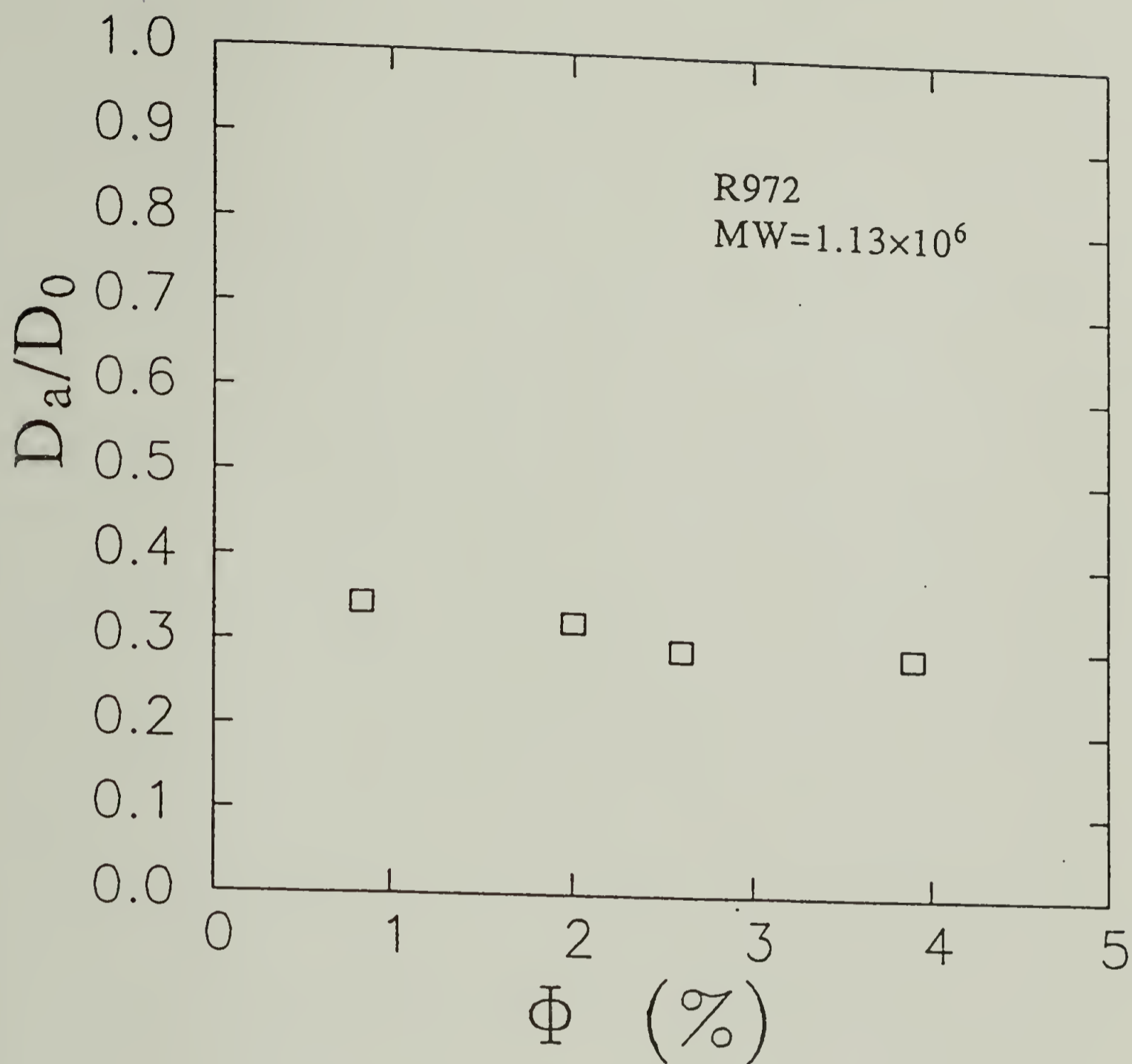


Figure 5.7 Hindrance factor  $D/D_0$  versus silica volume fraction  $\Phi$  for polystyrene ( $MW = 1.13 \times 10^6$ ) in R972 gels. The polymer diffusion is strongly hindered even at low  $\Phi$ . This hindrance is slightly dependent on  $\Phi$ .

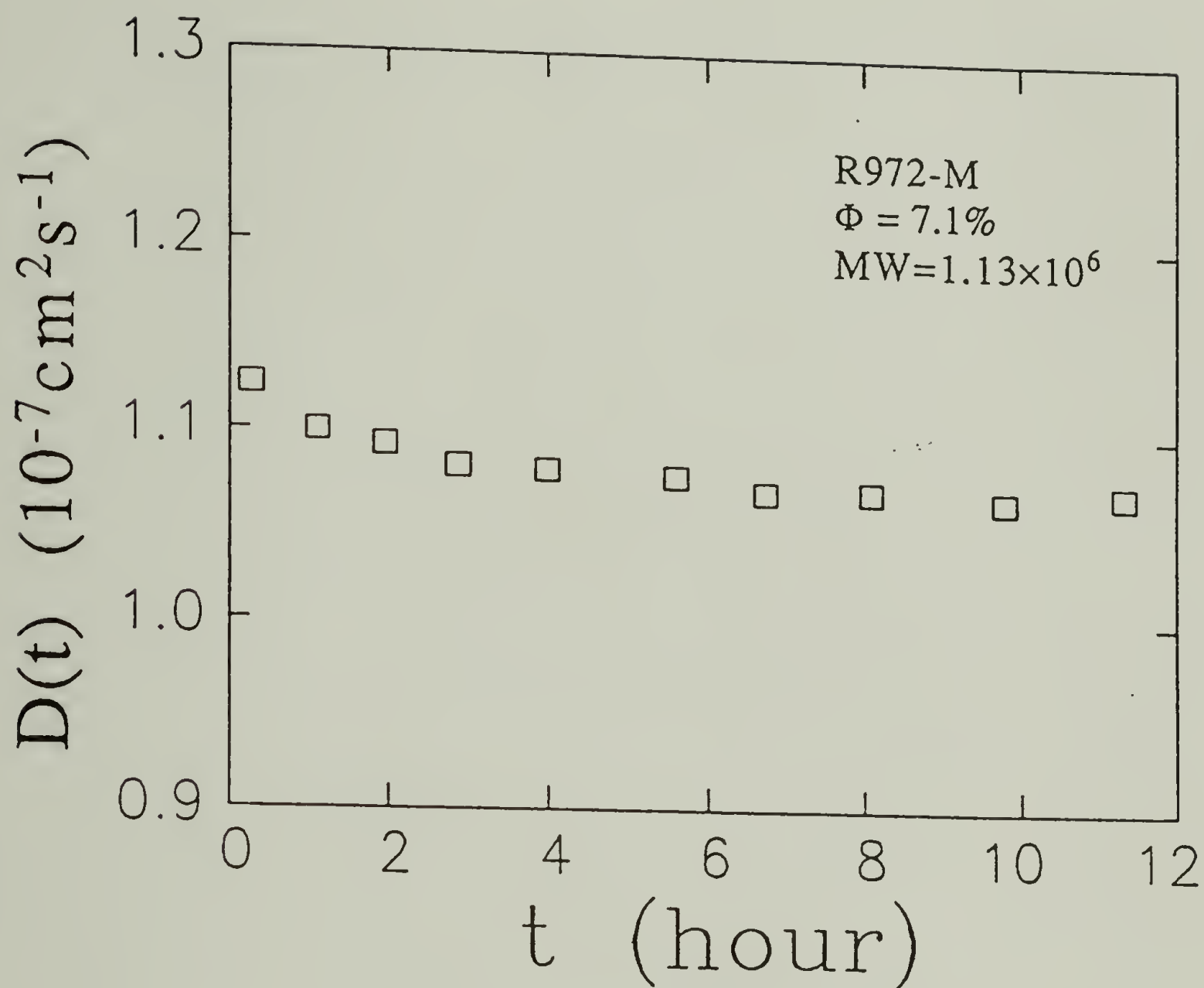


Figure 5.8 Diffusion coefficient  $D$  versus time during the gelation process for a R972-M gel ( $\Phi = 7.1\%$ ). The time for stabilization of the diffusion coefficient (approximately 5 hours) is comparable to that needed for the silica suspension to gel.



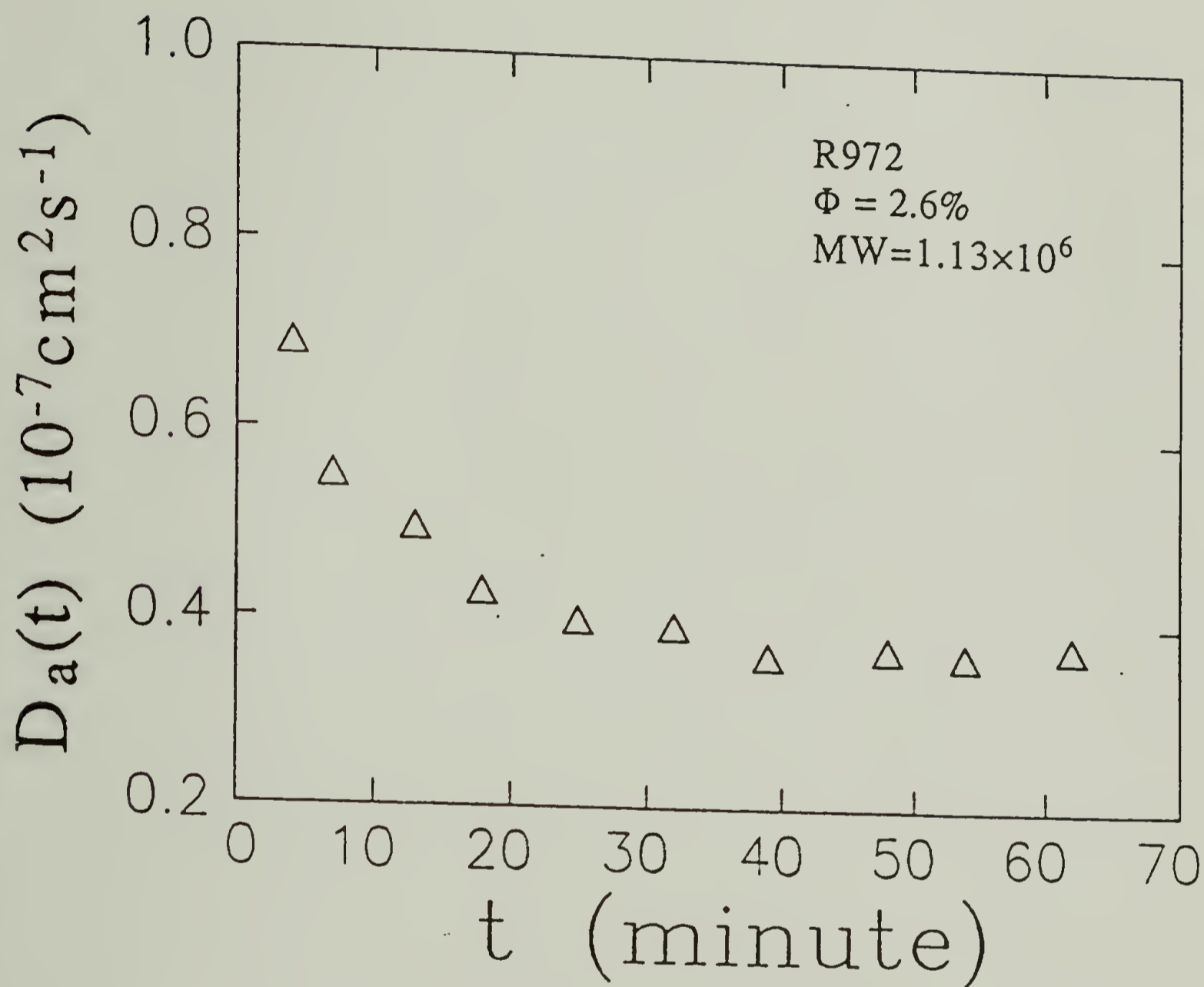


Figure 5.9 Diffusion coefficient  $D$  versus time during the gelation process for a R972 gel ( $\Phi = 2.6\%$ ). The time for stabilization of the diffusion coefficient (approximately 10 minutes) is much shorter than that needed for the silica suspension to gel.

# CHAPTER VI

## CONCLUSIONS

### A. Summary

In this dissertation, light scattering spectroscopies (DLS and FRS) have been employed to study hindered diffusion of macromolecules in liquid-filled pore spaces of porous materials, which are: (a) porous glass with controlled pore size, and (b) porous medium of fumed silica. The porous glasses studied have tortuous and roughly cylindrical pores that are highly branched and multiply interconnected. The fumed silica porous media (including silica gel and silica suspension) have very large pore spaces with random structures. We have used several polymers as diffusants: starburst-dendritic polyamidoamine, linear polystyrene, and dye-labeled polystyrene. Forced Rayleigh scattering apparatus was set up in this work, which was used, in addition to the existing dynamic light scattering apparatus, for direct measurement of polymer diffusion in "transparent" (due to the matching indices of refraction) porous materials. Supplemental to the above experimental measurements, computer simulation was also performed to study diffusion within cylinders that are interconnected to form a three-dimensional cubic lattice.

The experimental systems (of polymer samples and porous materials) and the analytical techniques used for each system are listed in table 6.1.

In all the systems studied, a macromolecule diffuses more slowly than in a free solution. This hindrance resulted from several factors each manifesting its effects to a different extent under different conditions. This dissertation investigated the mechanisms of the individual factors, such as steric obstruction, hydrodynamic interactions between the polymer and the pore walls, and entropy barrier at high confinement, and interpreted the results of hindered diffusion based on these factors.

Figure 6.1 schematically depicts the diffusion behavior as a function of three most important parameters — time scale ( $t$ ), hydrodynamic radius of the polymer diffusant ( $R_H$ ) and pore radius ( $R_P$ ), which are the three axes. The arrows represent our experimental approaches in this study. The effects of different factors in different regimes are summarized in the following.

In Figure 6.1, in the volume enclosed by the dashed frame and the shaded rhombic plane, single-pore diffusion was observed. In this regime, the time scale of observation is short, and the average displacement of a diffusant is smaller than the pore size; the diffusion is a manifestation of microscopic Brownian motion without fully experiencing the steric obstruction from the solid matrix. In the transition region ( $qR_P \approx 1$ ), the measured apparent diffusion coefficient at small  $t$  is larger than that at larger time or equivalently length scales. The hindrance in this regime is mainly due to the hydrodynamic interactions.

Inside the volume encompassed by the planes denoted by solid lines, macroscopic diffusion was measured. This corresponds to large time scales or equivalently large length scales of observation. Diffusion in this regime

involves tortuosity of the porous material, in addition to the hydrodynamic interactions. When a polymer molecule diffuses over distances large compared to the pore size, the diffusion averages over microscopic heterogeneities and obtains macroscopic features. Macroscopic diffusion which is slower than the single pore diffusion can be measured under either of the two conditions: (a)  $qR_P \ll 1$ , or (b)  $qR_P \approx 1$  and  $t \gg t_1$ , where  $t_1$  is the crossover time from single pore to macroscopic diffusion.

Dynamic light scattering at fixed scattering wavevector revealed faster apparent diffusion at short times (corresponding to single pore diffusion) followed by a slower macroscopic diffusion. Monte Carlo simulation has been performed which also showed the crossover from single pore to macroscopic diffusion, in qualitative agreement with DLS measurement. In both DLS experiments and computer simulation, we found that the time preceding the emergence of macroscopic diffusion is roughly equal to the time period for the polymer to diffuse a distance comparable to the pore size. The shaded rhombic plane represents the crossover time ( $t_1$ ) at different values of  $R_H$  and  $R_P$ . In DLS measurements,  $t_1$  was found to increase linearly with  $R_H$ , and in computer simulation, it was found  $t_1 \propto R_H \times R_P$ .

The square cross section in the front illustrates the macroscopic diffusion behavior. At a fixed pore size, as the polymer dimension increases, or as  $\lambda_H$  increases, the diffusion rate decreases monotonically. The diffusion behavior in the entire  $\lambda_H$  range is a continuously evolving process influenced by several factors. Each factor affect the diffusion to a different extent depending on the degree of confinement. The division of

the macroscopic diffusion into several regimes is to demonstrate conceptually that different factors dominate diffusion in different regimes, or different ranges of  $\lambda_H$ .

Though Figure 6.1 was mostly based on the systematic study of polystyrene chains in controlled pore glasses, it should be generally valid for other systems with non-ideal pore geometries, if we substitute  $R_p$  with some other equivalent average pore dimension.

When  $\lambda_H \ll 1$  (in the lower right triangle), a polymer molecule can be approximated by a point diffusant. In this regime, only the steric obstruction contributes to the hindrance. The hindrance factor  $D/D_0$  is a measure of intrinsic conductivity ( $X$ ) which is characteristic of the porous material. In the study of polystyrene diffusion in porous glasses, the value of  $X$  was obtained by extrapolating  $D/D_0$  to the limit  $\lambda_H = 0$ .

The diffusion study of dye-labeled polystyrene in a porous medium of fumed silica falls equivalently into this regime since the pore spaces were much larger than the diffusant; the hindrance is mainly due to the steric hindrance independent of polymer size. The measured diffusion in a porous medium of fumed silica was compared to a prediction based on a much simpler but somewhat similar model (by Neale and Nader) — a point particle in a homogeneous swarm of hard spheres of arbitrary size distribution. [36] It was found that at low silica concentrations our diffusion results were in reasonable agreement with the NN theory. At a high silica concentration, a silica suspension can transform into a gel. Diffusion in the silica gel was slower than that predicted by the NN theory, a result we attribute to the interconnection of fumed silica particles. The

measured hindrance factor  $D/D_0$  was found to be within the bounds calculated by Prager based on the principle of minimum entropy production for a homogeneous suspension of solid particles of arbitrary shape[85].

When the polymer radius is comparable to but still smaller than the pore radius ( $\lambda_H < 1$ ), the size dependent hydrodynamic drag comes in effect, in addition to the structural effect. It was assumed that the structural effect and the hydrodynamic effect were separable for controlled pore size glasses[19,20]. Under this assumption the normalized ratio  $D/(XD_0)$  measured the hindrance due to hydrodynamic interactions. In this regime, two types of polymers have been studied which are dendritic polyamidoamine and linear polystyrene. We found that the dendritic polymer molecule diffuses more slowly than the linear polymer, which was attributed to less compressibility of the dendritic polymer due to the higher architectural compactness. The experimental results were in quantitative agreement with the Brenner-Gaydos theory *without* using any fitting parameters such as  $\kappa$  to correlate  $R_H$  to  $R_S$ . In other words, we found  $\lambda_S \approx \lambda_H$  for dendritic polymer, compared to  $\lambda_S = 0.76\lambda_H$  for linear polystyrene.

In this regime ( $\lambda_H < 1$ ), the diffusion of polystyrene chains in porous glasses was studied more extensively than in the previous works[19-21]. The diffusion results were directly compared to a theoretical prediction (by Davidson and Deen) for a *flexible* polymer chain in a cylindrical pore[9,15]. Quantitative agreement was found for diffusion at  $\lambda_H$  values up to 0.3. In this comparison, no fitting parameter was used, and the theory of Davidson and Deen was directly tested.

When the size ratio  $\lambda_H$  is even larger ( $\lambda_H \approx 1$ ), polymer diffusion was largely determined by the conformational entropy changes. Diffusion under very high confinement in porous glasses with small pore radius was measured; we achieved measurements at size ratios as high as  $\lambda_H = 1.4$ . At large  $\lambda_H$ , we observed a molecular weight dependence stronger than that predicted by the scaling model of "elongated cigar"[27-30]. We suggest that the variation in local pore size imposes restrictions on polymer conformations and thus requires conformational entropy adjustments for polymer movement, which greatly hinders diffusion. Our experimental data are consistent with a scaling model of these entropy barriers[31]. The emergence of the entropy effect and the deviation from the prediction of the "elongated cigar" model happened at similar molecular weights, which were equivalent to  $R_G \approx R_P$ , where  $R_G$  is the radius of gyration of the polymer.

When a polymer chain is extremely confined ( $\lambda_H \gg 1$ ), diffusion may adopt the "reptation"[29] behavior, which has a scaling relation  $D \sim M^{-2}$ . We have not been able to reach this regime of extreme confinement, limited by the difficulty of a larger macromolecule to move into a much smaller pore.

### B. Suggestions for Future Work

This dissertation has employed light scattering techniques to study polymer diffusion in two kinds of porous materials, namely, porous glasses and silica gels. Proposed here are some suggestions to solve the problems encountered during the course of this project, and some

suggestions to extend the current work to other porous materials and polymers, and to the use of other complementary techniques.

From time to time, surface adsorption caused complication to the study. It may drastically slow down the diffusive motion, and sometimes impart abnormality to the observed diffusion behavior. Measures were taken to minimize adsorption, but even a well quenched surface can sometimes have enough excess energy to adsorb molecules in adjacency. In this situation, effort to understand the effect of adsorption on diffusion is not nonsense. This understanding will also be practically useful as adsorption abounds in practical transport processes.

As an example of adsorption effect, the diffusion coefficient (measured by FRS) of DABITC in surface treated Vycor porous glass is surprisingly slow:  $D \approx D_0/30$ , though the decay rate  $1/\tau$  is proportional to  $q^2$  within experimental error. Later we found that chemisorption was absent in the surface-treated Vycor fragment, known from the fact that the dye molecules which had permeated into the Vycor pores could be all washed out by soaking in solvent. We postulate that physisorption be present and the adsorption-desorption process is fast with respect to the data acquisition speed, so that diffusion law is still preserved (reflected in  $1/\tau \propto q^2$ ). Diffusion of polystyrenes in this same Vycor glass was studied and it was found not to be affected seriously by surface adsorption (see Chapter IV). The difference is the attached dye molecules whose molar concentration is less than 1% of the polymer concentration.

One way of studying the effect of adsorption is to monitor the diffusion over a wide temperature range. This can be difficult for light



scattering because of the requirement of index matching. Though different compositions of a mixture of solvent can be used at different temperatures, more confusion can arise by changing the properties of the solvent.

Another dynamic technique, pulsed field gradient NMR (PFGNMR), proves a good alternative, which is briefly described in the ensuing paragraph.

Although the advantageous light scattering techniques were used in this dissertation, they are not without limitations; hence the additional use of other complementary techniques is suggested. Recently, one of the most used dynamic technique to measure transport in porous materials is PFGNMR[32-34] which follows the diffusion of nuclear spins and thus unambiguously measures the self-diffusion coefficient ( $D_s$ ). By measuring  $D_s$ , studies can be made at higher concentration thus enhancing signal-to-noise ratio. This technique looks at diffusion over long distances such that it is well suited for studying macroscopic diffusion; this is especially valuable for materials with large pore sizes, or with longer range of heterogeneity.

Another complementary technique is conductivity measurement. The degree of hindrance is phenomenologically described by the ratio  $\sigma/\sigma_0$ , where  $\sigma$  and  $\sigma_0$  are the conductivity in porous material and in free solution respectively. Despite the disadvantages of the complicated involvement of boundary resistance and partitioning effect, conductivity measurement offers an independent and relatively simple way of measuring hindrance to transport. One important difference between conductivity measurement and light scattering measurement is that porosity and partition coefficient come into the conductivity ratio as,

$$\sigma/\sigma_0 = \phi K X \quad (6.1)$$

where  $\phi$  is porosity,  $K$  is partition coefficient, whereas in light scattering measurement,  $D/D_0 = X$ . In both these equations, the diffusant is assumed to be a point particle.

Another extension of the current work is to other porous materials. Thick track-etched membranes with almost cylindrical pores suggested by Bishop[20] remains of great interest. Diffusion of starburst-dendritic polymers in these pores will provide an experimental system more parallel to many hydrodynamic theories based on the model of hard sphere in cylindrical pores. Also diffusion of flexible polymer chains such as polystyrene in these cylindrical pores will better correspond to the hydrodynamic prediction of Davidson and Deen[9,15]. Since commercial membranes are unsuitable for light scattering experiments, many efforts are needed in making suitable track-etched materials. Information about the preliminary work can be found in the Ph.D. thesis of Matthew T. Bishop.

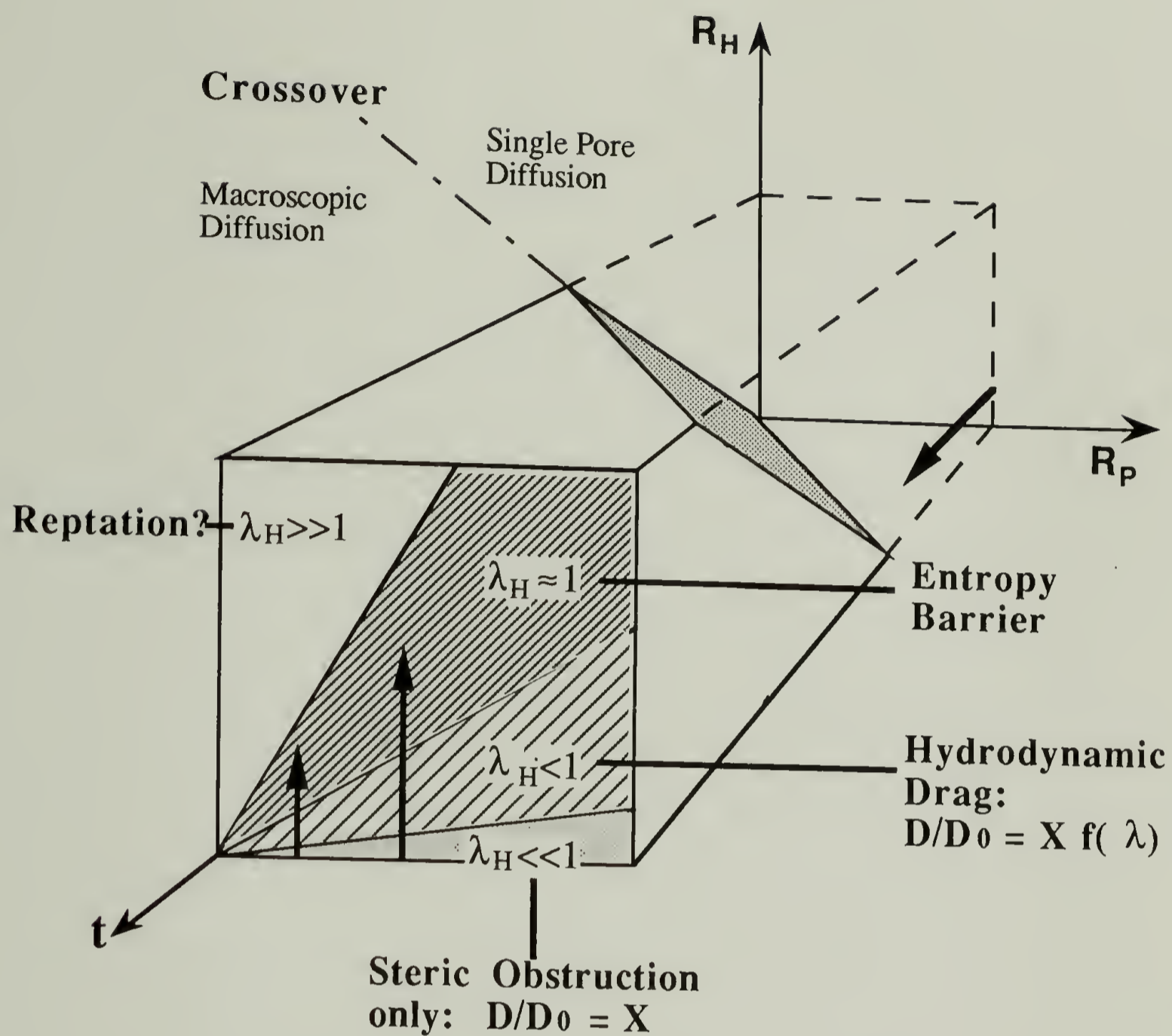
Also suggested is another porous material — colloidal silica aggregates, which have been extensively used as experimental systems for the study of the fractal nature of materials. Small angle scattering techniques such as SAXS and SANS have been employed to explore the fractal aspect of silica gel and the relation between structure and gelation conditions[124-129]. The silica gels made from colloidal silica are similar to but more regular than the silica gels made from fumed silica. The most commonly used colloidal silica is LUDOX(Du Pont), which is an aqueous dispersion of silica colloids. There are three different particle diameters

available: 7nm, 12nm, and 22nm. The highest silica volume fraction of stock suspension is 20%. The colloidal silica particles, dispersed in alkaline medium (pH = 8.1~10.0), repel one another because of the negative charge, thus resulting in stable products. By bringing the pH value down to 5-6, the silica colloids will aggregate and form a silica gel. Three problems have to be addressed: (1) index matching; (2) surface adsorption; and (3) miscibility of polymer in the solvent (water or alcohols), before the diffusion coefficient in this kind of silica gel can be successfully measured.

Table 6.1

Systems studied in this dissertation

Polymer	Porous Material	Technique	Chapter
Linear polystyrene	Porous glass	DLS, simulation	III, IV
Dendritic PAMAM	Porous glass	DLS	IV
Dye-labeled polystyrene	Silica gel and suspension	FRS	V



$R_H$  — Hydrodynamic radius of polymer

$R_P$  — Pore radius  $\lambda_H = R_H/R_P$

$t$  — Time scale of observation

→ Experimental approaches

Figure 6.1 Systematic scheme of diffusion behavior in different regimes

## APPENDIX A

### SOME PROPERTIES OF THE SOLVENTS

The selection of solvents is important to the light scattering experiments. In addition to the obvious requirement of matching the index of refraction ( $n$ ) to that of the porous materials (silica in all cases of this work), a larger  $dn/dc$  is also sought for higher scattering power as a dilute solution has to be used. We experimentally selected the solvents for different systems based on the criterion of a higher signal-to-noise ratio and a higher coherence function value. Three solvents have been used: 2-fluorotoluene, transdecahydronaphthalene, and fluorobenzene, all from Aldrich Chemical Co.

Following the choice of Bishop, we used 2-fluorotoluene for polystyrene in CPGs; 2-fluorotoluene is a good solvent for polystyrene. The viscosity of 2-fluorotoluene at different temperature was measured by Bishop using an Ubbelohde type viscometer. He the expressed viscosity ( $\eta$ ) as a function of T as:

$$\eta(\text{poise}) = 2.033 \times 10^{-4} \exp(1025/T) \quad (\text{A-1})$$

A value of index of refraction  $n=1.467$  was always used for 2-fluorotoluene, regardless of temperature or solution concentration. Under our experimental conditions, the error in  $q^2$  calculated by neglecting

concentration and temperature dependence of index of refraction was estimated at <0.5%. [20]

Transdecahydronaphthalene was chosen to be the solvent for starburst-dendritic polyamidoamine in CPGs. Compared to 2-fluorotoluene, transdecahydronaphthalene gives not only a larger  $dn/dc$  value (known from a higher experimentally measured coherence function), but also a higher viscosity that allows the use of longer sample time on the correlator thus enhancing the signal-to-noise ratio. (The dilute solution of polyamidoamine was found to have weak scattering power). Transdecahydronaphthalene offers the advantage of well known properties. The index of refraction as a function of  $\lambda_0$  and T, derived based on literature data[136] is:

$$n = 1.4524 + 4.39 \times 10^3 / \lambda_0^2 + (t - 30)(4.23 \times 10^{-4} + 4.06 / \lambda_0^2) \quad (\text{A-2})$$

where  $\lambda_0$  is in nm and T in °C. The viscosity of decahydronaphthalene, based on the literature data[137], can be approximated by:

$$\eta(\text{poise}) = 8.01 \times 10^{-5} \exp(1637/T) \quad (\text{A-3})$$

with error of less than 0.5% over the range of 20-45°C.

For VYCOR porous glass and fumed silica, fluorobenzene was found to have a better matching index of refraction at room temperature. The viscosity of fluorobenzene versus temperature was found to follow Arrhenius law and is expressed by:

$$\eta(\text{poise}) = 1.672 \times 10^{-4} \exp(1049/T) \quad (\text{A-4})$$

with error  $<0.5\%$  over the range 20-60 °C, based on literature data.  
The index of refraction is  $n=1.463$  at 25°C, and  $n=1.465$  at 20°C. [138]



## APPENDIX B

### TECHNICAL DETAILS OF FORCED RAYLEIGH SCATTERING

1. **Electrical Connections** of the key components are described here. The flow diagram is shown in Figure 2.4 and the connections (or interfacings) are shown in Figure B.1. At the beginning of the measurement, a TTL pulse from the computer (through the printer port) triggers the delay/pulse generator. This generator has four independent pulse outputs A, B C and D; the delay times for channels A, B, C and D are independently programmable. There are also four gate outputs AB, -AB, CD and -CD. The AB output provides a "high" level during the interval between the time set for channel A and channel B. During gate AB, the "writing" shutter blocking the Ar<sup>+</sup> laser is open; during gate "CD", the "reading" shutter passing the diffracted light is open. At delayed pulse B, the digital oscilloscope is triggered to record the transient voltage which is proportional to the intensity of the diffracted light. After recording, the data are sent to the computer via an RS232 interface.

2. **Optical Alignment** procedure is described in the following.

(a) Laser

Choose the desired light frequency using the coarse and fine tuner for vertical adjustment. Adjust the four screws that support the laser to make the

the output laser beam parallel to the table and at the same height as that of the pinhole on the detection arm, by checking at two different positions.

#### (b) Reference Pinhole Stand

The pinhole stand was specially designed for FRS alignment. The aluminum ring can hold a plate with a pinhole in the center. Different plates with different pinhole diameters from 1mm to 5mm can be used according to the beam width at different positions. A rod is attached to the ring such that the assembly can be rod-mounted onto the optical bench. On the rod, there is a collar to fix the pinhole height. The height of pinhole is adjusted to be the same as that of the output laser beam before it hits any mirror. The pinhole stand is used in the alignment procedure to guide the beam, so that the beam passes right over the a specific screw hole at a fixed height. By checking with the pinhole stand at two or more positions, one can assure that the beam is parallel to the optical bench.

#### (c) Beam Splitter

Ideally once the y-axis of the beam splitter is vertical to the incident beam, the transit and the reflected beams should have the same vertical direction. Unfortunately this is not exactly the case. One way out is to keep the reflected beam parallel to the table (at this time the transit beam is not parallel), and to compensate using mirrors A and B, shown in Figure B.2, such that the beam reflected from mirror B is again parallel to the table and at the correct height.

#### (d) Mirrors

Leave out the prisms and the parabolic mirror at this point. Adjust mirrors C, D and E to achieve coincidence between beam paths BDEC and

CEDB. For instance, the beam coming from A, B to D hits a pinhole placed in between B and D, and the beam from C, E, D to B should hit the same pinhole from the opposite direction. Also check positions between D and E, E and C.

#### (e) Prisms

Put the prisms in place. Rotate the prism (using the screw knobs of the prism stand) to let the reflection path (from the two perpendicular surfaces) to coincide with the incident path. Move the two prism platforms using the micrometers to place the outgoing beams right over and parallel to two rows of holes that are 2 inches apart. Since the parabolic mirror is not in yet, we can check the beam position at the far end of the table to obtain best parallelism. This step is crucial. Vertical deviation from parallelism will cause a skewed fringe pattern, horizontal deviation and error in spacing between two beams will result in error in the calculation of the fringe spacing which directly affects the final results. Note the readings of the micrometers on the platforms supporting the prisms. These readings are the basis for adjusting the prism spacing later. It was found that moving the platforms along the micrometer axes does not change the beam parallelism to any degree of significance.

#### (f) Reading Beam

Adjust the He-Ne laser, which is the reading beam source, and mirrors F, G to assure that both paths, from F to G and reflected by G, are parallel to two perpendicular rows of holes and at the same height as the reference pinhole. Still check at the far end of the table. Make the reading beam 1 inch away from the writing beam (the upper one shown in Figure

B.2) using the micrometer on the mirror mount for G. Note the micrometer reading. Move the reading beam to the calculated position that satisfies the Bragg's condition.

**(g) Off-Axis Parabolic Mirror**

Position the parabolic mirror appropriately. Mark the axis and the focal point on the table based on the specifications. Rotate the parabolic mirror horizontally (by the micrometer on the mirror mount) to make the crossing point of two beams to be on the marked axis and on the marked focal point as nearly as possible. Put the pinhole on the detection arm at the other far end of the table and check the position of all the three reflected beams from the off-axis parabolic mirror. Use the vertical controller at the back of the mirror mount to swing the mirror vertically. At this point, there may be some difference in direction among the three beams. Further fine adjustment will be conducted with the the help of a telescope.

**(h) Assembly of Sample Cell and Detection Arm**

The assembly includes a blackened aluminum sample cell holder sitting on a poly(methyl methacrylate) platform. The detection arm is connected to this platform by a pivot mechanism that made it possible to rotate the arm to pick up the diffracted light. In this step, only the sample cell block is to be fixed. It should be placed at the focal point with such a position that all the three beams enter and exit the block near the centers of the front and the rear openings. A piece of slide glass is inserted into the sample slit. The block is rotated to reflect each incident writing beam to the parabolic mirror at the spot of the other writing beam. This is to assure that the two writing beams impinge onto the sample symmetrically.

### (i) Telescope

The telescope is only used in the alignment, not in the measurement. It projects, with an enlargement, the image at its focal point onto a distant screen. This facilitates very fine adjustment. It is used to find the crossing point by achieving coincidence of its focal point with the crossing point that is also the focal point of the off-axis parabolic mirror. At this time, the two projected spots from the writing beams should merge. Adjust the knobs at the prism mounts slightly and translate the telescope to make two spots from the writing beams coincide. Adjust mirror G slightly to make the projected spot from the reading beam concentric with the writing spots.

The sample block is translated now using the micrometer to make the crossing point at the center of the sample slit. A stack of microscope slides, with a hair sandwiched in the middle, is inserted into the sample slit. The block is moved until a sharp image of the hair is seen in the telescope. By now, the center of the sample slit coincides with the focal point of the telescope, which was previously adjusted to coincide with the crossing point of the beams from the parabolic mirror.

### (j) Focal Lens for Reading Beam

The reading beam is much wider than the writing beams. A focal lens with a focal length of about 2 m is used to narrow the light intensity distribution. This improves the signal-to-noise ratio as a greater part of the reading intensity will be diffracted by the fringe pattern that is smaller than the initial reading beam width. This focal lens is adjusted to make the reading spot still concentric with the writing spots.

### (k) Fluorescent Gel

Fluorescein (about 0.05mg/ml final concentration) is dissolved in a warm solution of gelatine (about 0.15mg/ml), which is then cooled to form a fluorescent gel. Once it is exposed to the writing light fringes, a similar grating of concentration of photoexcited fluorescein is imprinted onto the gel. This pattern remains for more than several days and facilitates the alignment for the detection arm.

#### (1) Detection Arm

Select the #2 pinhole which is slightly smaller than the beam width of the diffracted light. Swing the arm to let the diffracted beam hit the pinhole, and then fix the arm. Put in the reading shutter at a position where the diffracted light hits the center of the shutter. Switch the pinhole to #4 whose aperture is larger than the beam width. Mark the diffraction spot on the screen. Put in the focal lens for the fiber optic and adjust the x-y micrometers on the mount of the lens to make the diffuse spot concentric with the previous mark. Connect the fiber optic.

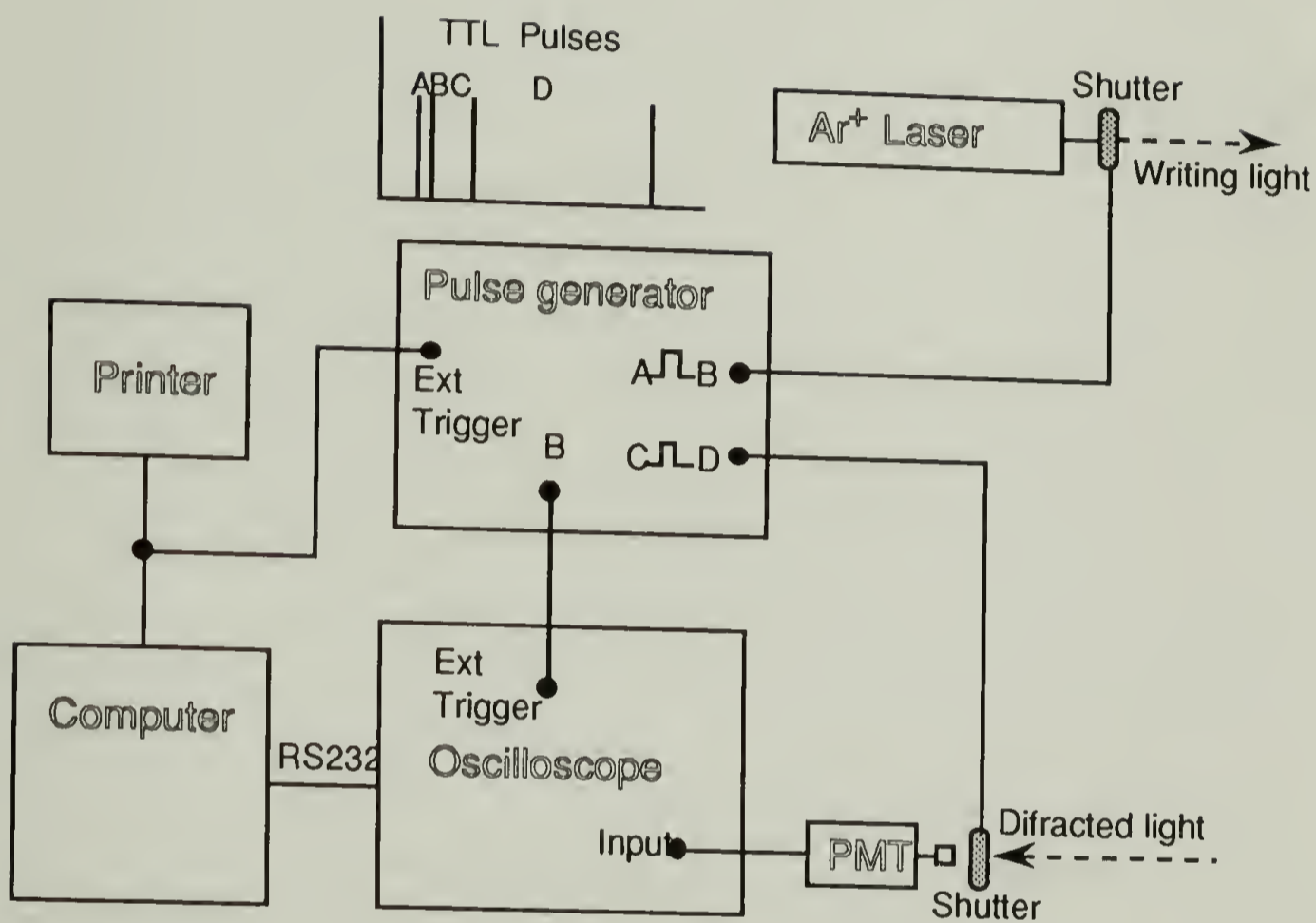


**Figure B.1** Connections among different units of the forced Rayleigh scattering apparatus.

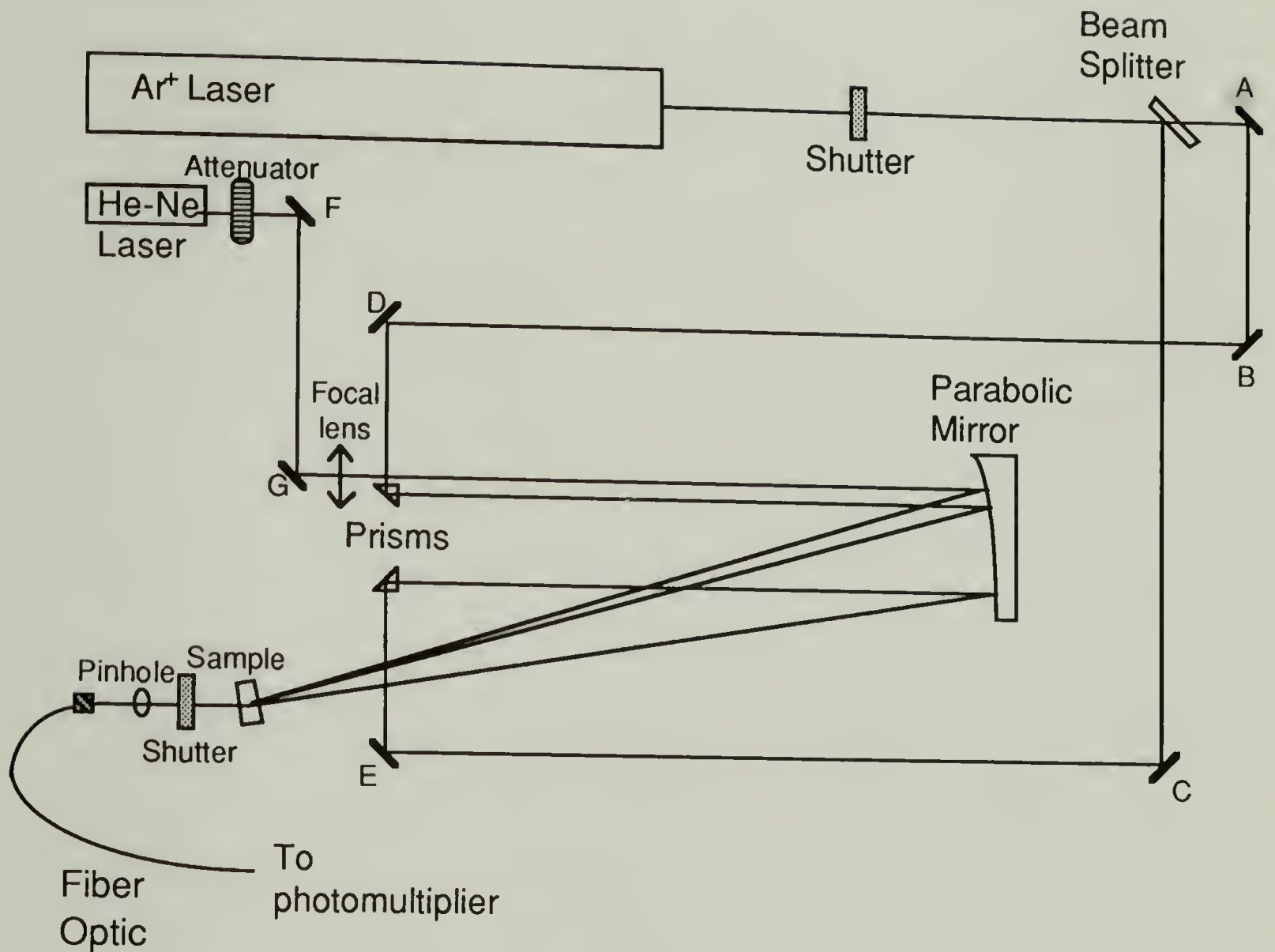


**Figure B.2** Optical layout of the for forced Rayleigh scattering spectroweter.



## REFERENCES

1. Drake, J. M.; Klafter, J., *Phys. Today*, **41**, 46 (1990).
2. Klafter, J.; Rubin, R. J.; Shlesinger, M. F., "Transport and Relaxation in Random Materials", World Scientific, 1986.
3. Klafter, J.; Drake, J. M., "Molecular Dynamics in Restricted Geometries", Wiley, New York, 1989.
4. Scheidegger, A. E., "The Physics of Flow through Porous Media", MacMillan, New York, 1960.
5. Bear, J., "Dynamics of Fluids in Porous Media", American Elsevier, New York, 1972.
6. Dullien, F. A. L., "Porous Media: Fluid Transport and Pore Structure", Academic, New York, 1979.
7. Happel, J.; Brenner, H., "Low Reynolds Number Hydrodynamics", Prentice-Hall, New Jersey, 1965.
8. Renkin, E. M., *J. Gen. Physiol.*, **38**, 225 (1954).
9. Davidson, M. G.; Deen, W. M., *Macromolecules*, **21**, 3474 (1988).
10. Deen, W. M.; Bohrer, M. P.; Epstein, N. B., *AIChE J.*, **33**, 1409 (1987).
11. Bohrer, M. P.; Patterson, G. D.; Carroll, P. J., *Macromolecules*, **17**, 1170 (1984).
12. Bohrer, M. P.; Fetters, L. J.; Grizzuti, N.; Pearson, D. S.; Tirrell, M. V., *Macromolecules*, **20**, 1827 (1987).
13. Guillot, G., *Macromolecules*, **20**, 2600, 2606 (1987).
14. Guillot, G.; Leger, L.; Rondelez, F., *Macromolecules*, **18**, 2531 (1985).

15. Davidson, M. G.; Deen, W. M. *J. Membrane Sci.*, **35**, 167 (1988).
16. Tennikov, M. B.; Belen'kii, B. G.; Nesterov, V. V.; Anan'eva, T.D., *Colloid. J. USSR*, **41**, 526 (1979).
17. Giddings, J. C.; Bowman, L. M., Jr.; Myers, M. N., *Macromolecules*, **10**, 443 (1977).
18. Klein, J.; Gruneberg, M., *Macromolecules*, **14**, 1411 (1981).
19. Bishop, M. T.; Langley, K. H.; Karasz, F. E., *Macromolecules*, **22**, 1220 (1989), *Phys. Rev. Lett.*, **57**, 1741 (1986).
20. Bishop, M. T., Ph.D. Thesis, University of Massachusetts, Amherst, 1986.
21. Easwar, N.; Langley, K. H.; Karasz, F. E., *Macromolecules*, **22**, 3492 (1989).
22. Colton, C. K.; Satterfield, C. N.; Lai, C.-J., *AIChE J.*, **21**, 289 (1975).
23. Bean, C.P., "Membranes: A Series of Advances", Eisenman, G., Ed., Marcel Dekker, New York, Vol. 1, pp.1, 1972.
24. Anderson, J. L.; Quinn, J. A., *Biophys. J.*, **14**, 130 (1974).
25. Brenner, H.; Gajdos, L. J., *Coll. Interface Sci.*, **58**, 312 (1977).
26. Paine, P. L.; Scherr, P., *Biophys. J.*, **15**, 1087 (1975).
27. Brochard, F., *J. Phys. (Paris)*, **38**, 1285 (1977).
28. Brochard, F.; de Gennes, P. G., *J. Chem. Phys.*, **67**, 52 (1977).
29. de Gennes, P. G., "Scaling Concepts in Polymer Physics", Cornell University Press, Ithaca, NY, 1979.
30. Daoud, M.; de Gennes, P. G., *J. Phys. (Paris)*, **38**, 85 (1977).
31. Muthukumar, M.; Baumgärtner, A., *Macromolecules*, **22**, 1937, 1941 (1989).
32. Halperin, W. P.; O'Drazio, F.; Bhattacharja, F.; Tarczon, J. C., "Molecular Dynamics in Restricted Geometries", Klafter, J.; Drake, J. M., Eds.; Wiley, New York, pp.311, 1983.

33. Karger, J.; Lenzner, J.; Pfeifer, H.; Schwabe, H.; Heyer, W.; Janowski, F.; Wolf, F.; Zdanov, S. P., *J. American Ceramic Soc.*, **66**, 69 (1982).
34. Stejskal, E.O.; Tanner, J. E., *J. Chem. Phys.*, **42**, 288 (1965).
35. Axelrod, D.; Koppel, D.; Schlessinger, J.; Lison, E.; Webb, W. W., *Biophys. J.*, **16**, 1055 (1976).
36. Neale, G. H.; Nader, W. K., *AIChE J.*, **19**, 112 (1973).
37. Fricke, H.; Morse, S., *Phys. Rev.*, **25**, 361 (1925).
38. De la Rue, R. E.; Tobias, C. W. *J. Electrochem. Soc.*, **106**, 827 (1959).
39. Willie, M. R.; Gregory, A. R., *Trans. AIME*, **198**, 103 (1953).
40. Klein, J.; Grüneberg, M., *Macromolecules*, **14**, 1411 (1981).
41. Sargent, R. W. H.; Whitford, C. J., *Adv. Chem.*, **102**, 155 (1971).
42. Quig, A.; Rees, L. V. C., *J. Chem. Soc. Faraday Trans.*, I **72**, 771 (1976).
43. Chu, B., "Laser Light Scattering", Academic, New York, 1974.
44. Berne, B.J.; Pecora, R., "Dynamic Light Scattering: With Applications to Chemistry, Biology and Physics", Wiley, New York, 1976.
45. Cummins, H. Z.; Pike, E. R., Eds., "Photon Correlation and Light Beating Spectroscopy", John Wiley and Sons, New York, 1976.
46. Scarlet, R. I., *Phys. Rev.*, **A6**, 2281 (1972).
47. Eichler, H.; Salje, S. E.; Stahl, H., *J. Appl. Phys.*, **44**, 5358 (1973).
48. Pohl, D. W.; Schwarz, S. E.; Irniger, V., *Phys. Rev. Lett.*, **31**, 32 (1973).
49. Pohl, D. W., *IBM J. Res. Development*, **23**, 604 (1979).
50. Rondelez, F., "Light Scattering in Liquids and Macromolecular Solutions", Degiorio, V.; Corti, M., Eds., Plenum, New York, 1980.

51. Urbach, W.; Hervet, H.; Rondelez, F., *J. Chem. Phys.*, **83**, 1877 (1985).
52. Fayer, M. D., *Ann. Rev. Phys. Chem.*, **33**, 63 (1982).
53. Johnson, Jr., C. S., *J. Chem. Phys.*, **81**, 5384 (1984).
54. Shibata, J. H.; Johnson, Jr., C. S., *Appl. Spectroscopy*, **39**, 786 (1985).
55. Roman, M., *J. Molec. Structure*, **141**, 289 (1986).
56. Chiang, K.; Levenson, M. D., *Appl. Phys. B*, **29**, 23 (1982).
57. Barish, A.; Bradley, M. S., *Rev. Sci. Instrum.*, **57**, 904 (1986).
58. Eichler, H.; Enterlein, G.; Glozbach, P.; Munschau, J.; Stahl, H., *Appl. Optics*, **11**, 372 (1972).
59. McGraw, D. J., *J. Chem. Phys.*, **86**, 2536 (1987).
60. Chan, W. K.; Pershan, P. S., *Biophys. J.*, **23**, 427 (1978).
61. Hara, M.; Takezoe, H.; Fukuda, A., *Japanese J. Appl. Phys.*, **23**, 1420 (1984), **25**, 1756 (1986).
62. Takezoe, H., Hara, M.; Ichikawa, S., *Molec. Cryst. Liq. Cryst.*, **122**, 169 (1985).
63. Hervet, H.; Urbach, W.; Rondelez, F., *J. Chem. Phys.*, **68**, 2725, (1978).
64. Zhang, J.; Wang, C. H.; Chen, Z.-X., *J. Chem. Phys.*, **85**, 5359 (1986).
65. Wang, C. H.; Xia, J. L., *Macromolecules*, **22**, 2020 (1989).
66. Wesson, J. A.; Takezoe, H.; Yu, H. Chen, S. P., *J. Appl. Phys.*, **53**, 6513 (1982).
67. Lee, J. A.; Lodge, T. P., *J. Phys. Chem.*, **91**, 5546 (1987).
68. Lodge, T. P.; Wheeler, L.; Hanley, B.; Huang, W. J.; Landry, M. R.; Frick, T. S.; Lee, J. A.; Tirrell, M., *Makromol. Chem., Macromol. Symp.*, **10/11**, 151 (1987).

69. Wesson, J. A.; Noh, I.; Kitano, T; Yu, H., *Macromolecules*, **17**, 782 (1984).
70. Lèger, L.; Hervet, H.; Rondelez, F., *Macromolecules*, **14**, 1732 (1981).
71. Deschamps, H.; Léger, L., *Macromolecules*, **19**, 2760 (1986).
72. Qui, T.-C.; Chang, T.; Han, C. C., *Polymer*, **29**, 2261 (1988).
73. Kim, H.; Chang, T.; Yohanan, J. M.; Wang, L.; Yu, H., *Macromolecules*, **19**, 2737 (1986).
74. Hervet, H.; Léger, L.; Rondelez, F., *Phys. Rev. Lett.*, **42**, 1681 (1979).
75. Chang, T.; Yu, H., *Macromolecules*, **17**, 115 (1984).
76. Antonietti, M.; Sillescu, H., *Macromolecules*, **18**, 1162 (1985).
77. Coutandin, J.; Sillescu, H., *Makromol. Chem., Rapid Commun.*, **3**, 649 (1982).
78. Antonietti, M.; Coutandin, J.; Grutter, R.; Sillescu, H., *Macromolecules*, **17**, 798 (1984).
79. Kim, H.; Chang, T.; Yu, H., *J. Phys. Chem.*, **88**, 3944, 3946 (1984).
80. Johnson, Jr., C. S., *J. Chem. Phys.*, **81**, 5384 (1984).
81. Arunyawongsakorn, U.; Johnson, Jr., C. S.; Gabriel, D. A., *Anal. Biochem.*, **146**, 265 (1985).
82. Chang, T.; Han, C. C., *Macromolecules*, **21**, 1870 (1988).
83. Lever, L. S.; Bradley, M. S.; Johnson, Jr., C. S., *J. Magnetic Resonance*, **68**, 335 (1986).
84. Smith, B. A., "Photophysical and Photochemical Tools in Polymer Science", Winnik, M. A., Ed., Reidel, 1986.
85. Prager, S., *Physica*, **29**, 129 (1963).
86. Tomalia, D. A.; Baker, H.; Dewald, J.; Hall, M.; Kallos, G.; Martin, S.; Roech, J.; Ryder, J.; Smith, P., *Polymer J.*, **17**, 117 (1985).

87. Ross, D. L.; Blanc, J., "Photochromism", Brown, G. H. Ed., Wiley-Interscience, New York, 1971.
88. Brode, W. R.; Gould, J. H.; Wyman, G. M., *J. Amer. Chem. Soc.*, **74**, 4641 (1952), **75**, 1856 (1953).
89. Fischer, E.; Frei, Y., *J. Chem. Phys.*, **27**, 328 (1957).
90. a. Haller, W., *Nature*, **206**, 693 (1965).  
b. Haller, W., *J. Chem Phys.*, **42**, 686 (1965).  
c. Haller, W., *Phys. Chem. Glasses*, **9**, 153 (1968).
91. Nordberg, M. E., *J. Am. Ceram. Soc.*, **27**, 299 (1944).
92. Hood, H. P.; Nordberg, M. E., U. S. Patent 2,106,744 (1938).
93. A special issue devoted to mercury porosimetry, *Powder Technol.* **29**, (1981).
94. Adamson, A.W., "Physical Chemistry of Surfaces", 4th Ed., Wiley-Interscience, New York, 1982.
95. Technique Bulletin Pigments, **6**, "Hydrophobic AEROSIL: Manufacture, Properties and Applications", Degussa Corporation, 1986.
96. Schaefer, D. W.; Hurd, A. J.; Christen, D. K.; Spooner, S.; Lin, J. S., *Mat. Res. Soc. Sym. Proc.*, **121**, 305 (1988).
97. Farwell, S. O.; Gluck, S. J., *Anal. Chem.*, **52**, 1968 (1980).
98. Cooper, A. R.; Johnson, J. F., *I. Appl. Polym. Sci.*, **13**, 1487 (1969).
99. Koppel, D. E., *J. Chem. Phys.*, **57**, 4814 (1972).
100. Provencher, S. W., *Makromol. Chemie*, **180**, 201 (1979).
101. Bevington, P. R., "Data Reduction and Error Analysis for the Physical Sciences", McGraw-Hill, New York, 1968.
102. Marquardt, D. W., *J. Soc. Ind. Appl. Math.*, **11**, 431 (1963).
103. Kremer, K.; Binder, K., *J. Chem. Phys.*, **81**, 6381 (1984).
104. Baumgärtner, A.; Muthukumar, M., *J. Chem. Phys.*, **87**, 3082 (1987).

105. Evans, K. E.; Edwards, S. F., *J. Chem. Phys.*, **77**, 1891, 1913, 1929 (1981).
106. (a) Famularo, J., D. Eng. Sci. Thesis, New York University, 1962.  
(b) Hirschfeld, B. R., Ph. D. Thesis, New York University, 1972.
107. Peterson, D. D.; Porter, M. C., "Kirk-Othmer: Encyclopedia of Chemical Technology", 3rd Ed., V.16, John Wiley and Sons, New York, pp.826, 1981.
108. Lehner, F. K., *Chem. Eng. Sci.*, **34**, 821 (1979).
109. Lodge, T. P.; Wheeler, L. M.; Tirrell, M. V., *Polym. Bull.*, **15**, 35 (1986).
110. Pismen, L. M., *Chem. Eng. Sci.*, **29**, 1277 (1974).
111. Casassa, E. F.; Tagami, Y., *Macromolecules*, **2**, 14 (1969).
112. Giddings, J. C.; Kucera, E.; Russell, C. P.; Myers, M.N., *J. Phys. Chem.* **72**, 4397 (1968).
113. Cifra, P.; Bleha, T.; Romanov, A., *Polymer*, **29**, 1644 (1988).
114. Yamakawa, H., "Modern Theory of Polymer Solutions", Harper & Row, New York, 1971.
115. Aklonis, J. J.; MacKnight, W. J.; Shen, M., "Introduction to Polymer Viscoelasticity", Wiley, New York, 1983.
116. Bantle, S.; Schmidt, M.; Burchard, W., *Macromolecules*, **15**, 1604 (1982).
117. Shiflett, W. K., Shell Development Co., personal communication.
118. Dozier, W. D.; Drake, J. M.; Klafter, J., *Phys. Rev. Lett.*, **56**, 197 (1986); results also cited in references 1-3.
119. Portella, M. T.; Montelmacher, P.; Bourdon, A.; Duran, J., *J. Phys.: Condensed Matter*, **1**, 981 (1989).
120. Horiguchi, Y.; Hudgins, R. R.; Silveston, P. L., *Canad. J. Chem. Eng.*, **49**, 76 (1971).
121. Okazaki, M.; Taman, H.; Hyodo, T.; Toei, R., *AIChE J.*, **27**, 1035 (1981).

122. Höhr, A.; Neumann, H.-B.; Schmidt, P. W.; Pfeifer, P.; Avnir, D., *Phys. Rev. B*, **38**, 1462 (1988).
123. A special issue devoted to disordered solids, *Phys. Today*, **39(12)**, (1988).
124. Schaefer, D. W., *Science*, **243**, 1023 (1989).
125. Aubert, C.; Cannell, D. S., *Phys. Rev. Lett.*, **56**, 738 (1986).
126. Dietler, G.; Aubert, C.; Cannell, D. S., *Phys. Rev. Lett.*, **57**, 3117 (1986).
127. Martin, J. E., *Phys. Rev. A*, **36**, 3415 (1987).
128. Schaefer, D. W.; Keefer, K. D., *Phys. Rev. Lett.*, **53**, 1383 (1984).
129. Martin, J. E.; Wilcoxon, J. P., *Phys. Rev. A*, **39**, 252 (1989).
130. Gefen, Y.; Aharony, A.; Alexander, S., *Phys. Rev. Lett.*, **50**, 77 (1983).
131. Rammal, R.; Toulouse, G., *J. de Physique, Lett.*, **44**, L13 (1983).
132. Guyer, R. A., *Phys. Rev. A*, **32**, 2324 (1985).
133. O'Shaughnessy, B.; Procaccia, I., *Phys. Rev. Lett.*, **54**, 455 (1985).
134. Van Brakel, J.; Heertjes, P. M., *Int. J. Heat Mass Transfer*, **17**, 1093 (1974).
135. Prigigine, I., "Introduction to Thermodynamics of Irreversible Processes", Charles C. Thomas, Illinois, Chap. 5, 1955.
136. Camin, D.L.; Rossini, F. D., *J. Phys. Chem.*, **59**, 1173 (1955).
137. Seyer, W. F.; Leslie, J. D., *J. ACS*, **64**, 1912 (1942).
138. Weast, R. C.; Selby, S. M., Eds., "Handbook of Chemistry and Physics", 48th Ed., Chemical Rubber Co., Ohio, 1967-1968.



